

UNCLASSIFIED

32 635

Reproduced

Armed Services Technical Information Agency

ARLINGTON HALL STATION; ARLINGTON 12 VIRGINIA

NOTE: WHEN GOVERNMENT OR OTHER DRAWINGS, SPECIFICATIONS OR OTHER DATA ARE USED FOR ANY PURPOSE OTHER THAN IN CONNECTION WITH A DEFINITELY RELATED GOVERNMENT PROCUREMENT OPERATION, THE U. S. GOVERNMENT THEREBY INCURS NO RESPONSIBILITY, NOR ANY LIABILITY WHATSOEVER; AND THE FACT THAT THE GOVERNMENT MAY HAVE FORMULATED, FURNISHED, OR IN ANY WAY SUPPLIED THE SAID DRAWINGS, SPECIFICATIONS, OR OTHER DATA IS NOT TO BE REGARDED BY ANY OTHER PERSON OR CORPORATION, OR CONVEYING ANY RIGHTS OR PERMISSION TO MANUFACTURE, USE OR SELL ANY PATENTED INVENTION OR MAY IN ANY WAY BE RELATED THERETO.

UNCLASSIFIED

LOAN COPY

RETURN IN 90 DAYS TO

ASTIA

ARLINGTON HALL STATION
ARLINGTON 12, VIRGINIA

Attn: TISSS

FILE COPY

Return to

ASTIA

ARLINGTON HALL STATION
ARLINGTON 12, VIRGINIA

Attn: TISSS

SUNDSTRAND

SUNDSTRAND

TURBO

S /TD No. 1735
**STUDY OF TURBINE AND TURBOPUMP
DESIGN PARAMETERS**

Final Report - Volume I

A Study of High Pressure Ratio Re-Entry Turbines

Hans D. Linhardt

Contract No. NONR-2292(00)

Task No. NR 094-343

For the Period 1 February 1958 through 30 January 1960

**Department of the Navy
Office of Naval Research**

**Reproduction of this data in whole or in part is permitted for any purpose
of the United States Government**

**Sundstrand Turbo
a Division of Sundstrand Corp.
Pacoima, California**

Rockford, Ill



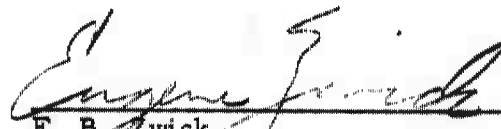
**S U N D S T R A N D T U R B O
DIVISION OF SUNDSTRAND CORPORATION**

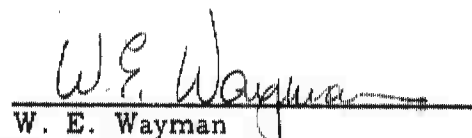
FOREWORD

This document was prepared by the Turbine Research Section of Sundstrand Turbo, Division of Sundstrand Corporation, under U. S. Navy Contract Nonr-2292(00) Task No. 094-343 and is one of four parts comprising the final report. The work described in this volume was accomplished during the period 1 February 1958 through 30 January 1960.

The original turbine design and analysis were the work of Mr. D. Silvern and W. Nerenstein. The author acted as Project Engineer during the test and analysis phases of the research program. Mr. M. Dubey supervised the program as Head of the Turbine Research Section. Messrs. H. Gavenman, F. Beach and H. Goodknight assisted with hardware procurement and testing and Mrs. R. E. Deere with the data evaluation. Dr. O. E. Balje, engineering consultant on turbomachinery, contributed advice on technical problems.

Approved by:


E. B. Zwick
Associate Chief Engineer


W. E. Wayman
Chief Engineer

Except for use by or on behalf of the United States Government, all rights with respect to this report, including without limitation, technical information, data, drawings and specifications contained herein, are reserved by the Sundstrand Corporation.

TABLE OF CONTENTS

	<u>Page</u>
FOREWORD	i
I. ABSTRACT	1
II. INTRODUCTION	1
III. TECHNICAL SUMMARY	2
IV. TECHNICAL DISCUSSION	4
A. Analysis	4
B. Design of Test Turbine	31
C. Objective of Experimental Program	34
D. Apparatus and Instrumentation	35
E. Analysis and Discussion of Experimental Results	39
F. Correlation of Test Results with Analysis	73
V. CONCLUSIONS	75
VI. RECOMMENDATIONS	77
VII. REFERENCES	79
VIII. APPENDICES	82
Appendix A	Nomenclature and Symbols 82
Appendix B	Derivation of Basic Relations for Equal Spouting Velocity in Both Stages 87

TABLE OF CONTENTS

	<u>Page</u>
Appendix C Derivation of Performance Relations for the Case of Unequal Spouting Velocities in Both Stages	90
Appendix D Derivation of Leakage Functions F_1 and F_2	94
Appendix E Duct Loss Analysis	97
Appendix F Illustrations and Figures	101

LIST OF FIGURES

<u>Figure No.</u>		<u>Page</u>
1	Leakage Passage of Two Stage Re-entry Turbine without Cross-over Duct.	101
2	N_s - D_s Diagram of Two-stage Re-entry Turbine with Equal Head in Both Stages and 300:1 Over-all Pressure Ratios.	102
3	N_s - D_s Diagram of Two-stage Re-entry Turbine with Equal Head in Both Stages and 17:1 Over-all Pressure Ratios.	103
4	N_s - D_s Diagram of Two-stage Re-entry Turbines with Equal Pressure Ratios in Both Stages and 300:1 Over-all Pressure Ratios.	104
5	Comparison of Optimum Turbine Performance Using Equal Heads or Equal Pressure Ratios in Both Stages. Over-all Pressure Ratio 300:1.	105
6	Comparison of Leakage Due to Equal Head and Equal Pressure Ratios in Both Stages.	106
7	Turbine Performance versus N_s for $D_s = 2.58$ and $P_{r_{tot}} = 300:1$.	107
8	Exploded view of Test Turbine.	108
9	Turbine Installation within the High Altitude Chamber.	109
10	High Altitude Facility of Sundstrand Turbo.	110
11	Test Chamber of the High Altitude Facility.	111

LIST OF FIGURES

<u>Figure No.</u>		<u>Page</u>
12	Recording Instruments of the High Altitude Facility.	112
13	Dynamometer with Torque Ring.	113
14	Schematic Instrumentation Stations.	114
15	Downstream Measuring Station.	115
16	Calibration of Re-entry Duct in High Altitude Chamber	116
17	Instrumentation	117
18	Description of Instrumentation.	118
19	Performance of Two-stage Re-entry Turbine:- Torque Coefficient versus (u/c_0).	119
20	Performance of Two-stage Re-entry Turbine for Clearance $C^* = 0.005$ and $C^* = 0.17$.	120
21	Comparison of Torque and Temperature Efficiency for Clearance $C^* = 0.005$.	121
22	Total Leakage.	122
23	Static Leakage	123
24	Comparison of Measured and Theoretical Predicted Amount of Static Leakage.	124
25	Static Pressure Variation Inside the Test Turbine Near the Design Point.	125

LIST OF FIGURES

<u>Figure No.</u>		<u>Page</u>
26	Static Pressure Variation Inside the Test Turbine for Off-design Performance.	126
27	Leakage Function F_1 .	127
28	Leakage Function F_2 .	128
29	Absolute Rotor Discharge Mach Number of First Stage versus	129
30	Illustration of Turning Loss at Inlet to Re-entry Duct.	130
31	Static Pressure Loss Coefficient for Re-entry Duct.	131
32	Recovery Factor.	132
33	Static Pressure Loss Coefficient for Turning and Friction Losses in the Re-entry Duct.	133
34	Nozzle Coefficient of First Stage.	134
35	Nozzle Coefficient of Second Stage.	135
36	Predicted Nozzle Coefficients of Reference (5).	136
37	Illustration of Incidence Loss.	137
38	Mach Number Relation for Subsonic Blade Configurations.	138
39	Form Factor versus Free-Stream Mach Number.	139

LIST OF FIGURES

<u>Figure No.</u>		<u>Page</u>
40	Stage Performance of Two-Stage Re-entry Turbine for Pressure Ratio 300:1 and Axial Clearance $C^* = 0.005"$.	140
41	Performance of First Stage.	141
42	Performance of Second Stage.	142
43	Final N_s - D_s Diagram for Two-stage Re-entry Turbines with Equal Pressure Ratios in Both Stages and 300:1 Over-all Pressure Ratios.	143
44	Comparison of Performance of Two-stage Re-entry Turbine with Theoretical Performance Predicted by Refined Analysis and Performance of Equivalent Single-stage Turbine.	144

I. ABSTRACT

The design point analysis of two-stage, axial re-entry type turbines is presented for the case of low weight flow and high over-all pressure ratios. The optimum pressure split between both stages is investigated approximately by evaluating the optimum performance for two-stage re-entry turbines with equal heads or equal pressure ratios in both stages. The optimum efficiency for both pressure splits is analyzed and a theoretical method of determining the detailed design criteria is presented for each optimum design. The method of analysis is substantiated by test of a two-stage re-entry turbine designed according to the analysis. Deviations from this analysis were found to be caused by increased leakage and off-design performance of the second-stage nozzle. (C)

II. INTRODUCTION

This report has been prepared in accordance with the requirements of ONR Contract Nonr 2292(00), Phase II, Re-entry Turbine Study. It deals with the performance of a two-stage re-entry turbine at the design or "best efficiency" point and is not concerned with detailed analysis of the off-design performance. Tests of a single disc turbine with seventeen passes, which were later reduced to four passes, were conducted at Sundstrand Turbo during

early 1959, but the results were inconclusive. The work is not described herein since the information would confuse rather than clarify the analysis.

III. SUMMARY

The design analysis of two-stage re-entry turbines presented in Reference (1) for the case of moderate over-all pressure ratios is extended for designing two-stage re-entry turbines with high pressure ratios. The optimum pressure split between both stages is investigated approximately by analyzing the special cases of equal head and equal pressure ratio in both stages. For the Reynolds number range considered, $10^4 < Re < 10^6$ it is found that equal pressure ratios in both stages results in higher efficiencies than that obtained with turbines having equal heads in both stages. General design criteria are presented for both cases in the form of preliminary $N_s D_s$ diagrams. Finally, a two-stage re-entry turbine, designed according to the criteria developed for equal pressure ratios in both stages, is subjected to an extensive and detailed test program. It is found that the over-all performance, as well as the performance of the components can be substantiated by the analysis. Discrepancies between preliminary analysis and test results are found to be caused by off-design performance of the second stage nozzle as well as increased leakage. It is found that leakage consists of two parts designated as the static and the dynamic component. The test results con-

cerning leakage are correlated with theoretical equations developed in this report. It is found that the axial clearance between the first stage nozzle and the rotor is a major parameter which affects the over-all performance of two stage re-entry turbines. In addition, it is found that the blade element performance is determined mainly by the entering relative Mach number. The blade coefficients are correlated with data published in the literature, and are valid for blade designs of subsonic configuration. The test performance curves are correlating well with final analysis of two-stage re-entry turbines. The analysis is presented in general equations, and design criteria are presented in the form of a final $N_s D_s$ diagram for two-stage re-entry turbines with a 300:1 pressure ratio.

It is concluded that the over-all performance of the turbines concerned can be estimated properly by application of one-dimensional streamline concepts. However, refined analyses and test procedures are necessary to investigate the flow phenomena in the turbine itself. This indicates the necessity of a detailed program for investigation and study of the cascade performance of impulse blades subjected to high Mach number conditions. Comparison of the two-stage turbine with an equivalent single stage design, both with subsonic blade configurations, overwhelmingly demonstrates the merit of the

two-stage turbine. However, preliminary calculations have indicated that a one-stage turbine designed with a supersonic blade configuration, might perform comparably or even more efficiently.

IV. TECHNICAL DISCUSSION

A. ANALYSIS

The analysis of axial, multistage, re-entry turbines, using partial admission in all stages, is presented in Reference (1) for the case of moderate pressure ratios. This analysis was based on a one-dimensional streamline concept, which uses proper corrections to account for three-dimensional effects and to include all "partial-admission-losses" known to the state-of-the-art at that time. Three-dimensional-effects are caused by non-uniformity of the flow field, which leads to secondary losses mainly at hub and tip section of the rotor cascade. In addition, disturbance of the channel flow can be caused by separation of the blade surface boundary layers. This effect is not included in the previous analysis and will not be investigated in this work. The partial admission losses consist of blade pumping losses, scavenging losses, filling and emptying losses, additional interstage leakage losses, and some additional cascade losses all of which are not encountered in the field of full admission turbines.

The theory developed in Reference (1) for the case of moderate pressure ratios is extended in this work for application to high pressure ratio, two-stage, re-entry turbines. For this purpose it was found necessary to use a compressible flow model rather than adhere to the nearly incompressible flow model used in Reference (1). In the case of highly efficient, high pressure ratio turbines it is possible to use isentropic flow relations as a first approximation. However, for less efficient turbine stages it is necessary to modify the isentropic equations by proper efficiency corrections.

Since it is not obvious, when designing a two-stage, re-entry turbine, what pressure split between the stages will result in the maximum turbine efficiency, the cases of equal heads and of equal pressure ratios in both stages are investigated in the following chapter, leading to two $N_s D_s$ diagrams, as shown in Figure 2 & 4. These diagrams are used as a basis for the design of the test turbine and for comparison of the actual turbine performance with the theory, developed in Reference (1) and extended herein.

1. Special Case of Equal Heads or Equal Spouting Velocities in Both Stages.

- 1.1 Turbine efficiency

Generally, the turbine efficiency or over-all efficiency is defined

by the following relation, which does not include bearing losses.

$$\eta_T = \eta_h(1 - L_t) - L_b - L_d - L_{sc} \quad (1)$$

where

η_T = turbine efficiency

η_h = hydraulic efficiency

L_t = total leakage as percentage of total mass flow

L_b = blade pumping loss as percentage of available power

L_d = disc friction loss as percentage of available power

L_{sc} = scavenging loss as percentage of available power

η_h is the hydraulic efficiency, which is derived in Reference (1) from Euler's equation for the change of momentum in single stage impulse turbines. This equation, only valid for the design point performance without incidence-losses, can be written in the convenient form

$$\eta_h = 2(u/c_{oi})^2 (1 + \psi_R) (\psi_N \cos \alpha - u/c_{oi}) \quad (2)$$

where

u = tip speed

c_{oi} = spouting velocity of a single stage

ψ_R = blade coefficient

ψ_N = nozzle coefficient

In the case of two stages having equal spouting velocities or equal velocity triangles equation (2) is modified by introducing average blade and nozzle coefficients and by observing the relation

$$C_{oI} = C_{oII} = \frac{C_o}{\sqrt{2}} \quad (3)$$

This results in the following expression for the hydraulic efficiency.

$$\bar{\eta}_h = 4(u/c_o)(1 + \bar{\psi}_R) \left(\frac{\bar{\psi}_N}{\sqrt{2}} \cos \alpha - u/c_o \right) \quad (4)$$

where

$\bar{\eta}_h$ = average hydraulic efficiency

C_o = total spouting velocity

$\bar{\psi}_R$ = average blade coefficient

$\bar{\psi}_N$ = average nozzle coefficient

The average blade coefficient is determined for partial admission stages by the equation derived in Reference (1)

$$\bar{\psi}_R = \bar{\psi}_{R_o} \left[1 - \frac{t}{4a_I} \left(1 + \frac{a_I}{a_{II}} \right) \right] \quad (5)$$

where

$\bar{\psi}_{R_o}$ = blade coefficient of an equivalent full admission stage

t = blade spacing

a_I = arc of admission of the first stage

a_{II} = arc of admission of the second stage

Introducing isentropic flow relations and neglecting leakage the ratio of the arcs of admission

$$\frac{a_I}{a_E} = \frac{p_I}{p_E} = \left(\frac{P_I}{P_E} \right) \left(\frac{T_I}{T_E} \right) \quad (6)$$

is only a function of the total pressure ratio $Pr = \frac{1}{\delta_{tot}}$ as seen from the simple relation which is derived in Appendix B, equations (B1) to (B7)

$$\left(\frac{a_I}{a_E} \right) = \frac{\delta_{tot}^{1/k}}{\left(\frac{1 + \frac{k-1}{2} M^2}{2} \right)^{1/(k-1)}} \quad (7)$$

The blade coefficient relation of an equivalent full-admission stage is derived in Reference (1) for the case of blade passages designed according to the method of characteristics and the theory of supersonic vortex flow (Reference 2). Such blade designs are called supersonic blades. The blade coefficient is determined by the following equation

$$\psi_{R_0} = \left[1 - 0.228 \left(1 - \frac{2\beta}{\pi} \right)^3 \right] \left[1 - 0.05 (1 - M_{W_2})^2 \right] \left[1 - 0.06 \left(\frac{\xi}{L} \right) \right] \quad (8)$$

where

β = blade angle

C = blade chord h = blade height M_{w_2} = relative Mach-number at rotor inlet

However, when subsonic blades are subjected to supersonic flow conditions, it is indicated by Reference (3) and by preliminary test information gathered at Sundstrand Turbo, that the resulting blade coefficients are lower. This is due to a disturbance of the uniform flow by shock patterns as observed in Reference (4) and by separation phenomena in the blade passages itself. For the case of subsonic blade passages with a blade angle $\beta = 30^\circ$ and chord to blade height ratio (C/h) = .86, it is found in the above mentioned references, that the blade coefficient ψ_{R_0} closely follows the empirically established equation:

$$\psi_{R_0} = 0.90 \left[1 - 0.12 (M_{w_2} - 1)^{1.5} \right] \quad (9)$$

Combining equation (4), (5) and (7), the hydraulic efficiency is determined by

$$\eta_h = 4 \cdot (u/c_0) \left\{ 1 + \psi_{R_0} \left[1 - \frac{t}{4a_1} \left(1 + \frac{\frac{1}{2} \frac{d_1}{d_2}}{\left(1 + \frac{d_1}{d_2} \right)^{\frac{1}{k-1}}} \right) \right] \right\} \left(\frac{\bar{\psi}_N}{\sqrt{2}} \cos \alpha - \frac{u}{c_0} \right) \quad (10)$$

The average nozzle coefficient,

$$\bar{\psi}_N = \frac{\psi_{N1} + \psi_{N2}}{2} \quad (11)$$

will be in the range for optimum designs $0.92 < \bar{\psi}_N < 0.96$, which is quoted by Reference (5) for nozzle designs in the range of the design Mach-number $1.38 < M_d < 3.375$. Other test data obtained by Reference (4) indicate the same trend.

1.2 Leakage

The part of the leakage flow lost entirely to both stages for a turbine configuration without a cross-over duct is analyzed approximately by accounting for the leakage paths as shown in Figure 1. In this design the first stage nozzle is located on the same side as the exhaust port of the second stage. From Figure 1 it can be seen that a tangential and radial leakage flow will likely occur between the first stage nozzle exit and the exhaust port of the second stage. This leakage flow is caused by the pressure gradient between the inlet and exhaust stations. The pressure gradient increases with an increasing over-all pressure ratio. In the case of high pressure ratio turbines, the pressure ratio between the nozzle exit of the first stage and the exhaust of the second stage will always be higher than the critical pressure ratio, and when the pressure gradient is due to pressure ratios above the critical

pressure ratio, the leakage flow is determined by the choked flow relation

$$W = \psi \cdot A^* \cdot \frac{P_0}{\sqrt{R T_0}} \quad (12)$$

where P_0 and T_0 describe the total conditions in front of the leakage throat area A^* . For the first approximation it is assumed that the static conditions at the nozzle exit represent the total condition in front of the tangential leakage area $A_t = 2c^*h$, and the radial leakage area $A_r = c^*a_I$. c^* denotes the axial clearance gap as shown in Figure 1, and a_I is the arc of admission of the first turbine stage.

The above assumption neglects the influence of the tangential component of the nozzle-jet on the leakage flow. In Reference (1) it was estimated that the tangential leakage in the direction of the rotating wheel will be larger by a ratio of $\sqrt{2}$ than the leakage in the opposite direction. The amount of leakage due to the above described effect is not included in the preliminary leakage equations, but will be investigated in the turbine test program as described in section E of this report.

The total leakage is determined by the following relation:

$$\Delta W = C_F \cdot \psi (A_r + A_t) \frac{P_2}{\sqrt{T_2 R}} \quad (13)$$

where

P_2 = static pressure at nozzle exit

T_2 = static temperature at nozzle exit

C_F = restriction factor

Ψ = nozzle function for choked flow

The nozzle function Ψ is given for choked flow by the equation

$$\Psi = \sqrt{2g \frac{\kappa}{\kappa+1}} \left(\frac{2}{\kappa+1} \right)^{\frac{1}{\kappa-1}} \quad (14)$$

The total leakage, as a ratio of the total inlet mass flow W_1 ,

$$W_1 = \Psi \cdot A_I^* \cdot \frac{P_{01}}{\sqrt{R T_{01}}} \quad (15)$$

where

A_I^* = nozzle throat of first stage

P_{01} = total inlet pressure

T_{01} = total inlet temperature

is determined by combining equation (13) and (15) and using isentropic flow relations for presenting temperatures in terms of pressure, as shown in Appendix B, equation (B8) to (B13). This leads to the following leakage equation, valid for the case of equal head in both stages and pressure ratios across the leakage areas larger than the critical pressure ratio:

$$L_4 = C_F \cdot \left(\frac{C^*}{D}\right) \cdot \left(\frac{D^2}{A_t^*}\right) \cdot \left[2 \frac{h}{D} + \frac{2}{D}\right] \cdot \left(\frac{1 + \sqrt{\frac{K}{1+K}}}{2}\right)^{\frac{K+1}{2(K-1)}} \quad (16)$$

The restriction coefficient C_f is estimated to be $C_F \approx 0.70$ assuming no labyrinths. The tip leakage is neglected.

1.3 Pumping Loss and Disc-friction Loss

The pumping or windage loss is derived by Reference (6) as a horsepower loss

$$\Delta HP_p = 0.458 \cdot 10^{-6} (1-\epsilon) \cdot D^{2.5} \cdot \left(\frac{h}{D}\right)^{1.5} \cdot g \cdot n^3 \quad (17a)$$

where ϵ denotes the total percent of admission of both stages together. For a two stage turbine of equal head in both stages the pumping loss, expressed as percentage of the available energy, amounts to

$$L_p = 16.2 \cdot \sqrt{2} \cdot 10^{-3} \left(\frac{D^{2.5}}{A_{N1}}\right) (1-\epsilon) \left(\frac{h}{D}\right)^{1.5} \cdot \left(\frac{u}{c_0}\right)^3 \quad (17b)$$

A_{N1} is the exhaust area of the first stage nozzle. Writing the above equation in dimensionless form for a rotor diameter $D = 5$ to 6 inches, results in the relation:

$$L_P = 40.5 \cdot 10^{-3} \cdot \sqrt{2} \left(\frac{D^2}{A_{N_I}} \right) \left(\frac{h}{b} \right)^{1.5} (1-\epsilon) \left(\frac{u}{c_0} \right)^3 \quad (17c)$$

The total admission ratio ϵ is given for two stages by

$$\epsilon = \frac{q_I}{\pi \cdot D} \left[1 + \frac{\left(\frac{1 + \delta_{t2}^{\frac{k-1}{k}}}{2} \right)^{\frac{1}{k-1}}}{\delta_{t2}^{\frac{1}{k}}} \right] \quad (18)$$

The disc-friction loss presents also a power loss according to Stodola

Reference (6)

$$\Delta H_D = 0.06 \cdot 10^{-3} \cdot \gamma \cdot D^2 \cdot n^3 \quad (19a)$$

The disc-friction loss as a percentage of available energy is determined for the two-stage turbine by the relation

$$L_d = 2.12 \cdot \sqrt{2} \left(\frac{D^2}{A_{N_I}} \right) \frac{\delta_{t2}^{\frac{1}{k}}}{\left(\frac{1 + \delta_{t2}^{\frac{k-1}{k}}}{2} \right)^{\frac{1}{k-1}}} \cdot \left(\frac{u}{c_0} \right)^3 \quad (19b)$$

1.4 Scavenging Loss

The scavenging loss of a single stage, partial-admission turbine is derived in Reference (7) and amounts to

$$\Delta H_{sc} = f \cdot g \cdot u \cdot c \cdot h \cdot \frac{u^2}{2g} \quad (20a)$$

The scavenging loss as a percentage of the available power of a two-stage re-entry turbine of equal head in both stages can be expressed by the following equation:

$$L_{sc} = 1.4 \sqrt{2} \chi \left(\frac{c}{a_1} \right) \frac{(u/c_0)^3}{\sin \alpha_1 \psi_{u_1}} \left[\frac{1}{z_1 - 1} + \frac{\frac{1}{\sin \alpha_1}}{\left(\frac{1 + \frac{1}{\sin \alpha_1}}{2} \right)^{\frac{1}{k-1}}} \right] \quad (20b)$$

Where χ represents the blade density factor. This factor was not included in the preliminary analysis. For typical impulse blades it was found that χ amounts to about $\chi \approx 0.60$. z_1 denotes the number of nozzles of the second stage. Evaluation of equation (20b) for $u/c_0 = 0.20 - 0.30$ and over-all pressure ratio $P_r = 300:1$ indicates that the scavenging loss is nearly negligible in this region. This may be explained by the fact that the stagnant fluid left in the buckets from the second stage is of lower density than the fluid of the first-stage nozzle jet. Furthermore, it appears that only one or two nozzles of the second stage are blowing out the stagnant fluid left over from the first stage.

1.5 Preliminary N_s - D_s Diagram for Equal Heads

A preliminary N_s - D_s diagram for two-stage re-entry turbines having equal heads in both stages and a total pressure ratio 300:1 is shown in Figure 2.

The efficiency equation, derived in the foregoing section, is related to the basic design parameters specific speed, N_s , and specific diameter, D_s , by employing a method similar to that demonstrated in Reference (1) for the case of the single stage, partial admission turbine.

The specific speed is defined as

$$N_s = \frac{N \cdot \sqrt{Q}}{H_{ad}^{3/4}} \quad (21)$$

and specific diameter by

$$D_s = \frac{D \cdot H_{ad}^{1/4}}{\sqrt{Q}} \quad (22)$$

when Q denotes the amount of flow passing through the rotor discharge area, N the rotation speed (rpm) and H_{ad} , the adiabatic head of the passing gas (feet).

The specific diameter can also be expressed as a function of the over-all pressure ratio, P_{tot} and the dimensionless parameter (A_1^*/D^2) as demonstrated in Reference (1) according to the equation:

$$D_s = \frac{\sqrt{\frac{\kappa}{\kappa-1}} \cdot \sqrt{1 - \epsilon_{tot}^{\kappa-1/\kappa}}}{\sqrt{\left(\frac{A_1^*}{D^2}\right)} \cdot \sqrt{\psi} \cdot \sqrt{P_{tot}} \cdot \sqrt{1 - \gamma_T (1 - \epsilon_{tot}^{\kappa-1/\kappa})}} \quad (23)$$

the reciprocal of the total pressure ratio. In the case of a two-stage turbine it is necessary to define the specific diameter of each stage. This can be done with an expression analogous to equation (23), yielding the following relations for D_{sI} and D_{sII} . The equations are written in squared form for convenience of the later calculations. The specific diameter of the first stage is

$$D_{sI}^2 = \frac{\sqrt{\frac{k}{k-1}} \sqrt{1 - \delta_I^{\frac{k-1}{k}}} \cdot \delta_I}{\left(\frac{A_I^*}{D^2}\right) \psi [1 - \psi_N^2 (1 - \delta_I^{\frac{k-1}{k}})]} \quad (24)$$

and the specific diameter of the second stage is

$$D_{sII}^2 = \frac{\sqrt{\frac{k}{k-1}} \sqrt{1 - \delta_{II}^{\frac{k-1}{k}}} \cdot \delta_{II}}{\left(\frac{A_{II}^*}{D^2}\right) \psi \sqrt{1 - \eta_I (1 - \delta_I^{\frac{k-1}{k}})} [1 - \psi_N^2 (1 - \delta_{II}^{\frac{k-1}{k}})]} \quad (25)$$

δ_I denotes the reciprocal of the pressure ratio of the first stage and δ_{II} is the reciprocal of the pressure ratio of the second stage. It is to be noted, that Equations (24) and (25) present only approximate relations, which neglect leakage and assume the flow conditions at the exhaust of each stage are similar to the flow at each nozzle exit. For further calculations it is convenient to define the ratios of the stage specific diameters to the over-all specific

diameter, which can easily be derived from combination of Equation (23) and (24) or (25). The ratio of the first stage specific diameter to the over-all specific diameter (squared) is defined by

$$K_1 = \left(\frac{D_{sI}}{D_{s+II}} \right)^2 = \sqrt{\frac{1 - \delta_I^{\frac{K-1}{K}}}{1 - \delta_{+II}^{\frac{K-1}{K}}}} \frac{[1 - \eta_{+II}(1 - \delta_{+II}^{\frac{K-1}{K}})]}{[1 - \psi_N^2(1 - \delta_I^{\frac{K-1}{K}})]} \left(\frac{P_{r+II}}{P_{rI}} \right) \quad (26)$$

and the ratio of the second stage specific diameter to the over-all specific diameter is given by

$$K_2 = \left(\frac{D_{sII}}{D_{s+II}} \right)^2 = \sqrt{\frac{[1 - \eta_I(1 - \delta_I^{\frac{K-1}{K}})][1 - \delta_I^{\frac{K-1}{K}}]}{[1 - \delta_{+II}^{\frac{K-1}{K}}]}} \quad (27)$$

In addition a function K_3 is used according to the relation:

$$K_3 = \frac{P_{r+II} \cdot \psi [1 - \eta_I(1 - \delta_{+II}^{\frac{K-1}{K}})]}{\sqrt{\frac{K}{K-1}} \sqrt{1 - \delta_{+II}^{\frac{K-1}{K}}}} \quad (28)$$

K_3 is the reciprocal of the dimensionless parameter $\left(\frac{A_I^*}{D^2} \right)$, as can be seen from Equation (23). The geometric parameters $\left(\frac{t}{a_I} \right)$, $\left(\frac{h}{D} \right)$, $\left(\frac{a_I}{D} \right)$ and $\left(\frac{A_I^*}{D^2} \right)$ are now expressed in terms of N_s - D_s functions by considering the definite interrelation of these parameters with the similarity parameters as already derived in Reference (1). There it is shown that the

parameter $\left(\frac{t}{a_I}\right)$ is related to D_{sI} by

$$\left(\frac{t}{a_I}\right) = \sin \alpha_I \psi_N \sqrt{2g} \cdot \left(\frac{h}{D}\right) \cdot \left(\frac{\pi}{2}\right) \cdot D_{sI}^2 \quad (29)$$

and that the ratio $\left(\frac{a_I}{D}\right)$ is determined by the equation:

$$\left(\frac{a_I}{D}\right) = \frac{1}{\left(\frac{h}{D}\right) D_{sI}^2 \psi_N \sin \alpha_I \sqrt{2g}} \quad (30)$$

These expressions can be presented as a function of the over-all specific diameter by replacing D_{sI}^2 with $K_I D_{sH}^2$, as shown by equation (26).

For the final equation it is necessary to find a relation between $\left(\frac{h}{D}\right)$ and D_{sH} or D_{sI} and D_{sH} . This can be done immediately by observing the definition of the total admission ratio

$$\varepsilon = \left(\frac{a_I + a_H}{\pi \cdot D} \right) \quad (31)$$

which relates $\left(\frac{h}{D}\right)$ and D_{sI}^2, D_{sH}^2 when considering equation (30) and (31), and yields the expression

$$\varepsilon = \frac{1}{\left(\frac{h}{D}\right) \psi_N \sin \alpha_I \sqrt{2g} \cdot D_{sI}^2} \left[1 + \frac{\sin \alpha_I}{\sin \alpha_H} \frac{D_{sH}^2}{D_{sI}^2} \right] \quad (32)$$

Inspection of the previous derived efficiency relations, in particular the blade coefficient ψ_R and the pumping loss, shows that it is desirable to use an ϵ value as high as possible. However, to assure a large enough exhaust port for the first stage, and to avoid interference effects from second-stage nozzles, that are too closely spaced, as well as to decrease leakage, it is found desirable to limit ϵ to values of $0.70 < \epsilon < 0.90$. Using a mean value of $\epsilon = 0.80$, equation (32) immediately determines (h/D) as a function of D_{SI}^2 , D_{SII}^2 and D_{Stot}^2 .

Considering now Equations (24) to (32) together with the efficiency relations presented by Equations (1), (10), (16), (17), (19) and (20), results in the final efficiency expression as a function of specific speed, specific diameter and total pressure ratio, Pr_{tot} :

In the case of a two-stage re-entry turbine with equal heads in both stages the functions K_1 , K_2 and K_3 can be approximated by the following relations,

$$K_1 = \frac{Pr_{tot}}{\sqrt{2}} \left[\frac{1 + \delta_{tot}^{\frac{K-1}{K}}}{2} \right]^{\frac{K}{K-1}} \quad (33)$$

$$K_2 = \frac{1}{r_2} \quad (34)$$

$$K_3 = \frac{P_{r+H} \cdot \psi}{\sqrt{\frac{K}{K-1}} \cdot \sqrt{2}} \quad (35)$$

Inserting these relations in Equation (32) results in the following blade to diameter ratio (h/D) :

$$h/D = \frac{1}{\varepsilon \cdot \pi \cdot \psi_N \cdot \sin \alpha_I \sqrt{2q_c \cdot K_1 \cdot D_{s+q}^2}} [1 + \sqrt{2} \cdot K_1] \quad (36)$$

The parameter $\left(\frac{t}{4a_I}\right)$ is given by considering Equation (30) and (36), yielding the simple relation

$$\left(\frac{t}{4a_I}\right) = \left(\frac{1 + \sqrt{2} K_1}{4 \varepsilon Z}\right) \quad (37)$$

Where Z denotes the number of rotor blades. Considering Equations (33) to (37) together with the efficiency relations presented in Equation (1), (10), (16) and (19) results in the following equation of the turbine efficiency:

$$\eta_T = \left(\frac{4}{154}\right) N_s D_s \left\{ 1 + \bar{\psi}_R \left[1 - \frac{1 + \sqrt{2} K_1}{4 \varepsilon Z} - \frac{\frac{\delta + \alpha}{2} \frac{1}{K-1}}{\left(1 + \frac{\delta + \alpha}{2}\right)^{\frac{1}{K-1}}} \right] \right\} \cdot \left(\bar{\psi}_N \frac{\cos \alpha}{12} - \frac{N_s D_s}{154} \right) (1 - L_T) - L_T \quad (38)$$

The above equation neglects the scavenging loss and the pumping loss which become very small. The total leakage amounts to

$$L_d = C_F \left(\frac{C^*}{D} \right) \left[\frac{2\psi (1 + \sqrt{2} K_1)}{\sqrt{\frac{K}{K-1}} \left(\frac{1 + \sqrt{\frac{K}{K-1}}}{2} \right)^{\frac{K}{K-1}} \varepsilon \cdot \pi \cdot \sin \alpha_I \cdot \sqrt{2g}} + \frac{\varepsilon \cdot \pi \cdot K_2 D_{s17}^2}{(1 + \sqrt{2} K_1)} \right] \left(\frac{1 + \sqrt{\frac{K}{K-1}}}{2} \right)^{\frac{K+1}{2(K-1)}} \quad (39)$$

Inspection of Equation (39) demonstrates that the leakage is mainly a function of the specific diameter D_{s17} for a given over-all pressure ratio and selected pressure split between both stages. Finally, it can be shown that the disc friction follows the simple relation

$$L_d = \frac{\sqrt{2g} K_d}{154^3} \cdot N_s^3 \cdot D_{s17}^5 \quad (40)$$

where K_d amounts about to $K_d = 0.00212$ assuming the Reynolds Number for the disc, $Re = \frac{u \cdot D}{\gamma}$ is about 10^6 .

Using Equations (38) to (40), an approximate N_s - D_s diagram is calculated for a two-stage re-entry turbine of equal head in both stages and 300:1 over-all pressure ratio. The resulting N_s - D_s diagram is presented in Figure 2. It is valid for the following design range:

Stator angle	$\alpha = 21^\circ$
Number of blades	$z = 120$
Aspect ratio	$c/h = 0.855$

Axial clearance ratio $C^*/D = 0.0008$ Over-all pressure ratio $Pr_{tot} = 300:1$

Selecting a typical design point for an APU-turbine suitable for space and missile applications, for example, $N_s=12$ and $D_s=2.6$, it can be seen from Figure 2 that an efficiency of about $\eta_T = .58-.59$ is predicted. Comparing Figure 2 with Figure 3, which represents the $N_s D_s$ diagram from Reference (1) for a 17:1 over-all pressure ratio, shows that an efficiency of about $\eta_T = .64$ will be achieved for the moderate pressure ratios of 17:1. The difference is mainly due to increased leakage (Equation (39)) and reduced blade coefficients, according to Equation (9) and (38). In the next section the case of equal pressure ratios in both stages is investigated. It will be compared later with the present case, to determine approximately the optimum pressure split for the test turbine under consideration.

2. Special Case of Equal Pressure Ratios in Both Stages

2.1 Efficiency relation

The special case of equal pressure ratios in both stages can be derived easily by considering first the general case of unequal spouting velocities in both stages. For this application the hydraulic efficiency has to be modified according to the spouting velocity split $\left(\frac{C_{sI}}{C_{sII}}\right)$.

$$\bar{\eta}_h = \left(\frac{C_{0I}}{C_0} \right)^2 \eta_{hI} + \left(\frac{C_{0II}}{C_0} \right)^2 \eta_{hII} \quad (41)$$

Combining Equation (2) and Equation (41) the average hydraulic efficiency is determined by the following relation, which is derived in Appendix C, Equations (C1) to (C8):

$$\bar{\eta}_h = 4 \cdot \left(\frac{u}{C_0} \right) (1 + \bar{\psi}_R) \left(\bar{\psi}_N \cos \alpha - \frac{u}{C_0} \right) \quad (42a)$$

The average blade coefficient $\bar{\psi}_R$ of both stages is the same as for the previous case, and determined by Equations (5) and (9). However, the average nozzle coefficient $\bar{\psi}_N$ has to be replaced by the nozzle-coefficient parameter

$$\bar{\psi}_N = \frac{1}{2} \left[\left(\frac{C_{0I}}{C_0} \right) \psi_{NI} + \left(\frac{C_{0II}}{C_0} \right) \psi_{NII} \right] \quad (42b)$$

The spouting velocity ratio $\left(\frac{C_{0I}}{C_0} \right)$ is

$$\left(\frac{C_{0I}}{C_0} \right) = \sqrt{\frac{1 - \frac{\delta_I^{\frac{K-1}{K}}}{\delta + \eta}}{1 - \frac{\delta_{II}^{\frac{K-1}{K}}}{\delta + \eta}}} \quad (43)$$

and the ratio $\left(\frac{C_{0II}}{C_0} \right)$ can be approximated by a simple relation which neglects interstage leakage:

$$\left(\frac{C_{1h}}{C_0}\right) = \sqrt{\mu^2 - \left(\frac{C_T}{C_0}\right)^2} = K_2 \quad (44)$$

μ denotes a factor in the range of $1.1 < \mu < 1.2$, which accounts for the inefficiency of the first stage. The over-all turbine efficiency is then defined by Equation (1) in connection with Equation (42).

In the case of equal pressure ratios for both stages, the above derived relations are still valid, when the relation

$$\delta_I = \delta_{II} = \delta_{+n}^{\frac{1}{2}}$$

is observed. The leakage is determined by modifying Equation (16), according to the similar expression:

$$L_t = C_F \cdot \left(\frac{D^2}{A^*}\right) \left[2 \left(\frac{h}{D}\right) + \frac{a_I}{D} \right] \cdot \delta_{+n}^{\frac{\kappa+1}{4\kappa}}$$

The disc friction is determined by Equation (40). Scavenging losses and pumping losses are neglected over the considered design range, as discussed in Section 1.

2.2 N_s - D_s diagram for equal pressure ratios in both stages.

In the case of equal pressure ratios for both stages, the functions K_1 , K_2 and K_3 are given by the following relations, derived from combining Equations (26), (27) and (28) with Equation (45):

$$K_1 = \sqrt{\frac{1 - \delta_{tot}^{\frac{K-1}{2K}}}{1 - \delta_{tot}^{\frac{K-1}{K}}} \cdot \frac{[1 - \eta_T (1 - \delta_{tot}^{\frac{K-1}{K}})]}{[1 - \psi_N^2 (1 - \delta_{tot}^{\frac{K-1}{2K}})]}} \sqrt{P_{r_{tot}}} \quad (47)$$

$$K_2 = \sqrt{\frac{[1 - \eta_T (1 - \delta_{tot}^{\frac{K-1}{2K}})] [1 - \delta_{tot}^{\frac{K-1}{2K}}]}{(1 - \delta_{tot}^{\frac{K-1}{K}})}} \quad (48)$$

$$K_3 = \frac{P_{r_{tot}} \psi [1 - \eta_T (1 - \delta_{tot}^{\frac{K-1}{K}})]}{\sqrt{\frac{K}{K-1}} \cdot \sqrt{1 - \delta_{tot}^{\frac{K-1}{K}}}} \quad (49)$$

Following the same method of analysis as outlined in Section 1.5, the blade-to-diameter ratio is still determined by Equation (32), when Equations (47) to (49) are used for K_1 , K_2 and K_3 .

$$\left(\frac{h}{D}\right) = \frac{1}{\epsilon \cdot \pi \cdot \psi_N \cdot \sin \phi \cdot I \sqrt{2g} \cdot K_1 \cdot D_{s_{tot}}^2} \left[1 + \frac{\sin \phi \cdot I}{\sin \phi \cdot II} \left(\frac{K_1}{K_2} \right) \right] \quad (50)$$

The parameter $\left(\frac{t}{4a_I}\right)$ is found by modifying Equation (37),

$$\left(\frac{t}{4a_I}\right) = \left(\frac{1 + \frac{K_1}{K_2}}{4\epsilon z}\right) \quad (51)$$

The ratio of the arcs of admission $\frac{a_I}{a_{II}}$, defined by

$$\frac{a_I}{a_{II}} = \frac{1}{\epsilon \pi \left(\frac{D}{a_{II}}\right) - 1} \quad (52)$$

is found by inserting Equation (50) in Equation (30), yielding the relation

$$\left(\frac{a_I}{D}\right) = \frac{\epsilon \cdot \pi}{\left[1 + \frac{\sin \phi_I}{\sin \phi_{II}} \cdot \left(\frac{K_1}{K_2}\right)\right]} \quad (53)$$

which, combined with Equation (52), results in the final expression:

$$\left(\frac{a_I}{a_{II}}\right) = \frac{K_2}{K_1} \quad (54)$$

Equation (54) assumes equal stator angles as a first approximation.

Combination of Equations (46), (49), (50) and (53) determines the total leakage for the case of equal pressure ratios:

$$L_t = L_s \left(\frac{C^*}{D} \right) \left[2 \cdot \left(\frac{K_3}{K_1} \right) \cdot \frac{1 + K_1/K_2}{\pi \cdot \bar{\psi}_N \cdot E \cdot \sin \alpha \cdot \sqrt{2g}} + \right. \\ \left. + \frac{E \pi \cdot K_3 \cdot D_{tot}^2}{[1 + K_1/K_2]} \right] \int_{tot} \frac{K+1}{4K} \quad (55)$$

Finally the turbine efficiency is obtained by combining Equations (42), (51), (52) and (55);

$$\eta_T = \left(\frac{4}{154} \right) \bar{\psi}_N \cdot D_s \left\{ 1 + \bar{\psi}_{Rc} \left[1 - \frac{1 + K_1/K_2}{4E} \left(1 + \frac{K_1}{K_2} \right) \right] \right\} \cdot \\ \left(\bar{\psi}_N \cos \alpha - \frac{N_s D_s}{154} \right) (1 - L_t) - L_d \quad (56)$$

where $\bar{\psi}_N$ is determined by Equation (42b), (43) and (44). $\bar{\psi}_{Rc}$ is given by Equation (9) for the case of "subsonic" blade design. The total leakage is found from Equation (55) and the disc-friction loss is still determined by Equation (40).

By application of Equation (56), an approximate N_s - D_s diagram is calculated for a two-stage re-entry turbine of equal pressure ratios in both stages and 300:1 over-all pressure ratio. The resulting N_s - D_s diagram presented in Figure 4, is valid for the same values of stator angle α , number of blades Z , aspect ratio $\left(\frac{C}{h} \right)$, and axial clearance ratio $\left(\frac{C^*}{D} \right)$ as the N_s - D_s diagram for equal heads in both stages.

3. Comparison of Design-Point Performance for Two Stage-Re-entry Turbines Having Equal Head or Equal Pressure Ratios in Both Stages.

3.1 Optimum performance

The optimum performance of a two-stage re-entry turbine is presented in Figure 5, where the cases of equal head and equal pressure ratios are compared. Figure 5 illustrates that the turbine efficiency is nearly the same for both cases for the low N_s range $1.5 < N_s < 3$. However, for the range of $N_s = 3$ to 100 it can be seen that equal pressure ratios in both stages result in higher efficiencies. This is because there is less leakage and higher percentages of admission in the first stage, as can be seen from inspection of Equations (39) and (55), and (37) and (51). The leakage of both cases is compared in Figure 6, where the leakage is plotted as a function of the axial clearances 0.005" to 0.030" for a turbine with $D = 6.3$ inches diameter. Finally it should be mentioned, that the above result is only valid for second-stage Reynolds numbers that do not affect the performance. In the case of low second-stage Reynolds number it seems desirable to perform more work in the first stage, where Reynolds number effects are not anticipated. However, because it is not known how low Reynolds number affects the performance of partial admission turbines with high pressure ratios, a final answer cannot be given at the present time for the optimum pressure split applicable for low Reynolds number operations.

3.2 Design performance for $D_{s+1} = 2.58$

Selecting a typical APU specific diameter of $D_s = 2.58$, the design performance is compared in Figure 7 for both cases, equal pressure ratio and equal head in both stages. Nearly the same trend is demonstrated as found in Figure 5, for the optimum performance. Therefore it seems to be advisable to design two-stage re-entry turbines with equal pressure ratios in both stages, when the turbine is operating in the specific speed range $3 < N_s < 50$.

B. DESIGN OF TEST TURBINE

For verification of the design-point analysis presented in Reference (1) and Chapter A of this report, a two-stage re-entry type turbine is now designed for the over-all pressure ratio of 300:1. The design point is selected at a tip speed to total spouting velocity ratio, $u/c_o = 0.20$. Specifying a total specific diameter of $D_s = 2.58$ determines the specific speed of the design point to be $N_s = 11.9$. For obtaining a highly efficient turbine it was decided to use equal pressure ratios in both stages, as indicated by Figure 7. This also seems to be desirable in view of anticipated Reynolds number effects in the second stage when tested with low back pressure in the high altitude facility of Sundstrand Turbo. The high altitude facility is used to achieve an over-all pressure ratio of 300:1 when testing the turbine with nitrogen at $T_o = 760^\circ R$ inlet temperature and $P_o = 90$ PSIA inlet pressure. The specific heat ratio for nitrogen is assumed to be constant, $K = 1.4$, for all calculations.

The geometric parameters are obtained by application of the method outlined in Chapter A, section 2. All other design parameters are selected in the range described by the N_s - D_s diagram for two-stage re-entry turbines with equal pressure ratios in both stages (see page 28). This results in the following design parameters:

Blade angle	$\beta = 30^\circ$
Stator angle	$\alpha_I = \alpha_{II} = 21^\circ$
Number of blades	$z = 120$
Aspect ratio	$c/h = .855$
Axial clearance ratio	$c^*/D = .0008$
Blade height-diameter ratio	$h/D = .055$
Ratio of arcs of admission	$c_{II}/c_I = 16$
Spacing to arc of admission ratio of first stage	$(t/c_I) = .180$
Stage pressure ratio	$P_{r_I} = P_{r_{II}} = 17.3:1$
Ratio of nozzle throats	$A_{II}^*/A_I^* = 16$

The ratio of nozzle throats is obtained from the approximate equation

$$\left(\frac{A_{II}^*}{A_I^*} \right) = \left(\frac{K_1}{K_2} \right) \frac{[1 - \psi_N^2 (1 - \delta_{tot}^{\frac{K-1}{2K}})]}{[1 - \eta_T (1 - \delta_{tot}^{\frac{K-1}{2K}})]} \quad (57)$$

which is derived in Appendix C, Equation (C9) to (14) by combination of the continuity equation with the specific diameter relations K_1 and K_2 , defined by Equations (47) and (48). Equation (57) neglects interstage leakage.

Using a design mass flow $W = 0.0368$ lb/s of nitrogen with $T_0 = 760^\circ R$

and $P_{01} = 90$ psia inlet-conditions, determines the turbine speed, N , and the turbine diameter according to the selected values of N_s and D_s . The design speed is $N = 20,000$ rpm and the turbine diameter is $D = 6.3$ inches. The final turbine configuration is shown in Figure (8). It can be seen that the first stage inlet and the second stage exhaust ports are located on the same side, as mentioned before when analyzing the leakage paths. This eliminates a so-called cross-over duct, which would provide parallel flow in both stages. However, the arrangement of opposed flows in both stages is somewhat simpler from the mechanical point of view, and is incorporated in the present design.

C. OBJECTIVE OF EXPERIMENTAL PROGRAM

The objective of the experimental program is to investigate the performance of the above described two-stage re-entry turbine in order to determine as accurately as possible:

1. Over-all performance
2. Nozzle and rotor performance of each stage
3. Losses in the re-entry duct
4. Effect of axial clearance on performance
5. Validity and range of application of theoretical performance predictions outlined in Chapter A.

D. APPARATUS AND INSTRUMENTATION

1. Apparatus

1.1 The two-stage test turbine is composed of a single, axial flow type wheel rotating in a housing with integrally machined nozzles and flow passages which provide two passes for the gases through the single wheel. Figure 8 shows an exploded view of the turbine with all of the components identified. The first stage collector ring contains a constant-area plenum chamber of a rectangular cross-section.

1.2 Figure 9 shows the complete turbine test setup installed within the altitude chamber to provide constant ambient conditions around the test apparatus. Figures (10), (11) and (12) show the altitude chamber facility, the test chamber, and recording instruments, respectively. Figure 9 also shows the flywheel loading device which was later replaced by the electrical dynamometer, shown in Figure 13.

1.3 Reference to Figure 14 indicates schematically the test setup with its controls clearly identified. The throttle valve for controlling the nitrogen mass flow rate is located upstream of a heat exchanger which increases the temperature of the cold nitrogen to approximately 760°R. Loss of heat

from the turbine is controlled by external insulation. Back pressure is controlled by the butterfly valve shown in Figure 15.

2. Instrumentation

2.1 General

Initial instrumentation during preliminary test runs employed a calibrated flywheel loading device for torque evaluation. The results of these tests demonstrated that thermodynamic and blade element performance can only be obtained under steady state conditions and not under dynamic conditions necessarily imposed by the flywheel acceleration technique. Furthermore, it was learned that the thermocouples located near the second stage exhaust were heated under the influence of first stage leakage flow and internal heat transfer, and therefore could not indicate the mean turbine exhaust temperature. Hence, these thermocouples were moved downstream to the location shown in Figure 15 where uniform flow conditions are expected.

2.2 Temperature and pressure measurement

For determining the thermodynamic performance of the test turbine, calibrated thermocouples and static pressure taps were installed at stations shown schematically in Figure 14. These instruments were located so as to evaluate the state point conditions at

- (1) turbine inlet
- (2) first stage nozzle exhaust
- (3) first stage exhaust port
- (4) re-entry duct
- (5) second stage nozzle inlet
- (6) second stage nozzle exhaust, and
- (7) turbine exhaust duct.

All instruments were calibrated several times to insure accurate measurement of the mass flow rate entering both stages. Figure 16 shows the re-entry duct being calibrated in the high-altitude chamber.

Shielded thermocouples were used at all positions where the flow direction was evident, while unshielded probes were employed at all other locations. Pictures of these thermocouples are presented in Figure 17 and their description in Figure 18.

The static pressure was measured by using static pressure taps connected to pressure transducers. The signals received from all twenty measuring points were relayed simultaneously to a calibrated Sanborn recorder. The instruments used and their accuracy is tabulated in Figure 18.

2.3 Torque Measurement

Torque measurements were made using a Wiancko Engineering Company force ring shown in Figure 17, in conjunction with an electric generator dynamometer and carrier oscillator. The oscillator serves as a power source to the deflection-measuring force ring. The deflection is translated into millimeter deflection readings on a Sanborn Recorder by a demodulation unit. The force ring has a range of ± 20 lbs with an accuracy of 0.5%, and is placed at a radius of 10 inches giving a range up to ± 200 in-lbs. The Sanborn recorder has an accuracy of 2% full scale.

2.4 Wheel Speed

The wheel speed was measured by a magnetic pickup using two lobes on a coupling. A Hewlett Packard Counter with a range of 0-99,999 cps was used. Its accuracy is 1.0%.

2.5 Mass-flow

The mass-flow rate is measured upstream of the heat exchanger using an orifice meter as shown in Figure 18. The orifice meter is built by the Barton Instrument Corporation and performs according to the ASME Power Code as determined by several calibration runs.

E. ANALYSIS AND DISCUSSION OF EXPERIMENTAL RESULTS

1. Over-all Performance

The over-all performance of the two stage re-entry turbine is obtained by measuring torque, speed, static pressure and total temperature at turbine inlet and exhaust. The performance evaluated by torque measurements is described by the dimensionless torque coefficient

$$\tau = \frac{T}{\left(\frac{W}{g}\right) \cdot D \cdot C_o} \quad (58)$$

which determines the over-all turbine efficiency according to the relation

$$\eta_T = 4 \cdot \tau \cdot u/C_o \quad (59)$$

The measured torque coefficients are presented in Figure 19 as a function of u/C_o . Two test curves are shown, one obtained for the axial clearance $C^*=0.005"$ and one for the axial clearance $C^*=0.017"$. Both curves are straight lines. The curve for the axial clearance $C^*=0.005"$ shows torque coefficients about six percent higher near the design point $u/C_o = .20$.

The respective turbine efficiencies are calculated for both clearances according to Equation (59) and are plotted as a function of (u/C_o) in Figure 20. For clearance $C^*=0.005"$ it can be seen that the efficiency of the design point

$u/c_o = 0.20$ amounts to about $\eta_T = 0.55$, while the peak efficiency occurs at $u/c_o = 0.30$ with an efficiency of $\eta_T = 0.63$. For $C^* = 0.017$ the design point efficiency is about $\eta = 0.505$ while the peak efficiency is shown to be about $\eta = 0.59$ at $u/c_o = 0.30$. The measured turbine performance for $C^* = 0.005$ is finally compared with the preliminary performance prediction of the $N_s - D_s$ diagram presented in Figure 4. The predicted performance curve is obtained for $D_s = 2.58$ and is plotted versus u/c_o in Figure 20. Comparison of this curve with the test performance reveals that the design point efficiency is about ten efficiency points lower than the predicted efficiency. Generally it can be seen that the actual performance is less than anticipated. This might be due to increased leakage, less efficient nozzle and blade performance, increased duct losses and some measuring errors. In order to determine the main sources of additional losses, not accounted for by the preliminary analysis presented in Chapter A, the turbine was instrumented in such a manner that the performance of all components could be determined. Their measurements and their evaluation are discussed in the following sections. Measuring errors may be estimated by comparison of the torque efficiency with the temperature or internal over-all efficiency η_i , which is defined as

$$\eta_i = \frac{1 - \frac{T_6}{T_{01}}}{1 - \left(\frac{P_6}{P_{01}}\right)^{\frac{K-1}{K}}} \quad (60)$$

The static temperature T_b is approximated by the total temperature T_{06} . This seems reasonable in view of the low velocity expected at the measuring station shown in Figure 15. Both efficiencies are compared in Figure 21. It can be seen that the temperature efficiency agrees nearly exactly with the torque efficiency for the design point $\eta/c_0 = 0.20$. However, for off design values it is indicated that the temperature efficiency is higher than the torque efficiency in the range $\eta/c_0 < 0.20$ and lower for the range $\eta/c_0 > 0.20$. This might be due to errors introduced by electronic measuring instruments or shifts of the calibration constants, non-uniform velocity distribution, heat-transfer effects, etc. However, it is demonstrated for the design point $\eta/c_0 = 0.20$, that both efficiencies agree well. Therefore, it can be concluded that quite accurate measurements are obtained for the range close to the design point. For all other performance points it is found that the temperature efficiency deviates up to 5% from the torque efficiency. The performance curve of the temperature efficiency also does not follow the trend of the torque efficiency which seems to follow a similar curve as presented by the theoretical performance curve. In view of this fact, it was decided to use only torque efficiencies for further analysis and discussion.

2. Leakage Measurements

The leakage is determined by measuring the difference in mass flow between the first and second stage nozzle inlets. For this purpose it was necessary to calibrate the first stage nozzle and the re-entry duct as accurately as possible. This was done using a calibrated orifice, which served as a reference instrument. The mass flow through each nozzle was then calculated by using the choked flow relation given by Equation (12) which has to be modified by the measured calibration constant, which amounts to about 0.96 to 0.98. The total leakage, occurring between both stages, is presented in Figure 22 as a function of the speed parameter u/c_0 . This curve is valid for the axial clearance $C^* = 0.005$ " and the over-all pressure ratio 300:1. Inspection of Figure 22 reveals that the total leakage apparently consists of two components, one dependent on the speed parameter u/c_0 and one independent of it. The speed dependent leakage is called "dynamic leakage" and the speed independent leakage value is described as "static leakage". Both components of the total leakage are investigated as indicated below.

2.1 Static leakage.

The static leakage was measured during stall conditions, in the high altitude chamber. This makes it possible to correlate the leakage measurements obtained during dynamic conditions. The measured amount of

"static leakage" is presented in Figure 23, where the leakage flow expressed as a ratio of the leakage to total inlet mass flow is plotted against the axial clearance, C^* . The leakage values were obtained by changing the clearance between rotor and first stage nozzle from $C^* = .001$ to $C^* = 0.017$ ". During all these tests the clearance remained unchanged on the other side of the rotor. That clearance amounted to $C^* = 0.005$ ". The tip clearance was kept constant during all test runs with $C_T^* = 0.006$ ". Figure 23 demonstrates that the leakage passes mainly through the clearance gap between rotor and first stage nozzle exhaust section, while leakage is found negligible on the other side of the rotor. The small amount of leakage shown for $C^* = 0$ in Figure 23 can be explained as tip leakage. The above finding indicates that the static leakage flow is lost entirely for turbine configurations with opposed flow conditions in both stages, as assumed by the preliminary leakage analysis of Reference (1) and of this report.

Inspection of Figure 23 also reveals that the static leakage varies linearly with changing axial clearance gap, C^* , as predicted by Equation (39) and (55), for constant over-all pressure ratio. However, it is noticed that the "static concept" underlying both Equations (39) and (55) does not explain satisfactorily the measured leakage values. For this purpose the leakage values indicated for equal head and equal pressure ratios are compared with the meas-

ured amount of leakage in Figure 24. It can be seen that the values obtained for the case of equal head are about 32 percent lower and those calculated for equal pressure in both stages are about 50 percent lower than the actual amount of leakage.

Because the predicted leakage for equal pressure ratio in both stages is far less than the actual measured amount of leakage, it is necessary to check the static pressure variation inside the turbine for the design point $u/c_o = 0.20$. This is done in Figure 25 where the actual static pressure variation inside the turbine is compared with the static pressure variation predicted by the design method. The dashed curve denotes the design values and the solid curve the actual test values which are obtained for the design point $u/c_o = 0.20$ and for one lower and one higher value. It can be seen that the static-to-inlet total pressure ratio is plotted at measuring stations (1) to (6). Measuring station (1) is at the nozzle inlet of the first stage, station (2) determines measurements at the nozzle exhaust or rotor inlet of the first stage, station (3) is the exhaust station of the first stage and the inlet to the re-entry duct, station (4) denotes the exhaust of the re-entry duct or the inlet to the second stage nozzle, station (5) is the nozzle exhaust station of the second stage and the rotor inlet of the second stage and station (6) represents the exhaust of the second stage.

Taking the design value $u/c_o = 0.20$ which is represented by circles, it can be seen that the static pressure variation of the design point is very close to the design static pressure variation. The same is true for the other values $u/c_o = 0.18$ and $u/c_o = 0.219$. The best correlation is found for the design point. The respective curve indicates a small amount of reaction in the first stage and nearly negligible reaction in the second stage. However, this might be due to leakage through the clearance gap which allows the jet to expand beyond the values measured at station (2). The duct losses appear to be small as do the losses occurring between nozzle and inlet to the second stage. A similar trend is found in Figure 26 for the off-design performance determined by the speed parameter values $u/c_o = 0.08$ and $u/c_o = 0.240$. However, deviations are apparently occurring in the first stage while the second stage is performing closer to the design values. At the lower value of u/c_o some shock losses apparently occur in the turbine rotor, while at $u/c_o = 0.24$ the same trend is indicated as for the design point shown in Figure 25. Altogether, it can be concluded that the test turbine is performing closely to the design values of static pressure variation inside the turbine. Therefore, equations based on equal pressure ratios in both states have to be used to calculate and analyze the measured amount of leakage. Looking at Figure 24 it can be seen that the leakage prediction, according to Equation (55) is about 50 percent less than the actual value. Equation (55) is derived for equal pressure ratios in

both stages. The difference between predicted and actual measured value of leakage can only be explained if supersonic velocities occur in front of the tangential leakage area in the direction of rotor rotation, because in this case, normal or oblique shocks can occur in front of the leakage area through which flow can only pass with sonic velocity. This leads to a higher pressure level and density level in front of the leakage areas than measured in the nozzle jet itself. Therefore, it seems logical that a larger amount of leakage passes through the leakage area in the tangential direction. To account approximately for this very complex effect, it is assumed that total conditions are predominant in the direction of the tangential jet component while static conditions are still used in the opposite direction. This concept leads to the following equation for predicting the actual measured leakage value. It also includes the tip leakage.

$$L_+ = C_F \cdot \left(\frac{C^*}{D}\right) \cdot \left(\frac{D^2}{A_I^*}\right) \left[\left(\frac{h}{D} + \frac{a_r}{D}\right) F_1(M_{i2}) + \left(\frac{h}{D}\right) F_2(M_{i2}) \right] \quad (61)$$

$$+ 2 C_{F_T} \left(\frac{C_T^*}{D}\right) \left(\frac{D^2}{A_T^*}\right) \left(\frac{C}{D}\right) F_1(M_2)$$

Equation (61) is of similar structure as the leakage Equations (39) and (55).

The only difference is that two functions are introduced F_1 and F_2 which describe static or total flow conditions in front of the respective leakage areas. Furthermore, the tip leakage is added to Equation (61). The function

F_1 denotes static conditions and the function F_2 determines the total conditions in the tangential direction. The leakage function F_1 is determined by the following equation:

$$F_1(M_{2i}) = \frac{\sqrt{1 + \frac{K-1}{2} \psi_{NI}^2 \cdot M_{2i}^2}}{\left(1 + \frac{K-1}{2} \psi_{NI}^2 M_{2i}^2\right)^{\frac{K}{K-1}}} \quad (62)$$

M_{2i} is the design Mach number of the first stage nozzle and is calculated by the well known relation

$$M_{2i} = \sqrt{\frac{2}{K-1} \left[\left(\frac{P_{01}}{P_{2i}} \right)^{\frac{K-1}{K}} - 1 \right]} \quad (63)$$

The leakage function F_2 includes the nozzle coefficient ψ_N and the nozzle angle δ_T as can be seen from the following expression which is derived in Appendix D, equation (E12) to (E14) (see page 47a)

The leakage function F_1 is plotted versus the nozzle design pressure ratio $\left(\frac{P_{01}}{P_{2i}}\right)$ in Figure 27. Two curves are presented, one for the ratio of the specific heat equal to $K = 1.4$ and the other, $K = 1.28$. Both curves nearly coincide for the higher pressure ratios. Figure 27 illustrates quite impressively that the static leakage decreases with increasing pressure ratio of the first stage, a fact known from general turbine practice. Figure 27 illustrates the behavior of the leakage function F_2 , which describes the total

S/TD No. 1735

30 January 1960
Page 47a

$$F_2 = \left[\frac{1 + \frac{K-1}{2} \psi_N^2 M_{i2}^2 \left\{ (\cos^2 \alpha + 1) + \frac{K-1}{2} \cos^2 \alpha \psi_N^2 M_{i2}^2 \right\}}{1 + \frac{K-1}{2} M_{i2}^2 \left\{ (\psi_N^2 + 1) + \frac{K-1}{2} \psi_N^2 M_{i2}^2 \right\}} \right] \quad (62b)$$

condition in front of the leakage area normal to the tangential jet velocity component of the first stage. Again, two curves are calculated for the different specific heat ratios in the range of $K = 1.28$ to 1.4 . The nozzle coefficient is assumed to be $\psi_N = 0.96$. Furthermore, a constant nozzle angle of $\alpha_I = 20.5$ degree was used for evaluating the function F_2 . Comparison of Figure 28 and 27 demonstrate that "total conditions" will increase the leakage to nearly the amount indicated in Figure 24. Finally, Equation (61) is combined with Equation (50), (53) and Equations (47) to (49), this results in a general $N_s D_s$ relation for predicting leakage in high pressure ratio turbines, as can be seen from the following equation.

$$L_{st} = C_F \cdot \left(\frac{C^*}{D}\right) \left[\left(\frac{K_3}{K_1}\right) \frac{[1 + K_1/K_2]}{\pi \cdot \psi_N \cdot E \cdot \sin \alpha_I \sqrt{2g}} (F_1 + F_2) + \right. \\ \left. + \frac{E \cdot \pi \cdot K_3}{[1 + K_1/K_2]} D_{st,t}^2 \cdot F_1 \right] + 2C_{F_T} \cdot \left(\frac{C_T^*}{D}\right) \cdot K_3 \cdot D_{st,t}^2 \cdot \left(\frac{E}{D}\right) \cdot F_1 \quad (65)$$

Since supersonic velocities are occurring at the exhaust of the first stage nozzle in a tangential direction, the above outlined concept is applied to the test turbine with equal pressure ratios in both stages. Evaluation of Equation (65) results in an excellent correlation of theoretical predictions and actual test values. It is found that the test points can be matched with the theory when the restriction factor is adjusted to $C_f = 2/3$ to account

for leakage in the radial and tangential directions. This restriction factor is predicted in Reference (1) and is a common factor employed in leakage calculations. The restriction factor C_{FT} attributed to the tip leakage amounts to $C_{FT} = 1/3$. This might be due to the fact that the circulation distribution in the cascade somehow restricts the leakage across the top of the blade. Also, boundary layer effects as well as separation phenomena may cause a restriction of the tip leakage flow. In the case of high turning impulse blades, it is noted that the radial pressure gradient is quite large and three-dimensional radial flows will occur, which might result in lower leakage values. However, all these very complex phenomena are not investigated in this report, as mentioned before. Such phenomena have to be studied in cascade tunnels and other arrangements where the flow can be made visible and where the pressure gradient can be studied as, for example in the work presented in Reference 8. Finally, it should be mentioned that Equation (65) neglects leakage on the other side of the rotor. This is the radial and tangential leakage through the clearance gap between re-entry duct and rotor. The reason for this was outlined before and can be seen from Figure 23. It was found during stall tests that the leakage can be explained by tangential and radial leakage between first stage nozzle and rotor as well as tip clearance. The small amount of leakage for zero axial clearance between first stage and rotor is found to be the amount predicted by the tip leakage equation.

Therefore, it is indicated that no leakage occurs on the other side of the wheel during static tests. An explanation for this finding may be stipulated by considering the case where supersonic velocities are involved at the exhaust of the first stage rotor. In this case leakage seems not to occur because total conditions in the tangential direction are existing simultaneously at the exhaust of the first stage and in the opposite direction at the exhaust of the second stage nozzles. When we assume that duct losses and nozzle losses are comparatively small, it seems to be logical that leakage may not occur. The next step is now to correlate the leakage measured under stall conditions with the total amount of leakage measured during turbine operation as shown on Figure 22. From Figure (22) it can be seen that the leakage increases above the static value shown for $u/c_0 = 0$ with increasing values of u/c_0 . This apparently is due to dynamic leakage. The dynamic leakage is discussed in the following section.

2.2 Dynamic Leakage

Dynamic leakage is apparently caused by an amount of fluid from the first stage

$$\Delta W_d = C_D \cdot X \cdot \rho \cdot h \cdot c \cdot u \quad (66)$$

which is trapped in the blade passage. Considering that vacuum cannot exist in a blade passage of a partial admission turbine, it seems obvious that dynamic leakage will always occur regardless how large the exhaust port is. The dynamic leakage expressed as a ratio of the total mass flow can be determined by the following relation;

$$L_d = C_D \cdot \chi \left(\frac{u}{c_0} \right) \cdot \left(\frac{c_0}{c_I} \right) \cdot \left(\frac{c_I}{c_{I2}} \right) \frac{1}{\psi_N \cdot \sin \alpha} \quad (67a)$$

which may be expressed in form of the basic design-parameters $N_s D_s$ and P_{tot} , resulting in the following equation,

$$L_d = C_D \cdot \chi \frac{N_s D_s}{154} \left[\left(\frac{c}{D} \right) \sqrt{\frac{1 - \delta_{tot}^{K-1/K}}{1 - \delta_{tot}^{K-1/K}}} \cdot \frac{[1 + K/2]}{\psi_N \sin \alpha I \cdot \pi} \right] \quad (67b)$$

χ denotes the blade density ratio and C_D is a restriction factor which might depend on exhaust geometry and second stage inlet pressure. The test result in Figure 22 agrees nearly with Equation (67) when using the measured blade density ratio of the rotor, $\chi = 0.60$. In this case it is found that the restriction factor C_D amounts to about $C_D = 0.35$. At this point it might be mentioned that a similar number for the restriction factor was found when evaluating the performance of a terry-drag turbine as shown in Reference (9). Therefore, it is indicated that the restriction factor

seems to be a constant. Inspection of Equation (67) reveals that the dynamic leakage will increase linearly with u/c_0 for a given pressure split between first and second stage. The pressure split is expressed in Equation (67) by the spouting velocity ratio c_0/c_{01} . It can be seen that dynamic leakage will decrease with an increasing spouting velocity of the first stage. Finally, it should be mentioned that the dynamic leakage for the design point u/c_0 is nearly the same amount as the static leakage. Inspection of Figure (22) indicates that about 10 percent leakage is occurring at the design point of $u/c_0 = 0.20$. This high amount of leakage was not included or predicted by the design and analysis method outlined in Reference (1), and in Chapter A of this report. In summary, it can be seen that the measured amount of leakage shown in Figure 22 is predictable by combining Equation (65) and (67). However, it has to be mentioned that the assumption of negligible leakage between first stage exhaust and re-entry duct is only valid for the case of small values of u/c_0 when the velocity vector of the leaving fluid is close to the direction of the relative velocity, because only in this case a cancellation might be assumed for the tangential components of the leaving velocity of the first stage and the tangential component of the nozzle jet of the second stage. In all other cases, some static

leakage might occur which could not be detected during static test or under running conditions. For this amount of leakage, which might occur between rotor and re-entry duct and which has done work in the first stage, it is assumed for simplification of later calculations, that the amount of work done in the first stage cancels losses caused by the leakage amount when passing through the clearance gap in tangential and radial directions as well when joining the nozzle jet of the second stage. Using this concept Equation (65) will be used for determining the static leakage, which occurs only between first stage nozzle and rotor. This amount of leakage is lost entirely for the turbine. The same is assumed in the case of the dynamic leakage. The last assumption was based on detailed calculations, investigating what amount of work could be done by the dynamic leakage involved. It is indicated very complex flow phenomena occur which cannot be accounted for by the simplified theories as presented herein. It is suggested that further analysis and tests are to be conducted in later tasks to evaluate secondary flow effects and phenomena similar to the "dynamic leakage" which effect the over-all turbine performance.

3. Duct Losses

Several static pressure and total temperature probes were located along the periphery of the re-entry duct for measuring the losses in total pressure. The total temperature was found to be constant throughout the

duct. This indicates negligible internal heat transfer. However, static pressure probes instead of total pressure probes could only be installed in the duct. Therefore, only an approximate method can be employed for evaluating the duct losses. Furthermore, it should be mentioned that the drop in static pressure through the duct is measured between station (3) and station (4). At station (3) a total pressure probe and a static pressure tap is located. Station (4), however, consists of several manifolded pressure taps located around the periphery of the duct together with total temperature probes also manifolded together. It was found that the correlation between the mass flow measured by the reference orifice meter and the several probes located around the periphery could only be obtained satisfactorily when manifolding these probes together. In view of this fact, it is nearly impossible to separate losses occurring during turning of the flow from the axial direction to the direction of the circumferential duct from the losses occurring due to friction along the walls. However, to estimate the losses, two methods are presented. The first one assumes that the turning loss might be neglected and friction losses are predictable by means of the laws of friction on rough walls. The second method assumes laminar flow in the re-entry duct and accounts later for the turning losses.

First, the case of negligible turning losses is presented. The assumption of negligible turning losses is based on the fact that the exhaust port of the first stage is about two times larger than the area necessary for the leaving amount of fluid. This indicates that the leaving flow of the first stage decelerates immediately and, therefore, low velocities occur during turning of the flow to peripheral direction. Comparison of the exhaust port area with the average inlet area to the peripheral duct also indicates that some acceleration will take place during turning. In this case it is found by several investigators, for example Reference (10), that turning losses are small, because boundary layer separation effects are suppressed by accelerating flow. Next, an average constant velocity through the duct is assumed. The losses are then determined by the total pressure loss coefficient

$$C_{p_{tot}} = \left(\frac{P_3}{P_{03}} \right) \left[1 - \frac{P_4}{P_3} \right] \quad (68)$$

where P_3 denotes the static pressure of the inlet and P_4 the static pressure at the exit of the duct. P_{03} is the total pressure at the inlet station. Since the total pressure loss coefficient is directly proportional to the static pressure loss coefficient

$$C_p = 1 - \frac{P_4}{P_3} \quad (69)$$

the latter is used primarily for detailed investigations. The measured static loss coefficients are presented in Figure 31 and are compared with the theoretical static pressure coefficient defined as

$$C_{p_{th}} = \frac{P_3 \cdot \frac{C_3^2}{2g}}{P_{03}} = \left[1 + \frac{\kappa-1}{2} M_3^2 \right]^{\frac{\kappa}{\kappa-1}} - 1 \quad (70)$$

Equation (70) assumes total loss of the dynamic head at the rotor discharge. M_3 is the absolute rotor discharge Mach number which is evaluated approximately by use of the total discharge temperature T_{03} and estimated values of nozzle coefficient ψ_N and blade coefficient ψ_R .

$$M_3 = \frac{u}{\sqrt{gKR \cdot T_{03}}} \frac{\psi_N \cdot \sin \alpha_2}{(u/c_{0I}) \cdot \sin \alpha_3} \quad (71)$$

The discharge angle of the rotor is found from the relation,

$$\alpha_3 = \cot^{-1} \left\{ \left(\frac{u/c_{0I}}{\psi_{NI} \cdot \sin \alpha_I} \right) (1 + \psi_{RI}) - \psi_{RI} \cot \alpha_I \right\} \quad (72)$$

For evaluation of Equation (72) values of $\psi_N = 0.92$ and $\psi_{RI} = 0.78$ were used as first approximations. The resulting discharge Mach numbers are plotted versus u/c_0 and are presented in Figure 29, indicating mainly subsonic flow in the re-entry duct. The theoretical pressure loss coefficient

is then obtained from Equation (70) and is compared with the test result in Figure 32. Inspection of this diagram indicates that the duct losses are apparently smaller than assumed in the analyses of Reference 1 and in chapter (A) of this report, where it was also assumed that the dynamic head at rotor discharge is lost entirely in the duct. To illustrate the percentage difference from the total dynamic head a recovery factor

$$C_R = 1 - \frac{C_{Pst}}{C_{Pth}} \quad (73)$$

was defined and is presented in Figure 33 for the turbine speeds of interest.

It can be seen that for the design point $u/c_o = 0.20$ only half the total dynamic head is lost. The total to total efficiency of the first stage can now be calculated by use of the following equation;

$$\eta_{Tot} = \eta_{hI} \frac{(1 - \delta_I)^{K-1/K}}{1 - \left(\frac{\delta_I}{1 - C_{Ptot}} \right)^{K-1/K}} \quad (74)$$

which corrects the total to static efficiency to total conditions. C_{Ptot} is defined by Equation (68). The static to total pressure ratio $\frac{P_3}{P_{o3}}$ needed for evaluation of Equation (68) was already calculated for the discharge Mach number M_3 .

The duct losses presented in Figure 32 indicate that the losses decrease slightly with increasing u/c_o . This seems to be due to small turning losses which are neglected by this method.

The losses caused by friction are found to be predictable by the following relation derived in Appendix E;

$$C_{Pst} = f \cdot \left(\frac{L}{r_h} \right) C_{Pth} \left[F_{Cm} \sin \alpha_3 (1 - L_t) \left(\frac{A_3}{A_4} \right) \right]^2 \quad (75)$$

where

f = friction coefficient

L = duct length

r_h = hydraulic radius

L_t = total leakage area

A_3 = flow area at duct inlet

A_4 = constant duct area

F_{Cm} = velocity function

C_{Pst} = theoretical pressure loss coefficient

α_3 = rotor discharge angle

The velocity function F_{Cm} accounts for the decreasing velocity with the channel-length due to mass flow leaving through each nozzle. A linear

velocity function was assumed for determining an average duct velocity

\bar{C}_m .

$$F = \frac{1}{2} \left[1 + \frac{1}{Z_{II}} \right] \quad (76)$$

where Z_{II} denotes the number of nozzles of the second stage.

Equation (75) is derived in Appendix E, Equation (E8) to (E14).

Application of Equation (75) shows that the test curve of Figure 32 agrees exactly with this equation when using a friction coefficient on the order of $f = 0.02$ to 0.025 . The average Reynolds number of the duct amounts to about $Re = 5 \times 10^4$. For this case, friction coefficients of $f = 0.02$ are predicted for rough walls in Reference (10). Therefore, it seems possible to use the assumption of negligible turning loss, which results in good correlation between test results and the approximate theoretical prediction. However, the measured duct losses may also be explained when assuming laminar flow through the duct. In this case the friction coefficient can be calculated according to the relation

$$f = \frac{.0559}{\sqrt{Re}} \quad (77)$$

which is quoted by Reference (11) for ducts of rectangular or square cross-area. In this case it can be seen from Figure 33 that the friction loss is quite small and, therefore, that the turning loss is the largest source of

static pressure loss. The turning loss can be calculated according to the simple relation

$$C_{p\alpha} = \left(\frac{\alpha_3}{180} \right) \cdot C_{p+h} \quad (78)$$

which assumes that the turning loss is directional proportional to the flow angle α_3 as indicated in Figure 30. For $\alpha = 0$, when the velocity is in the direction of the duct, the turning loss is zero.

Combining Equation (75) with (77) and (78) results in good correlation between test results and the prediction of turning loss and friction losses, as shown in Figure 33.

In summary, two concepts of approximate nature are presented to discuss the duct losses. Both concepts were able to correlate the measured losses. However, in reality it is indicated that laminar flow will not be predominant throughout the whole duct on one side and that turning losses cannot be neglected on the other side. Therefore, it might be concluded that the duct losses may be predicted by an average value from the application of both concepts, which means that the turning loss is somewhat smaller than indicated in Figure 33 and the friction loss is not as high as shown in Figure 31.

In conclusion, it can be seen that the assumption of total loss of the dynamic head of the first stage is somewhat conservative for the present case. However, it is found, for the second stage, that the dynamic head is lost entirely in the duct as shown in Figure 15. Therefore, it still may be convenient to use the assumption of loss of total dynamic head at both rotor discharge stations. The error introduced will be less than one to two points in turbine efficiency.

4. Nozzle Performance

The performance of turbine nozzles is usually represented by the nozzle or velocity coefficient ψ_N , the ratio of the mean gas velocity at the exit of the nozzle to the velocity if the flow were isentropic. The mean velocity is defined as the mass averaged velocity, and the velocity coefficient ψ_N is determined according to the following equation

$$\psi_N = \frac{\int C \cdot dm}{C_0 \int dm} \quad (79)$$

The nozzle coefficient can be obtained by measuring the values of the mass flow together with the reaction force on the nozzle (Reference 5) or by measurements of the distribution of the total pressure in the exit plane, from which the mean velocity can be calculated. However, for the present tur-

bine configuration, the nozzle coefficient could not be evaluated by application of the methods mentioned above, because reaction test facilities for turbine nozzles were not available. A total pressure survey at the nozzle exhaust station was not feasible in view of the small dimensions involved and the lack of special total pressure probes calibrated accurately for high Mach number conditions. Therefore, it was necessary to adopt an approximate method for estimating the nozzle performance during static and dynamic conditions. The approximate method is based on the assumption that a nearly uniform velocity profile exists at the nozzle exhaust section B-B as shown in Figure 34. The section B-B is parallel to the throat section A-A. The above assumption should be valid for the design point performance for which nozzle coefficients of $\psi_N = .92$ to $.96$ are commonly measured and predicted by Reference (5). In addition, it is found to be valid for the design point that shock waves disturb the nozzle-jet only beyond the nozzle section B-B (Reference (8)). This is also true for small deviations from the design performance as indicated in Reference (4). In the case of uniform flow the nozzle coefficient can be obtained by measuring the total to static pressure ratio between nozzle inlet and the nozzle exhaust section B-B where one static pressure tap is located as shown in Figure 34. For convenience the nozzle coefficient is defined as the ratio of the actual to the ideal isentropic Mach number

referred to the measuring station B-B.

$$\psi_N^* = \frac{M_z}{M_{id_2}} = \frac{\sqrt{\frac{2}{K-1}}}{M_{id_2}} \sqrt{\left(\frac{p_{0_2}}{p_2}\right)^{\frac{K-1}{K}} - 1} \quad (80)$$

It is realized that Equation (80) is only an approximate expression which does not include interference effects between the nozzle jet downstream of section B-B and the leading edges of the "subsonic" rotor configuration.

Since these effects cannot be measured with the present test setup, the above definition of ψ_N^* is believed to be the best approximation possible. The ideal Mach number is determined by the throat to exhaust area ratio according to the following equation

$$\left(\frac{A_I^*}{A_I}\right) = \frac{M_{2i} \left(\frac{K+1}{2}\right)^{\frac{K+1}{2(K-1)}}}{\left(1 + \frac{K-1}{2} M_{2i}^2\right)^{\frac{K+1}{2(K-1)}}} \quad (81)$$

The ideal nozzle-design Mach number is listed in the gas tables (Reference 12) together with the respective throat to exhaust area ratios. The nozzle coefficient ψ_N^* as defined by Equation (80) was measured for the first and second stage nozzles during dynamic and static test conditions. In Figure 34 the measured nozzle coefficients of the first stage and in Figure 35 the measured coefficients of the second stage are plotted versus the measured total to static pressure ratios. It can be seen that both nozzles are operat-

ing at off-design when tested with an overall pressure ratio of 300:1. Inspection of Figure 24 reveals that the pressure ratio between first stage nozzle throat and measuring station (2) at the exhaust of the first stage nozzle amounts to 15.72:1 and that the respective pressure ratio of the nozzles of the second stage amount to 14.2:1. For these pressure ratios Figure 34 indicates a nozzle coefficient of $\psi_{N_I}^* = 0.90$ for the first stage and Figure 35 indicates for the pressure ratio 14.2:1 a nozzle coefficient of $\psi_{N_{II}}^* = 0.84$. The test curves indicate good agreement between tests conducted under stalled conditions and during actual turbine operation. From these figures it can be seen that the first stage is operating close to the design value but the second stage is far less efficient than expected. It is realized that the nozzle coefficients defined by Equation (80) and obtained by use of only one pressure tap at each nozzle might introduce some error. To estimate this error the measured nozzle coefficients are compared with nozzle coefficients measured in Reference (5) and plotted in Figure 36. Here the nozzle coefficients of Figure 36 are measured by the reaction method. The nozzle coefficients are plotted versus the nozzle design Mach number. Several curves are presented illustrating the off-design performance of the nozzles tested in Reference (5). The off-design performance was investigated in the range of 40 to 100 percent of the design values.

The design Mach numbers are determined by the throat to exhaust area ratio as defined in Equation (81)

To verify the design Mach numbers of the present turbine, the nozzle area of the first and second stages were carefully inspected. It was found that the exhaust to throat area ratio of the first stage amounted to $(A/A^*)_I = 3.25$ and of the second stage $(A/A^*)_{II} = 3.65$. The respective design Mach numbers, corresponding to these area ratios, are calculated to be $M_I = 2.72$ and $M_{II} = 2.84$. This means, in other words, that the design pressure ratio of the first stage is $P_{rI} = 24:1$ and that of the second stage $P_{rII} = 28.9:1$. Keeping in mind that the design pressure ratio is 17:1 it can be seen that the second stage is far off the design value. The reason for the larger exhaust area to throat ratio of the second stage is believed due to errors in tolerances when the nozzles were manufactured. In addition, it should be noted that the second stage nozzles are of the same design as the first stage nozzle and, therefore, an error is introduced because integer number of nozzles had to be used.

If the design Mach numbers and the measured nozzle coefficients ψ_N^* , defined as the ratio of the actual to the design Mach number are used, Figure 36 indicates that the nozzle coefficient for the first stage should have been $\psi_{N1} = .93$ instead of $\psi_{N1} = .90$ for the design Mach number 2.72. This

indicates close agreement for the first stage between the prediction of Reference (5) and measurements. Larger deviation is found for the second stage where Figure 36 indicates a nozzle coefficient of $\psi_{N_I} = .88$ instead of $\psi_{N_I}^* = .84$ measured for the design Mach number 2.84. This suggests that a non-uniform velocity distribution exists in the second stage nozzles while the first stage nozzle is operating with a velocity profile as assumed. For further calculations it is advisable to use a nozzle coefficient of $\psi_{N_I} = .93$ for the first stage. The nozzle coefficient of the second stage should be between $\psi_{N_{II}} = .84$ and .88. Finally, it is mentioned that, besides a non-uniform velocity profile, incidence effects or interference effects of blades and nozzle might have caused the low velocity coefficient of the second stage. Therefore it is interesting to investigate the incidence angle and incidence loss occurring at the second stage. For this purpose, first the nozzle parameter $\bar{\psi}_N$ defined by Equation (42b) is calculated using a first stage nozzle coefficient $\psi_{N_I} = .93$ and a nozzle coefficient for the second stage of $\psi_{N_{II}} = .83$ to .84. This results in a nozzle parameter $\bar{\psi}_N = .669$. However, when using nozzle coefficients indicated by Figure 36, the nozzle parameter amounts to $\bar{\psi}_N = 0.76$ using $\psi_{N_I} = .93$ and $\psi_{N_{II}} = .88$. This result indicates a difference in efficiency

$$\frac{\eta}{\eta_0} = \frac{\bar{\Psi}_N \cos \alpha - u/c_0}{\Psi_N \cos \alpha - u/c_0} \quad (82)$$

where η_0 is the reference efficiency using the measured values for nozzle coefficients of first and second stage. Evaluation of Equation (82) shows that a second stage nozzle coefficient of $\Psi_N = .84$ instead of $\Psi_N = .88$ decreases the turbine efficiency nearly 2 percent. This might be due to incidence losses occurring at the second stage. The incidence angle of the second stage amounts to 3.5 degrees when evaluating the incidence angle from the following equation,

$$i_I = \beta - \tan^{-1} \left[\frac{\sin \alpha_I}{\cos \alpha_I - u/c_{0I}} \right] \quad (83)$$

where α_I denotes the actual flow angle and β denotes the blade angle of the rotor cascade. The actual flow angle is obtained from the relation

$$\cos \alpha_I = \sin \beta^2 \left[\left(\frac{u/c_{0I}}{\Psi_{N_I}} \right) + \sqrt{\left(\frac{u/c_{0I}}{\Psi_N} \right)^2 + \frac{\cot^2 \beta - \left(\frac{u/c_{0I}}{\Psi_N} \right)}{\sin^2 \beta}} \right] \quad (84)$$

used for evaluating Equation (83). The incidence angle, i_I , is illustrated in Figure 37. The incidence loss as a percent of the available power can now be obtained by the following equation

$$L_{iII} = \left(\frac{C_{oII}}{C_o} \right)^2 \cdot \left(\frac{\sin(i_{II}) \cdot \sin \alpha'_{II}}{\sin \beta} \right)^2 \quad (85)$$

where $\left(\frac{C_{oII}}{C_o} \right)$ denotes the spouting velocity parameter of the second stage determined by Equation (44). Equation (85) assumes that the velocity component normal to the blade inlet angle is lost as a total pressure loss due to the incidence angle, i , as indicated in Figure (37). This concept of incidence loss is also used in References (13, (14) and (15). Evaluation of Equation (85) indicates that the incidence loss as a percentage of the available power is nearly of the same order as the efficiency decrease due to the lower value of the nozzle coefficient of the second stage, as shown by Equation (82). Therefore, it might be concluded that using a nozzle coefficient $\psi_{N_{II}} = 0.84$ takes into account the incidence loss of the second stage. The incidence angle of the first stage is found to be negligible, therefore, the nozzle coefficient of $\psi_{N_I} = 0.93$ should compare closely with the actual nozzle performance of the first stage.

5. Blade Element Performance

The rotor or blade-element performance of each stage is determined in the case of impulse operation by the coefficient, ψ_{RI} which

is related to the hydraulic-stage efficiency according to Equation (2).

$$\psi_{RI} = \frac{\eta_{RI}}{2(u/c_o)_I [\psi_{RI} \cos \alpha - u/c_o)_I]} - 1 \quad (86)$$

Since additional losses, referred to as disc friction, pumping and scavenging losses were found to be negligible in the range of $u/c_o = 0.20$ and are beyond the accuracy of the measurements, the hydraulic stage efficiency is approximated by the internal or thermodynamic stage efficiency.

$$\eta_{RI} = \frac{1 - \frac{T_{03}}{T_{01}}}{1 - \left(\frac{P_3}{P_{01}}\right)^{\frac{K-1}{K}}} \quad (87)$$

Combining Equation (86) and (87) the blade coefficient of both the first stage, ψ_{RI} , and of the second stage, $\psi_{R_{II}}$, can be evaluated from the measurements. The blade coefficient presented in this report is the full admission blade coefficients, ψ_{R_0} , which is defined according to Reference (7) by the following relation.

$$\psi_{R_0} = \frac{\psi_R}{1 - \frac{t}{2a_I}}$$

where the geometric parameter t/a_I is determined by Equation (51). The full admission blade coefficient of the first stage is found to be $\psi_{RI_0} = 0.82$

occurring at the relative Mach number $M_{w_I} = 1.75$ and the full admission blade coefficient of the second stage amounts to $\psi_{R_{O_{II}}} = 0.87$ for a relative Mach number $M_{w_I} = 1.50$. This result is presented in Figure (38) together with another test point obtained at Sundstrand Turbo on an identical turbine wheel for a relative Mach number of $M_{w_{II}} = 2.50$. Figure (38) demonstrates that all three test points are nearly on a straight line. Comparison of this result with Equation (9) shows excellent agreement. Equation (8), however, indicates higher blade coefficients which apparently can only be achieved with supersonic blade configurations as mentioned before. The low blade coefficients shown in Figure (38) are believed due to separation phenomena occurring in the blade passages of subsonic type. This might be illustrated by a simple calculation employing the boundary layer concept, as outlined in Reference (16). This concept is usually applied for determining total pressure losses of compressor and reaction cascades. The basic loss coefficient is defined by

$$\omega_2 = \frac{\left(\frac{\Delta P_{tot}}{\rho}\right)}{\left(w_2^2/2g\right)} \quad (88)$$

where w_2 denotes the relative velocity at the rotor exit. In the case of impulse operation of an axial turbine, it can be seen from the Bernoulli equation of the relative flow

$$\left(\frac{W_1^2}{2g}\right) - \frac{u_1^2}{2g} + \frac{P_1}{\gamma} = \frac{W_2^2}{2g} - \frac{u_2^2}{2g} + \frac{P_2}{\gamma} + \frac{\Delta P_{tot}}{\gamma} \quad (89)$$

that the total pressure loss coefficient, w_2 , can be expressed by the simple relation

$$w_2 = \left(\frac{W_1}{W_2}\right)^2 \left[1 - \left(\frac{W_2}{W_1}\right)^2\right] = \frac{[1 - \psi_R^2]}{\psi_R^2} \quad (90)$$

Using the theoretical results of Reference (16) it can be seen that the basic loss parameter of the boundary layer theory, the momentum thickness of the trailing edge plane, is related to the total pressure loss coefficient by the simple relation

$$\left(\frac{\theta}{c}\right)_2 = \frac{w_2 \cdot \left(\frac{\cos \beta_2}{\sigma}\right)}{H_2 \cdot w_2 + \frac{4H_2}{3H_2 - 1}} \quad (91)$$

$(\theta/c)_2$ denotes the ratio of the discharge momentum thickness to the chord length, c , and σ is the solidity, defined as the ratio of the chord, c , to the blade spacing, $\sigma = (c/t)$. The momentum thickness determines the momentum loss occurring in the blade surface boundary layers, which displace the free stream by the displacement thickness, δ^* . The factor H occurring in Equation (91) is denoted as a "form factor" according to the definition

$$H = \left(\frac{\delta^*}{\theta} \right) \quad (92)$$

By applying this concept to the first stage of our test turbine, for a relative Mach number of $M_{w_1} = 1.725$, the form factor may be determined from application of theoretical and test results of Reference (17). Figure (39) presents the results of Reference (17) where the form factor is plotted against the relative Mach number. Using the discharge Mach number of $M_{w_2} = 1.36$ it can be seen from Figure (39) that a form factor of approximately $H = 2.2$ is suggested. Evaluating Equation (91) indicates a momentum thickness of $\theta/c = 0.0986$. The displacement thickness is calculated according to Equation (92) as $\left(\frac{\delta^*}{\theta} \right) = 0.262$. Now relating the ratio of displacement thickness to chord lengths to the ratio of displacement thickness to spacing determines the blockage effect at the exhaust section. It can be seen from the obtained value of the displacement thickness and the spacing that as much as 48 percent of the area at the discharge of the first stage is blocked by boundary layer development. This indicates heavy separation inside the blades and that three-dimensional interference effects must exist. To improve the passage, it is indicated that the area should be increased from the leading edge to the trailing edge, in a fashion which provides equilibrium of the cascade flow or, at least, linearly. Detailed calculations of how to

achieve equilibrium of the flow as outlined in Reference (18) are not included in this work. However, the equilibrium concept should be applied in future investigations of blade sections for high pressure-ratio turbines.

Finally, the performance of both stages is compared in Figure (40) which illustrates again the off-design performance of the second stage. The hydraulic efficiency of each stage is compared in Figures (41) and (42) with the equivalent single stage efficiency predicted by the $N_s D_s$ diagram of Reference (1). The hydraulic efficiency is used for comparison because this eliminates the leakage effect which is negligible for single-stage turbines. Figure (40) shows very good agreement between actual and predicted performance of the first stage while Figure (42) demonstrates the off-design performance of the second stage. The off-design performance of the second stage is due to off-design performance of the nozzle as well as some incidence losses as estimated in Section 4.

F. CORRELATION OF TEST RESULTS WITH ANALYSIS

The test results discussed in the foregoing chapter have shown that new leakage expressions and lower nozzle coefficients have to be used for calculating the design point efficiency. In view of this fact, it is found necessary to obtain a new $N_s D_s$ diagram for two-stage re-entry turbines, by combination of Equation (56), (9), (61), (62), (65) and (67). To account (approximately) for the incidence losses, it is advisable to use an average nozzle coefficient of $\psi_N = 0.90-0.92$ for both nozzle configurations. This results in a final $N_s D_s$ diagram for two stage re-entry turbines with equal pressure ratio in both stages. This diagram is presented in Figure (43), and is valid for the same 300:1 over-all pressure ratio and design parameters as indicated in the preliminary $N_s D_s$ diagram of Figure (4). From Figure (43) it can be seen that for the design values of N_s and D_s , an efficiency of approximately $\eta_t = 0.56-0.57$ is predicted. Finally, the performance curve of the test turbine is compared in Figure (44) with the design point performance curve predicted by the $N_s D_s$ diagram of Figure (43), for a constant $D_s = 2.58$. Comparison of both curves shows very close agreement. The design point deviates by about one efficiency point. This is apparently caused by the off-design performance of the second stage nozzle as discussed previously. The test curve is presented for the axial clearance 0.005. The test result for clearance $c^* = 0.017$ is already presented in Figure 20. Application of the

basic efficiency relations, modified by the new leakage relations also correlate well with the performance for $C^* = 0.017$. The dashed performance curve above the test curve of Figure (44) indicates the performance which would be expected when both nozzles would operate with optimum nozzle coefficients $\psi_N = 0.96$. Comparisons of the predicted design point performance with the off-design point performance of the test turbine reveal nearly the same trends. This is a surprising result because the efficiency Equation (4) is only true for the design point when

$$\cot \beta_2 = \cot \alpha_2 - \frac{u / c_{oi}}{\sin \alpha_i' \psi_{N_i}} \quad (93)$$

Without analyzing in detail the off-design performance, which is beyond the task of this report, it is noted that off-design performance and design point performance nearly coincide for the present turbine. This might be due to the fact that improper application of Equation (4), and neglect of the incidence losses and off-design performance losses of the nozzle and rotor cascade, cancel each other. It is suggested at this point, that a future program should be undertaken for studying the off-design point behavior and the possibility of analysis of same for high pressure ratio turbines. Finally, the performance of the two-stage re-entry turbine is compared with the optimum performance of an equivalent single stage turbine as shown in Figure (44).

The single stage performance is obtained from the respective $N_s D_s$ diagrams of Reference (1). However, the efficiency is corrected according to Equation (9) in the case of subsonic blade configurations. For the design point $u/c_o = 0.20$ it can be seen that the two stage turbine with $\frac{C^*}{D} = 0.008$ and nozzle operating at off-design is about 20 percent more efficient than the equivalent optimum single stage turbine. This demonstrates overwhelmingly the merit of the two-stage single disc turbine when employing subsonic blade configurations. However, preliminary investigations have indicated that, for the case of supersonic blade configurations, the single stage turbine might perform comparably or even more efficiently than the two-stage re-entry turbine. Therefore, it seems to be desirable to investigate supersonic single stage turbines. This future task should finally determine the most efficient turbine configuration for high energy level, low power output turbines.

V CONCLUSIONS

1. Reliable and internally consistent test data are obtained describing satisfactorily the over-all and blade element performance of the two-stage re-entry turbine under consideration.
2. Leakage measurements have revealed that the total leakage is larger than predicted by Reference (1). Leakage is found to be caused by

two components, the static and dynamic leakage, both of which can be predicted analytically.

3. Duct losses are found to be somewhat less than predicted by the common assumption that the dynamic head leaving the rotor of the first stage is totally lost. Analysis has shown that the duct losses may be predicted satisfactorily by empirical equations for friction and turning losses developed herein.

4. The blade coefficients presented in Reference (3) and employed in the analysis of this report are found to be valid for the present turbine. The blade coefficients can be predicted analytically and are valid for turbine cascades of subsonic configurations.

5. The nozzles of the test turbine were operating under off-design conditions due to inaccurate manufacturing procedures. The off-design performance could be correlated with published data of Reference (5) and it is indicated that some incidence losses are included in the nozzle coefficients.

6. A final $N_s D_s$ diagram for re-entry turbines with equal pressure ratios in both stages is constructed for 300:1 over-all pressure ratios and axial clearance parameter $\frac{c}{D} = 0.0008$. This $N_s D_s$ diagram uses an

average nozzle coefficient of $\psi_N = 0.92$ and blade coefficients computed from the respective equation presented in this report. The design point efficiency of the test turbine correlates well with this $N_s D_s$ diagram.

7. Two stage re-entry turbines are more efficient than equivalent single stage turbines for the case of subsonic blade configurations in the rotor.

8. The over-all performance of the two-stage re-entry turbine tested can be correlated with simple one dimensional-streamline theories as outlined in this report. However, it is indicated that complex three-dimensional flow phenomena occur inside the blade passages which should be investigated in further research tasks. In this case, it is desirable to investigate equilibrium conditions of the flow throughout the turbine cascades and to correlate the losses in total pressure with predictions from boundary layer concepts.

VI RECOMMENDATIONS

1. The program should be extended to investigate off-design performance of the two-stage re-entry turbine using the same analytical techniques that succeeded in this design point analysis.

2. Further investigations should be made to determine the performance of these turbine types with supersonic blade passages.

3. It is desirable to investigate the complex, three dimensional flow equilibrium conditions through the turbine cascade, and correlate the losses in total pressure with predictions from boundary layer concepts. In this respect, more analysis and test information are needed concerning the interaction of supersonic nozzle jets with moving cascades.

TABLE OF REFERENCES

1. Silvern, D. H., and Balje, O. E., A Study of High Energy Level, Low Power Output Turbines, Sundstrand Turbo Report AMF/TD 1196, 9 April 1958. *AD-161323*
2. Boxer, E., Sterrett, J. R., and Wlodarski, J., Application of Supersonic Vortex Flow Theory to the Design of Supersonic Impulse Compressor or Turbine Blade Sections, NACA RM L52B06, 24 April 1952.
3. Traupel, W., Thermische Turbomaschinen, Springer Verlag, Berlin, 1958.
4. Deich, M. E., Flow of Gas through Turbine Lattices, NACA TM 1393, May 1956. *AD-99721*
5. Keenan, J. H., Reaction Tests of Turbine Nozzles for Supersonic Velocities, ASME Paper 48-A-61, 1948.
6. Stodola, A., Steam and Gas Turbines, New York, Peter Smith, 1945.
7. Stenning, A. H., Design of Turbines for High Energy Fuel, Low Power Output Applications, Massachusetts Institute of Technology, Dynamic Analysis and Control Laboratory, Report No. 79, September, 1953.

TABLE OF REFERENCES

8. Heen, H. J., Non Steady Two-Dimensional Flow in a Partial Admission Turbine, The Hydraulic Analogy, PhD Thesis, M.I.T., September, 1958.
9. Spies, R., Dubey, M., Design of Low Speed Turbines for Long Duration Missile Secondary Power Units, Sundstrand Turbo Report S/TD No. 1769, December, 1959.
10. Schlichting, H., Grenzschicht-Theory, Verlag und Druck, G. Braun, Karlsruhe, 1954.
11. Kaufmann, W., Technische Hydro-und Aeromechanik, Springer-Verlag, Berlin, 1954.
12. Wang, C. J., Peterson, J. B., Anderson, R., Gas Flow Tables, Guided Missile Research Division, The Ramo-Wooldridge Corporation, Inglewood, California, 1957.
13. Kochendorfer, F. D., Nettles, J. C., An Analytical Method of Estimating Turbine Performance, NACA Report 930, 1949.
14. English, R. E., Caricchi, R. H., Comparison of Measured Efficiencies of Nine Turbine Designs with Efficiencies Predicted by Two Empirical Methods, NACA RM E51F13, 1951.

TABLE OF REFERENCES

15. Stewart, W. L., Evans, D. G., Analytical Study of Losses at Off-Design Conditions for A Fixed Geometry Turbine, NACA RM E53K06, February 4, 1954. *AD 24319*
16. Lieblein, S., and Rondebush, W. H., Theoretical Loss Relations for Low Speed Two-Dimensional Cascade Flow, NACA TN 3662, March, 1956. *AD 88530*
17. Stewart, W. L., Whitney, W. J., and Mieser, J. W., Use of Effective Momentum Thickness in Describing Turbine Rotor Blade Losses, NACA RM E56E29, 1956, (Declassified February 26, 1958). *AD 28962*
18. Hatch, J. E., Giamati, C. C., and Jackson, R. J., Application of Radial Equilibrium Condition to Axial Flow Turbomachine Design Including Consideration of Change of Entropy with Radius Downstream of Blade Row, NACA RM E54A20, April, 1954. *AD 28962*

APPENDIX A
NOMENCLATURE AND SYMBOLS

- A - area (inch²)
- A* - nozzle throat area (inch²)
- a - arc of admission (inch)
- C - coefficient
- c - absolute velocity or chord length (ft/sec; inch)
- C_f - restriction coefficient (dimensionless)
- C_o - spouting velocity (ft/sec)
- C_{Ptot} - total pressure loss coefficient (dimensionless)
- C_{Pst} - static pressure loss coefficient (dimensionless)
- C_{Pth} - theoretical static pressure loss coefficient (dimensionless)
- C_R - recovery coefficient (dimensionless)
- C* - axial clearance (inch)
- C_T* - tip clearance (inch)
- D - tip diameter (inch)
- D_s - specific diameter $D_s = \frac{D \cdot H_{ad}^{1/4}}{\sqrt{Q}}$
- F - function of ()
- F₁ - Mach number function for static conditions (dimensionless)
- F₂ - Mach number function for total conditions (dimensionless)

- $F_{(cm)}$ - velocity function (dimensionless)
- f - friction coefficient (dimensionless)
- g - gravitational constant $g = 32.2 \text{ ft/sec}^2$
- H_{ad} - adiabatic head (ft)
- HP - horsepower (HP)
- h - blade height (inch)
- L - developed length of re-entry duct (inch)
- L_b - blade pump loss (dimensionless)
- L_d - disc friction loss (dimensionless)
- L_{sc} - scavenging loss (dimensionless)
- L_t - total leakage loss (dimensionless)
- M - Mach number (dimensionless)
- N - revolutions per minute (RPM)
- N_s - specific speed $N_s = \frac{N \sqrt{Q}}{H_{ad}^{3/4}}$
- P_o - total pressure (psia)
- P - static pressure (psia)
- P_r - pressure ratio (dimensionless)
- Re - Reynolds number (dimensionless)
- r_h - hydraulic radius (inch)

- T_o - total absolute temperature ($^{\circ}R$)
- T - static, absolute temperature ($^{\circ}R$)
- t - blade spacing (inch)
- u - tip speed (ft/sec)
- W - mass flow (lb/sec)
- z - number of blades (dimensionless)
- z - number of nozzles of second stage (dimensionless)
- α - absolute flow angle [$^{\circ}$]
- β - blade angle [$^{\circ}$]
- δ - reciprocal of pressure ratio (dimensionless)
- ϵ - mixing coefficient (dimensionless)
- η - efficiency (dimensionless)
- η_t - turbine efficiency (dimensionless)
- η_h - hydraulic efficiency (dimensionless)
- η_i - internal or thermodynamic efficiency (dimensionless)
- k - ratio of specific heats (dimensionless)
- λ - partial admission function (dimensionless)
- μ - reheat factor (dimensionless)
- ρ - density (lb/ft³)
- τ - torque coefficient (dimensionless)

- χ - blade density ratio (dimensionless)
 ψ - nozzle function (dimensionless)
 ψ_N - nozzle coefficient (dimensionless)
 ψ_R - blade coefficient (dimensionless)
 ψ_{R0} - blade coefficient of full admission turbine (dimensionless)

Subscripts

- b - blade pumping
d - disc friction
f - restriction
h - hydraulic
i - ideal, internal
m - meridional
N - nozzle
o - total conditions
R - blade
sc - scavenging
st - static
t - turbine
th - theoretical
tot - total

- w - relative
- 1 - turbine inlet
- 2 - nozzle exhaust, first stage
- 3 - rotor discharge, first stage
- 4 - duct exit
- 5 - nozzle exhaust, second stage
- 6 - rotor discharge, second stage
- ex - exhaust second stage
- I - first stage
- II - second stage

Superscripts

- - average values
- ' - corrected values
- * - nozzle throat conditions

APPENDIX B

DERIVATION OF APPROXIMATE RELATIONS FOR EQUAL SPOUTING
VELOCITIES IN BOTH STAGES1. Derivation of Equation (6)

The ratio of the arcs of admission

$$\frac{a_r}{a_I} = \left(\frac{P_{II}}{P_I} \right) \cdot \left(\frac{T_I}{T_{II}} \right) \quad (B1)$$

is expressed as a function of the reciprocal of the total pressure ratio

$$\delta_{tot} = \delta_I \cdot \delta_{II} \quad (B2)$$

by introducing the isentropic relation

$$\frac{T_{II}}{T_I} = \left(\frac{P_{II}}{P_I} \right)^{\frac{k-1}{k}} \quad (B3)$$

in (B1)

$$\frac{a_r}{a_I} \approx \delta_I^{1/k} \quad (B4)$$

and relating δ_{II} to the total pressure ratio δ_{tot} . This is done by observing the condition of equal spouting velocities or equal heads in both stages

$$\frac{H_{II}}{H_{tot}} = \frac{1}{2} = \frac{T_{II} \left[1 - \delta_{II}^{\frac{k-1}{k}} \right]}{T_I \left[1 - \delta_{tot}^{\frac{k-1}{k}} \right]} \quad (B5)$$

and using (B3) to eliminate the temperature ratio. After simple re-arranging of the resulting equation, δ_{II} is found as a function of δ_{tot} .

$$\delta_{II} = \frac{\delta_{tot}}{\left(\frac{1 + \delta_{tot}^{\frac{k-1}{k}}}{2} \right)^{\frac{k}{k-1}}} \quad (B6)$$

Combining now (B6) and (B4) the final expression for $\left(\frac{a_I}{a_{II}} \right)$ is found:

$$\frac{a_I}{a_{II}} = \frac{\delta_{tot}^{\frac{k}{k-1}}}{\left(\frac{1 + \delta_{tot}^{\frac{k-1}{k}}}{2} \right)^{\frac{1}{k-1}}} \quad (B7)$$

2. Derivation of Equation (16)

Assuming static conditions in front of the leakage areas $A = 2 \cdot C^* \cdot h$ and $A = C^* \cdot A_I$, the leakage as a ratio of the total mass flow is expressed by

$$L_t = C_F \cdot \left(\frac{C^*}{D} \right) \cdot \left(\frac{D^2}{A^*} \right) \left[2 \cdot \frac{h}{D} + \frac{a_I}{D} \right] \cdot \left(\frac{P_2}{P_{01}} \right) \cdot \left(\frac{T_{01}}{T_2} \right)^{\frac{1}{2}} \quad (B8)$$

where the total mass flow is determined by the choked nozzle throat. The function

$$F(P, T) = \left(\frac{P_2}{P_{01}} \right) \left(\frac{T_{01}}{T_2} \right)^{\frac{1}{2}} \quad (B9)$$

is now related to the total pressure ratio δ_{tot} , by inserting (B3), in (B9)

$$F(P,T) = \delta_1^{\frac{K+1}{2K}} \quad (B10)$$

and observing (B2):

$$F(P,T) = \left(\frac{\delta_{tot}}{\delta_{II}} \right)^{\frac{K+1}{2K}} \quad (B11)$$

Finally δ_{II} of (B11) is eliminated by (B6). This yields the final relation:

$$F(P,T) = \left(\frac{1 + \delta_{tot}^{\frac{K-1}{K}}}{2} \right)^{\frac{K+1}{2(K-1)}} \quad (B12)$$

which determines L_t :

$$L_t = \left(\frac{C^*}{D} \right) \cdot \left(\frac{D^2}{A_I^*} \right) \left[2 \left(\frac{h}{D} \right) + \left(\frac{a_I}{D} \right) \right] \cdot \left(\frac{1 + \delta_{tot}^{\frac{K-1}{K}}}{2} \right)^{\frac{K+1}{2(K-1)}} \quad (B13)$$

APPENDIX C

DERIVATION OF PERFORMANCE RELATIONS FOR THE CASE OF UNEQUAL
SPOUTING VELOCITIES IN BOTH STAGES1. Derivation of Equation (42a)

The hydraulic efficiency of a two-stage turbine is given by the relation

$$\bar{\eta}_h = \eta_{h_I} \left(\frac{C_I}{C_o} \right)^2 + \eta_{h_{II}} \left(\frac{C_{II}}{C_o} \right)^2 \quad (C1)$$

Inserting the single stage relation (Equation (2))

$$\eta_h = 2 \cdot u_{coi} (1 + \psi_R) (\psi_N \cos \alpha - u_{coi}) \quad (C2)$$

in (C1) results in the expression

$$\begin{aligned} \bar{\eta}_h = & 2 \cdot u_{coI} \cdot \left(\frac{C_I}{C_o} \right)^2 [1 + \psi_{R_I}] (\psi_{N_I} \cos \alpha_I - u_{coI}) \\ & + 2 \cdot u_{coII} \cdot \left(\frac{C_{II}}{C_o} \right)^2 [1 + \psi_{R_{II}}] (\psi_{N_{II}} \cos \alpha_{II} - u_{coII}) \end{aligned} \quad (C3)$$

Expanding (C3), and assuming $\alpha_I = \alpha_{II}$ determines the average hydraulic efficiency:

$$\begin{aligned} \bar{\eta}_h = & 4 \cdot \frac{u}{C_o} \left\{ \frac{1}{2} \cos \alpha \left[\psi_{N_I} \frac{C_I}{C_o} + \psi_{N_{II}} \frac{C_{II}}{C_o} \right] \right. \\ & \left. + \frac{1}{2} \left(\psi_{R_I} \psi_{N_I} \frac{C_I}{C_o} + \psi_{R_{II}} \psi_{N_{II}} \frac{C_{II}}{C_o} \right) \cos \alpha - \frac{u}{C_o} \cdot \frac{\psi_{R_I} + \psi_{R_{II}}}{2} \right\} \end{aligned} \quad (C4)$$

(C4) suggests that average values can be defined as

$$\bar{\psi}_N = \frac{1}{2} \left[\psi_{N_I} \frac{C_I}{C_0} + \psi_{N_{II}} \frac{C_{II}}{C_0} \right] \quad (C5)$$

and

$$\bar{\psi}_R = \frac{1}{2} \left[\psi_{R_I} + \psi_{R_{II}} \right] \quad (C6)$$

and to approximate

$$\frac{1}{2} \left(\psi_{R_I} \cdot \psi_{N_I} \frac{C_I}{C_0} + \psi_{R_{II}} \cdot \psi_{N_{II}} \frac{C_{II}}{C_0} \right) \approx \bar{\psi}_R \cdot \bar{\psi}_N \quad (C7)$$

Finally, by combining Equations (C4), (C5), (C6) and (C7), the average efficiency equation is obtained for two-stage re-entry turbines.

$$\bar{\eta}_h = 4 \left(\frac{u}{C_0} \right) (1 + \bar{\psi}_R) (\bar{\psi}_N \cos \phi - u/C_0) \quad (C8)$$

2. Derivation of Equation (57)

The throat to area ratio $\left(\frac{A_{II}^*}{A_I^*} \right)$ is determined by the continuity equation for two nozzle-throats including the leakage occurring between them.

$$\psi A_I^* \cdot \frac{P_{0I}}{\sqrt{RT_{0I}}} = \psi \cdot A_{II}^* \cdot \frac{P_{0II}}{\sqrt{RT_{0II}}} + \Delta W \quad (C9)$$

Rearranging Equation (C9) and expressing the mass flow of the second stage and the leakage flow as percentages of the inlet mass flow results in the relation:

$$\left(\frac{A_{II}^*}{A_I^*} \right) = \frac{P_{r_{II}}}{\left(\frac{T_{0I}}{T_{0II}} \right)^{1/2} (1 - L_t)} \quad (C10)$$

Introducing the relation

$$\frac{T_{0I}}{T_{0II}} = 1 - \eta_I \left(1 - \delta_z^{\frac{K-1}{K}} \right) \quad (C11)$$

and combining Equations (C10), (C11), and using the condition of equal pressure ratios in both stages, results in the following equation:

$$\left(\frac{A_{II}^*}{A_I^*} \right) = \frac{\sqrt{P_{r_{tot}}}}{\sqrt{1 - \eta_I \left(1 - \delta_{tot}^{\frac{K-1}{K}} \right)}} \quad (C12)$$

The right side of Equation (C12) is now expressed by the functions K_1 and K_2 defined by Equations (47) and (48) giving the relation:

$$\frac{\sqrt{P_{r_{tot}}}}{[1 - \eta_I \left(1 - \delta_{tot}^{\frac{K-1}{K}} \right)]} = \left(\frac{K_1}{K_2} \right) \cdot \frac{[1 - \psi_N^2 \left(1 - \delta_{tot}^{\frac{K-1}{K}} \right)]}{[1 - \eta_T \left(1 - \delta_{tot}^{\frac{K-1}{K}} \right)]} \quad (C13)$$

which, combined with Equation (C12), determines the final expression for the throat area ratio of both stages.

$$\left(\frac{A_{II}^*}{A_I^*} \right) = \left(\frac{K_1}{K_2} \right) \cdot \frac{[1 - \psi_N^2 (1 - \delta_{to} + \frac{K-1}{K})]}{[1 - \eta_T (1 - \delta_{to} + \frac{K-1}{K})]} \quad (C14)$$

APPENDIX D

DERIVATION OF LEAKAGE FUNCTIONS F_1 AND F_2 1. Derivation of leakage function F_1

The Mach number function F_1 considers static conditions in front of the leakage area. Therefore

$$F_1 = \frac{P_2}{P_{01}} \cdot \left(\frac{T_{01}}{T_2} \right)^{\frac{1}{2}} \quad (D1)$$

By use of the Mach number relations

$$\frac{P_2}{P_{01}} = \left(1 + \frac{K-1}{2} \psi_N^2 M_{2i}^2 \right)^{\frac{-K}{K-1}} \quad (D2)$$

and

$$\left(\frac{T_{01}}{T_2} \right)^{\frac{1}{2}} = \sqrt{1 + \frac{K-1}{2} \psi_N^2 M_{2i}^2} \quad (D3)$$

$F_1(M_{2i})$ is defined:

$$F_1 = \frac{\sqrt{1 + \frac{K-1}{2} \psi_N^2 M_{2i}^2}}{\left(1 + \frac{K-1}{2} \psi_N^2 M_{2i}^2 \right)^{\frac{K}{K-1}}} \quad (D4)$$

M_{2i} is the design Mach number of the nozzle

$$M_{2i} = \sqrt{\frac{2}{K-1} \left[\left(\frac{P_{01}}{P_2} \right)_i^{\frac{K-1}{K}} - 1 \right]} \quad (D5)$$

and ψ_N is the nozzle coefficient defined as

$$\psi_N = \frac{M_2}{M_{2i}} \quad (D6)$$

2. Derivation of leakage function F_2

The leakage function F_2 considers total conditions in front of the leakage area, normal to the tangential component of the jet velocity c_2 :

$$F_2(M_2, \alpha_2) = \left(\frac{P_{02}}{P_{01}} \right) \left(\frac{P_{02t}}{P_{02}} \right) \quad (D7)$$

The efficiency of the nozzle is defined as

$$\eta \equiv \frac{P_{02}}{P_{01}} = 1 - \frac{\Delta P_{ad}}{P_{01}} = 1 - \frac{1 - \left(\frac{P_{02}}{P_{01}} \right)^{\frac{K-1}{K}}}{1 - \left(\frac{P_{2i}}{P_{01}} \right)^{\frac{K-1}{K}}} \quad (D8)$$

Re-arranging of Equation (D8) results in the expression

$$\frac{P_{02}}{P_{01}} = \left[\psi^2 + \left(\frac{P_{2i}}{P_{01}} \right)^{\frac{K-1}{K}} (1 - \psi^2) \right]^{\frac{K}{K-1}} \quad (D9)$$

which is related to the design Mach number M_{2i} by Equation (D2):

$$\frac{P_{02}}{P_{01}} = \left[\psi^2 + \left(1 + \frac{K-1}{2} M_{2i}^2 \right)^{-1} (1 - \psi^2) \right]^{\frac{K}{K-1}} \quad (D10)$$

Now Equation (10) is brought in the more convenient form:

$$\frac{P_{02}}{P_{01}} = \left[\frac{1 + \frac{K-1}{2} \psi_N^2 M_{2i}^2}{1 + \frac{K-1}{2} M_{2i}^2} \right]^{\frac{K}{K-1}} \quad (D11)$$

The ratio $\frac{P_{02t}}{P_{02}}$ is given immediately from the condition of constant static pressure P_2 and from the relation:

$$M_{2t} = M_2 \cdot \cos \alpha \quad (D12)$$

Therefore,

$$\frac{P_{0t}}{P_{02}} = \left(\frac{1 + \frac{\kappa-1}{2} \psi_N^2 M_{2i}^2 \cos^2 \alpha}{1 + \frac{\kappa-1}{2} \psi_N^2 M_{2i}^2} \right)^{\frac{\kappa}{\kappa-1}} \quad (D13)$$

Multiplication of (D11) with (D13) and re-arranging of the expanded equation yields the final expression

$$F_2 = \left[\frac{1 + \frac{\kappa-1}{2} \psi_N^2 M_{2i}^2 \{(\cos^2 \alpha + 1) + \frac{\kappa-1}{2} \cos^2 \alpha \psi_N^2 M_{2i}^2\}}{1 + \frac{\kappa-1}{2} M_{2i}^2 \{(\psi_N^2 + 1) + \frac{\kappa-1}{2} \psi_N^2 M_{2i}^2\}} \right]^{\frac{\kappa}{\kappa-1}} \quad (D14)$$

APPENDIX E

DERIVATION OF BASIC EQUATIONS FOR DUCT ANALYSIS

1. Rotor-discharge angle

The rotor-discharge angle is determined by the geometric relation of the discharge-velocity triangle:

$$\cot \alpha_3 = \frac{C_{u3}}{C_{m3}} \quad (E1)$$

The whirl component, C_{u3} , is related to the spouting velocity, blade coefficient and speed according to

$$C_{u3} = u - W_{u3} = u - \psi_R (C_{iI} \psi_N \cos \alpha_2 - u_2) \quad (E2)$$

The meridional component remains constant through the rotor, when perfect impulse operation is assumed. Therefore

$$C_{m3} = C_{m2} = \psi_N C_{oI} \cos \alpha_2 \quad (E3)$$

Combining (E1), (E2) and (E3) the final expression is obtained:

$$\alpha_3 = \cot^{-1} \left\{ \frac{u/C_I}{\psi_N \sin \alpha_2} [1 + \psi_R] - \psi_R \cot \alpha_2 \right\} \quad (E4)$$

2. Rotor discharge Mach-Number M_3

The rotor discharge Mach Number M_3 is defined

$$M_3 = \frac{\left(\frac{C_3}{u} \right) u}{C_{s3}} \quad (E5)$$

where the velocity ratio C_3/u is determined by the discharge velocity triangle:

$$C_3/u = (C_m/u) / \sin \alpha_3 \quad (E6)$$

Inserting (E3) into (E6) yields finally

$$H_3 = \left(\frac{u}{C_3} \right) \frac{\psi_u \cdot \sin \alpha_2}{(u K_{02}) \sin \alpha_3} \quad (E7a)$$

or

$$H_3 = \frac{u}{\sqrt{g K R T_3}} \frac{\psi_u \cdot \sin \alpha_2}{(u K_{02}) \sin \alpha_3} \quad (E7b)$$

3. Friction losses of re-entry duct

The friction loss of the re-entry duct is determined by the D'arcy Weisbach relation

$$\Delta h = f \cdot \left(\frac{L}{r_h} \right) \frac{\bar{C}_q^2}{2g} \quad [ft] \quad (E8)$$

\bar{C}_q denotes the average velocity through the duct, which is approximated by a linear relation

$$\bar{C}_q = C_{3m} \frac{1}{2} \left[1 + \frac{1}{\bar{C}_q} \right] = C_{3m} \cdot F(\bar{C}_{m4}) \quad (E9)$$

which accounts for velocity decrease due to the mass-flow leaving through each nozzle. Observing that

$$C_{m3} = C_3 \cdot \sin \alpha_3 \quad (E10)$$

and Equation (E9), the friction loss is expressed by

$$\Delta h = f \cdot \left(\frac{L}{r_h} \right) \frac{C_3^2}{2g} \left[\sin \alpha_3 \cdot F(C_{m4}) \right]^2 \quad (E11)$$

Introducing the leakage ratio L_t and accounting for the area change from A_3 to A_4 , Equation (E11) is modified as follows:

$$\Delta h = f \cdot \left(\frac{L}{r_h} \right) \frac{C_3^2}{2g} \left[\sin \alpha_3 F(C_{m4}) (1 - L_t) \frac{A_3}{A_4} \right]^2 \quad (E12)$$

Equation (12) is now brought into dimensionless form, by defining the static pressure loss coefficient, C_{Pst} ,

$$C_{Pst} = p_3 \cdot \frac{\Delta h}{p_3} \quad (E13)$$

and introducing this relation into the above equation. Therefore,

$$C_{Pst} = f \cdot \left(\frac{L}{r_h} \right) \left(\frac{p_3}{\rho_3} \right) \left(\frac{C_3^2}{2g} \right) \left[\sin \alpha_3 F(C_{m4}) (1 - L_t) \frac{A_3}{A_4} \right]^2 \quad (E14)$$

Since the theoretical pressure loss coefficient is defined as

$$C_{Pth} = p_3 \cdot \frac{G^2}{2g} = \left[1 + \frac{K-1}{2} M_3^2 \right]^{\frac{K}{K-1}} - 1 \quad (E15)$$

S/TD No. 1735

30 January 1960
Page 181

Equation (E14) can be rearranged to the final form:

$$C_{Pst} = f \cdot \left(\frac{L}{F_h} \right) C_{Pth} \quad (E16)$$

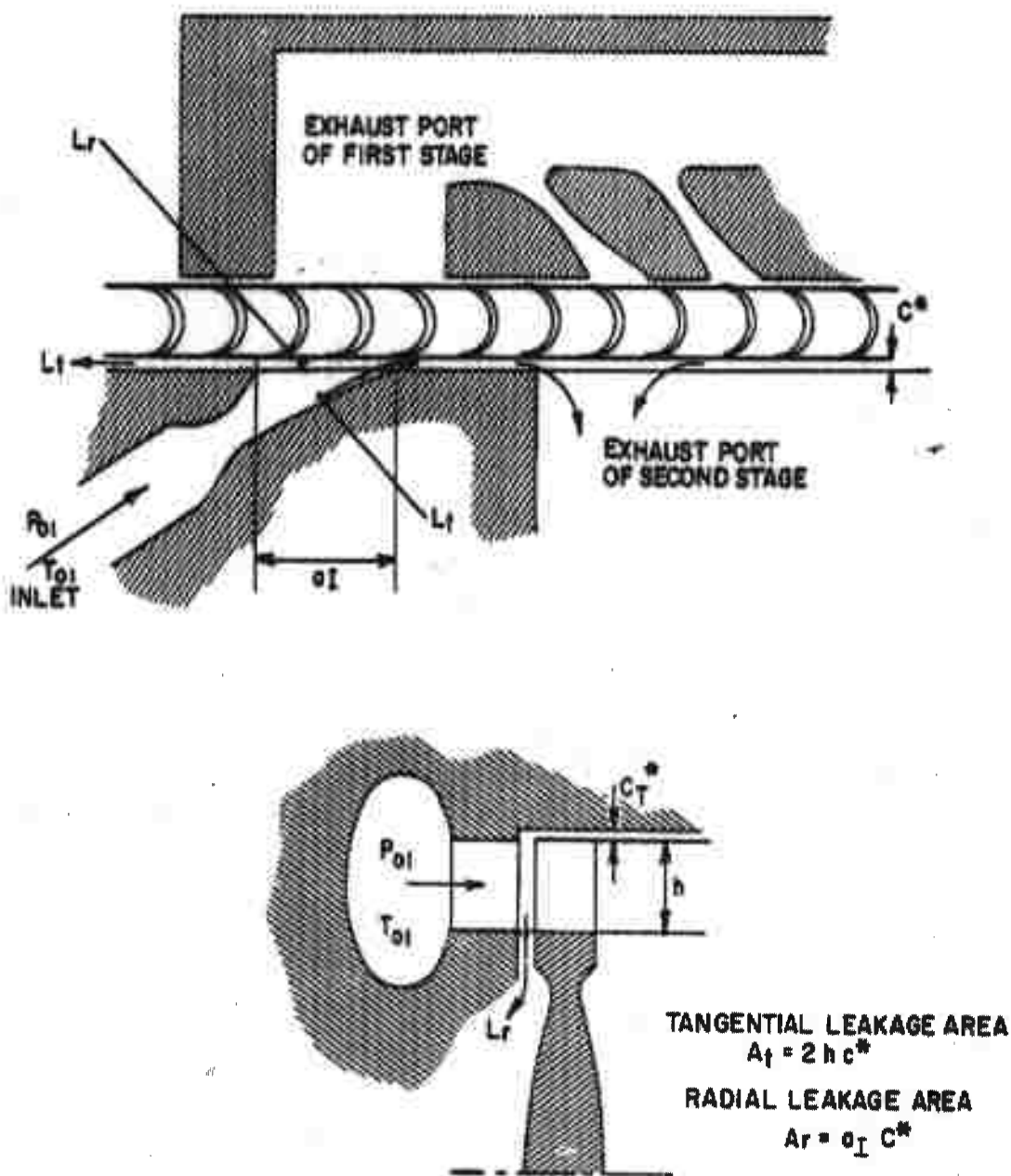


FIGURE 1.
LEAKAGE PATHS OF TWO STAGE REENTRY TURBINE WITH OPPOSED
FLOWS IN BOTH STAGES

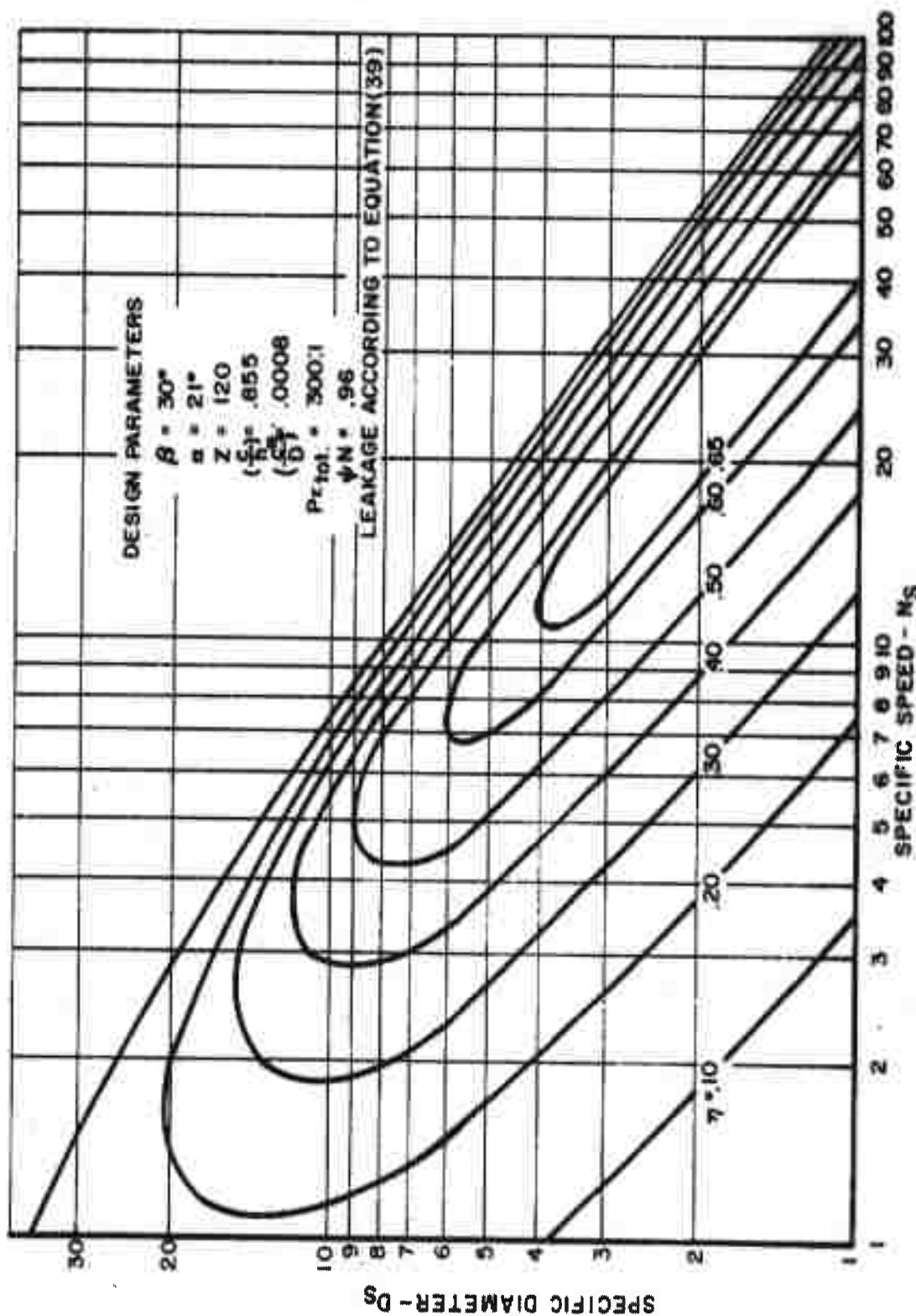


FIGURE 2.
 PRELIMINARY NS-DS DIAGRAM FOR TWO STAGE REENTRY TURBINES WITH EQUAL HEADS
 $H_{ad I} = H_{ad II}$ IN BOTH STAGES AND 300:1 OVER ALL PRESSURE RATIO

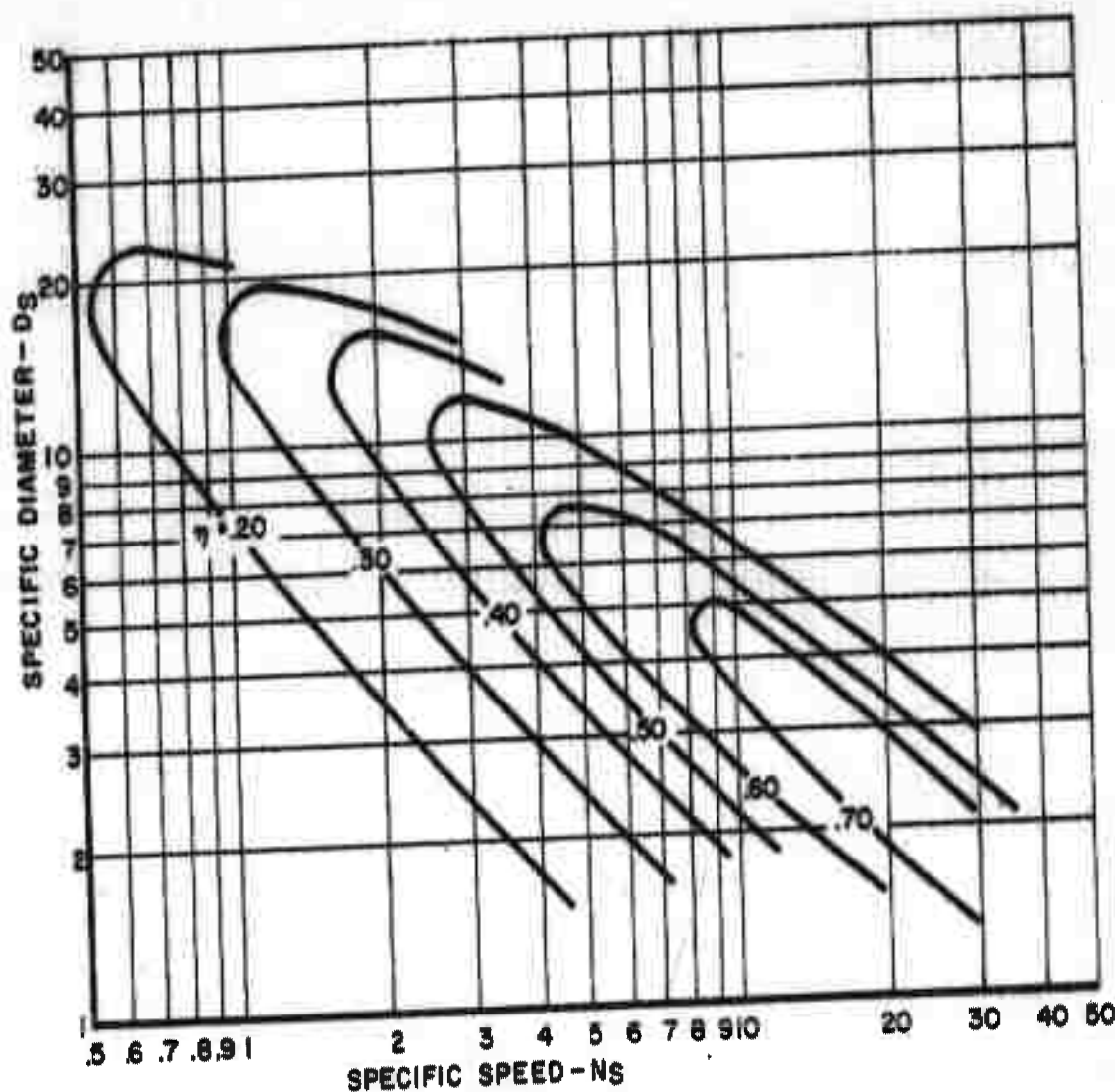


FIGURE 3.
 N_s - D_s DIAGRAM PREDICTED BY REFERENCE (1) FOR TWO STAGE RE ENTRY
 TURBINES WITH 17:1 OVERALL PRESSURE RATIO AND EQUAL HEADS
 IN BOTH STAGES

SUNDSTRAND TURBO
 DIVISION OF SUNDSTRAND CORPORATION

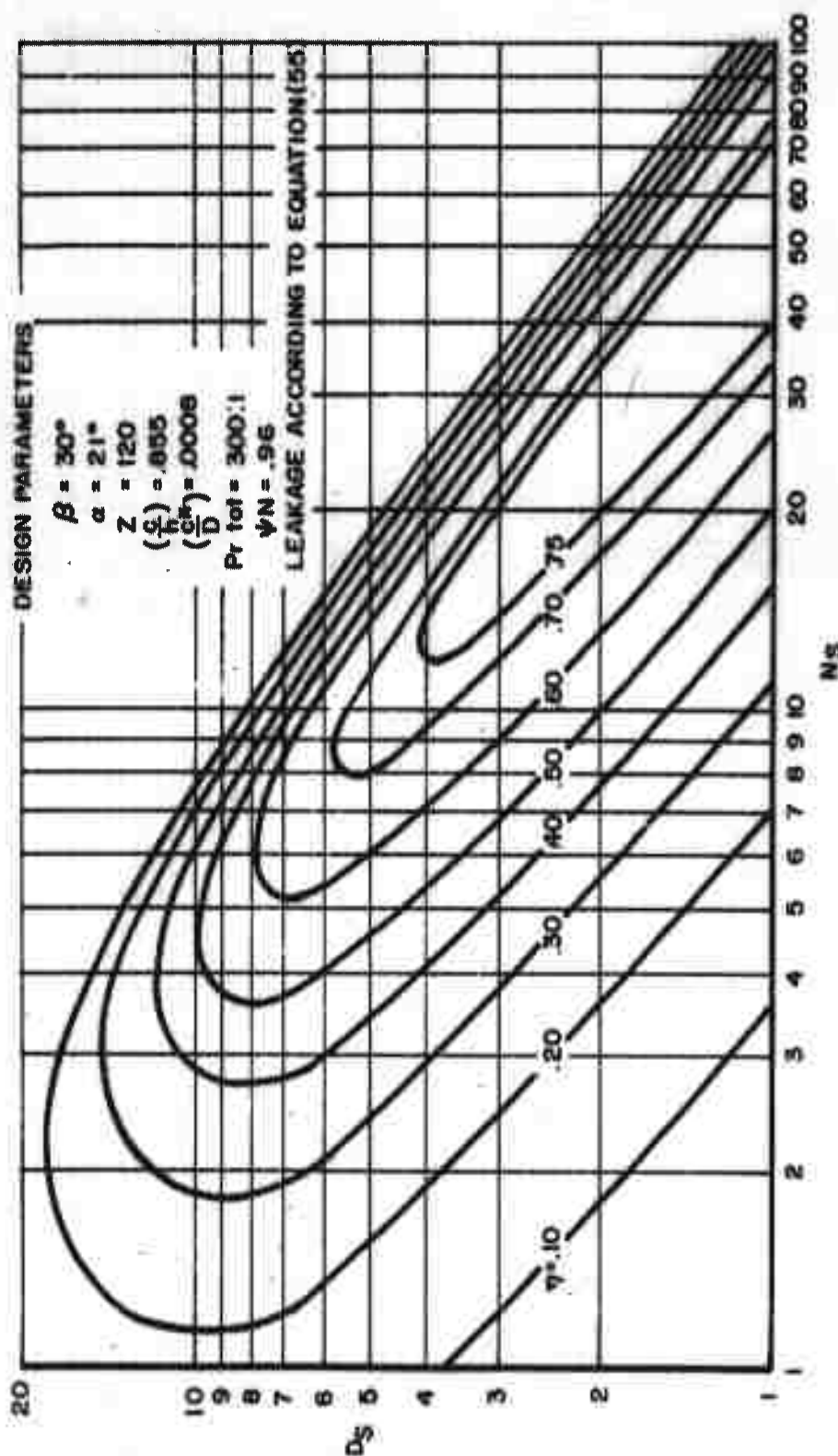
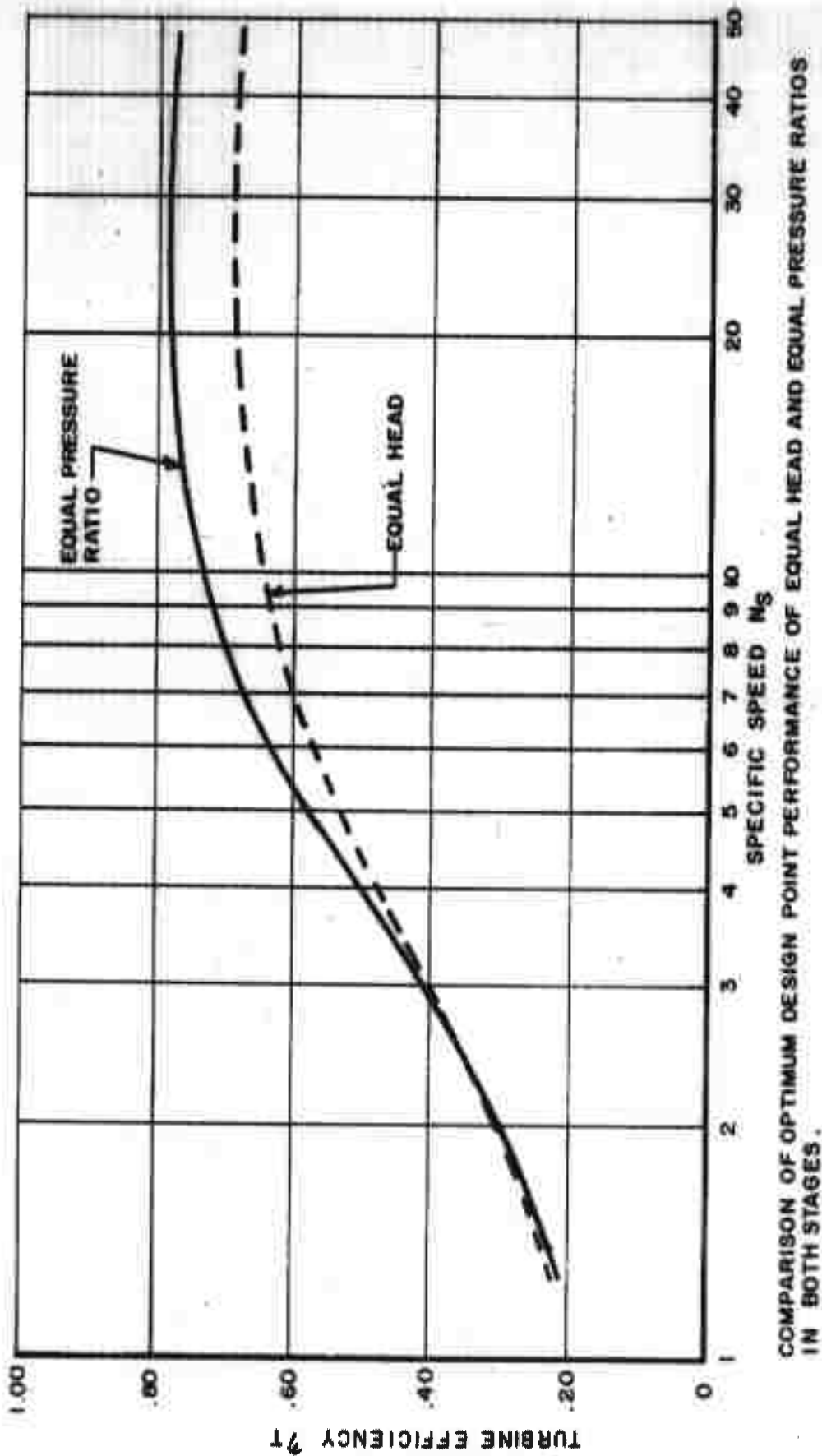


FIGURE 4.
PRELIMINARY N_s - D_s DIAGRAM FOR TWO-STAGE REENTRY TURBINES WITH EQUAL
PRESSURE RATIO IN BOTH STAGES AND 300:1 OVERALL PRESSURE RATIO



SUNDSTRAND TURBO
DIVISION OF SUNDSTRAND CORPORATION

FIGURE 5.
TWO-STAGE RE-ENTRY TURBINE FOR $P_{r \text{ total}} = 300:1$

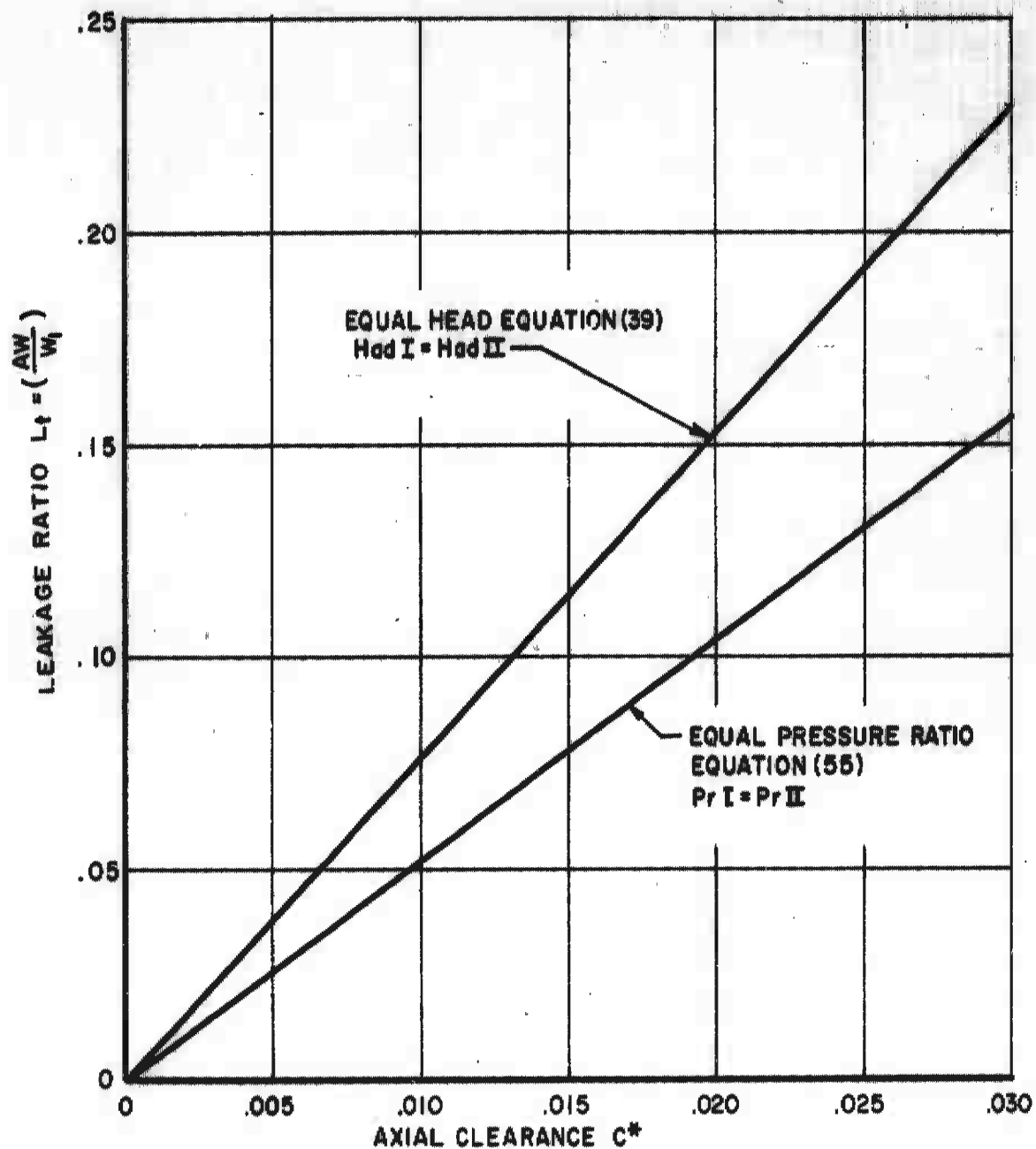


FIGURE 6.

COMPARISON OF LEAKAGE PREDICTED FOR TURBINES WITH EQUAL HEAD IN BOTH STAGES AND TURBINES WITH EQUAL PRESSURE RATIOS IN BOTH STAGES. TURBINE DIAMETER $D=6.3"$ OVERALL PRESSURE RATIO $Pr_{total}=300:1$

SUNDSTRAND TURBO
DIVISION OF SUNDSTRAND CORPORATION

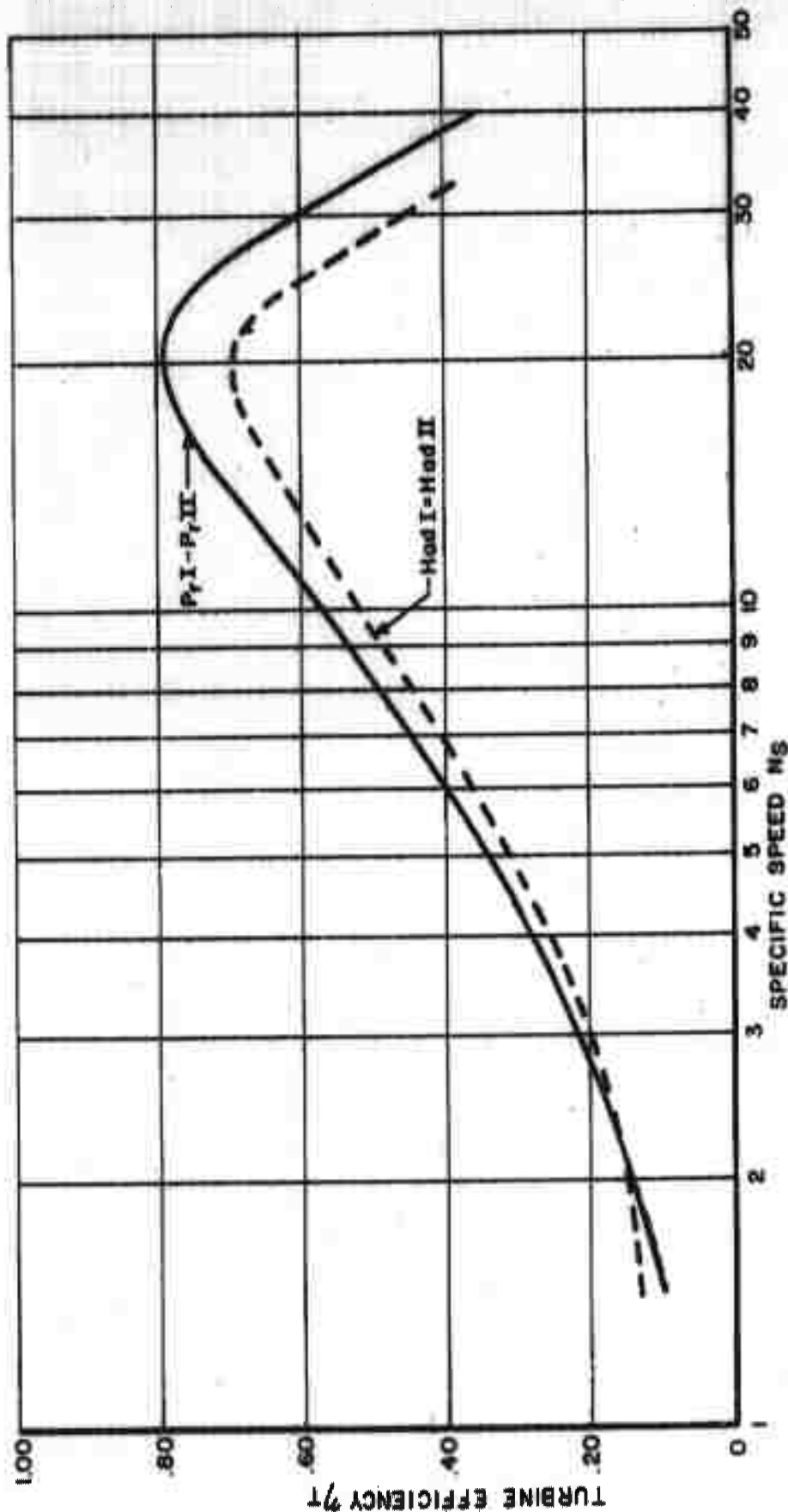


FIGURE 7.

COMPARISON OF DESIGN POINT PERFORMANCE OF TWO STAGE RE-ENTRY TURBINES OF EQUAL HEAD AND EQUAL PRESSURE RATIO FOR $D_S \text{ total} = 2.58 \text{ \& } P_r \text{ total} = 300.1$

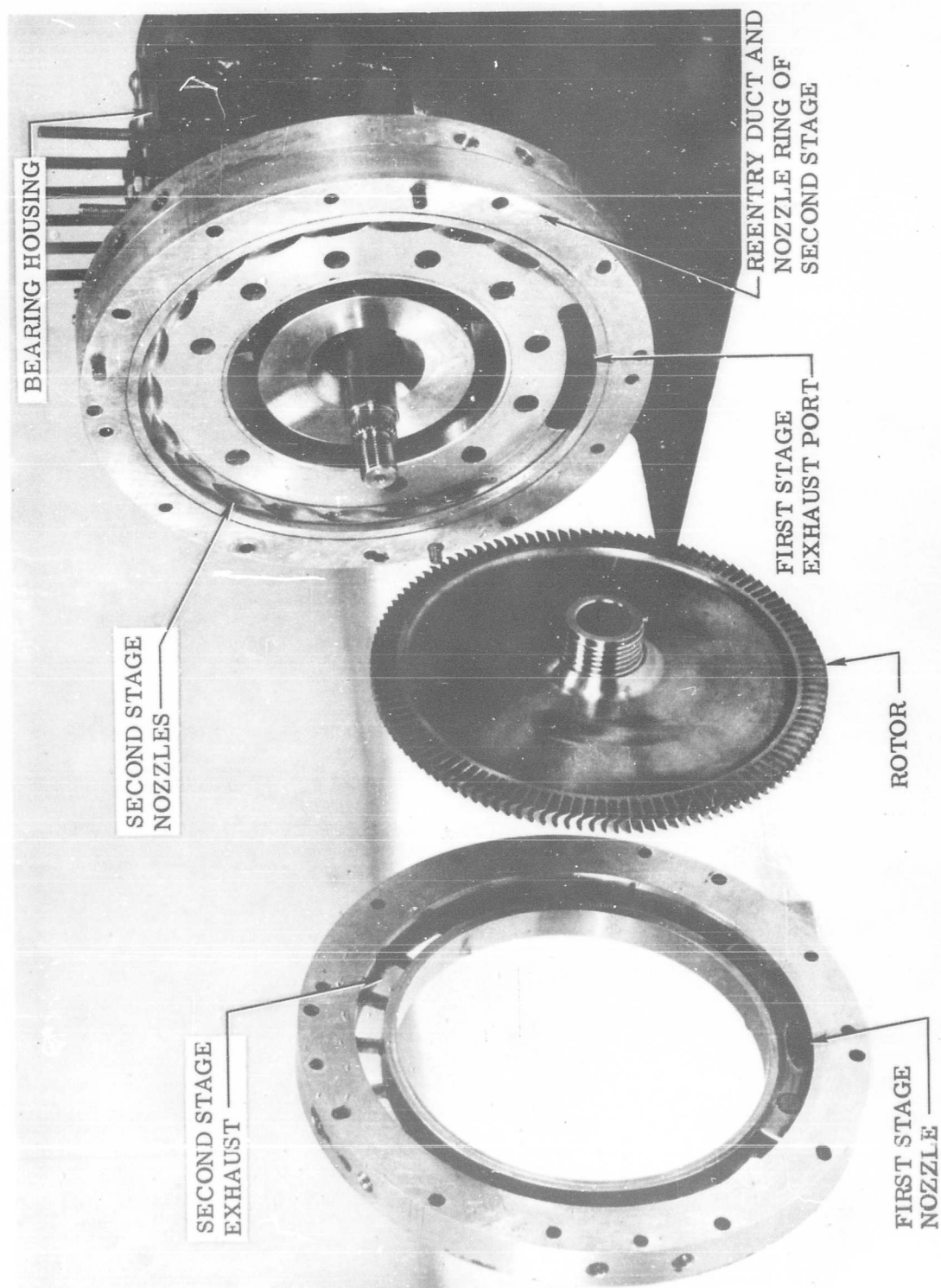


Figure 8. Exploded View of Test Turbine

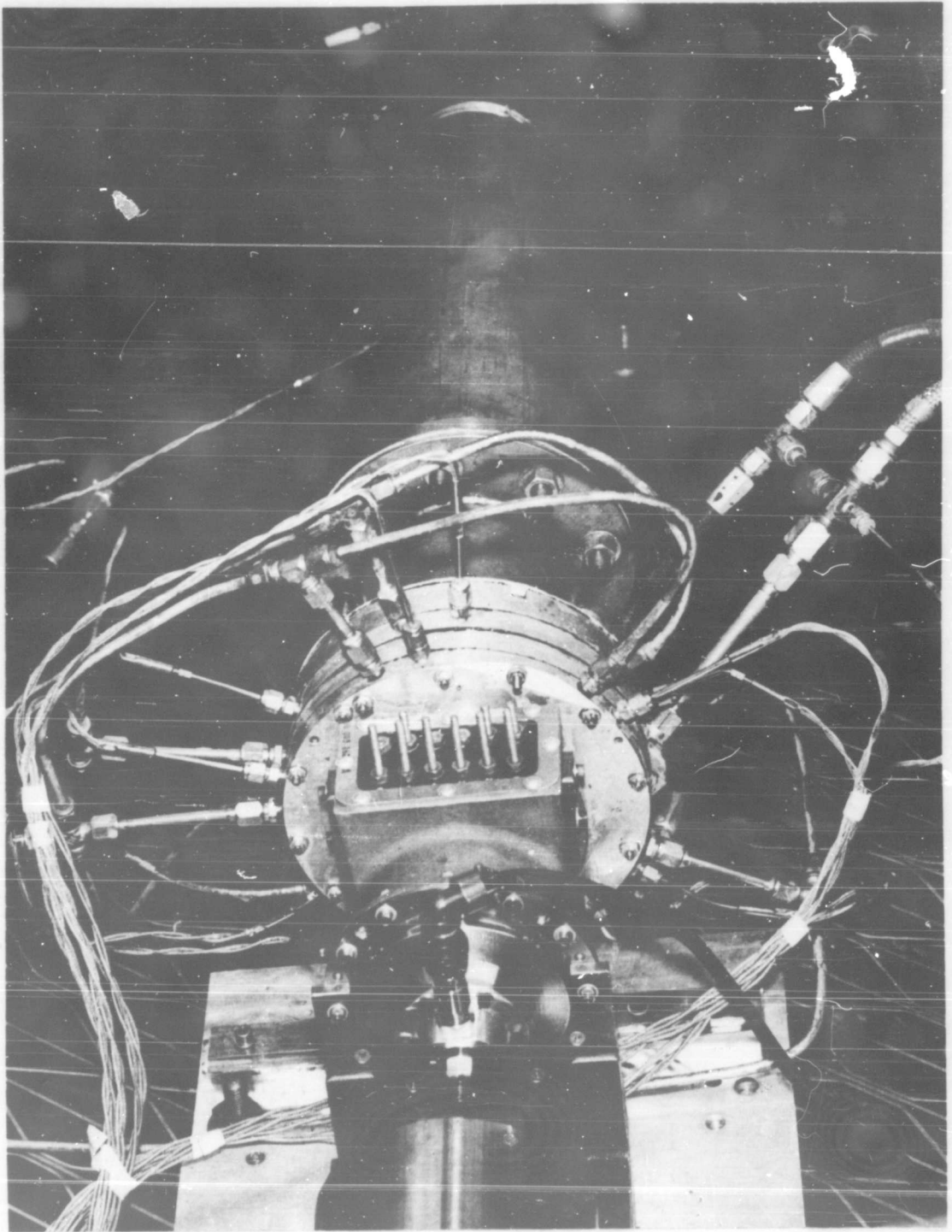


Figure 9. Turbine Installation Within the High Altitude Chamber

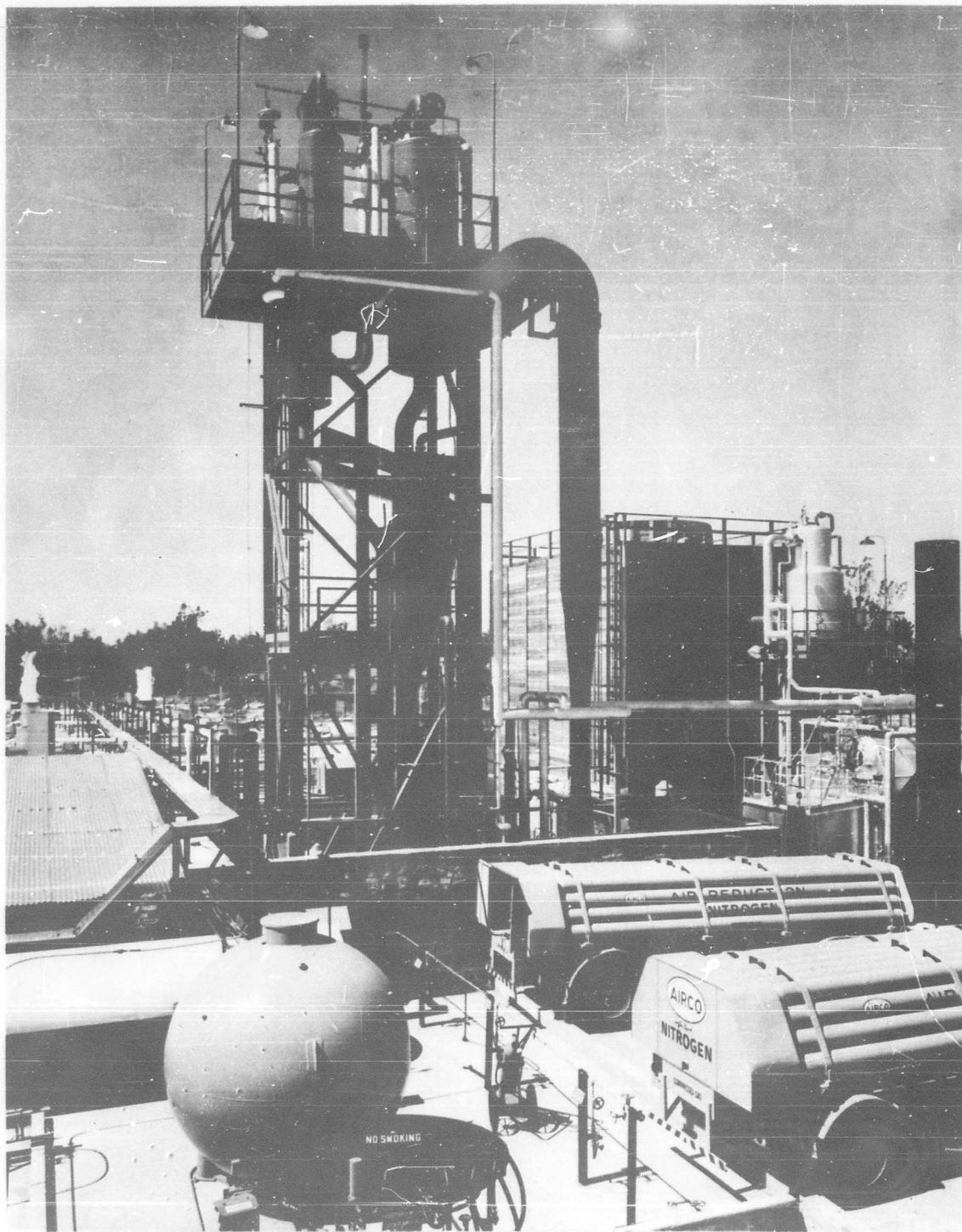


Figure 10. High Altitude Facility at Sundstrand Turbo

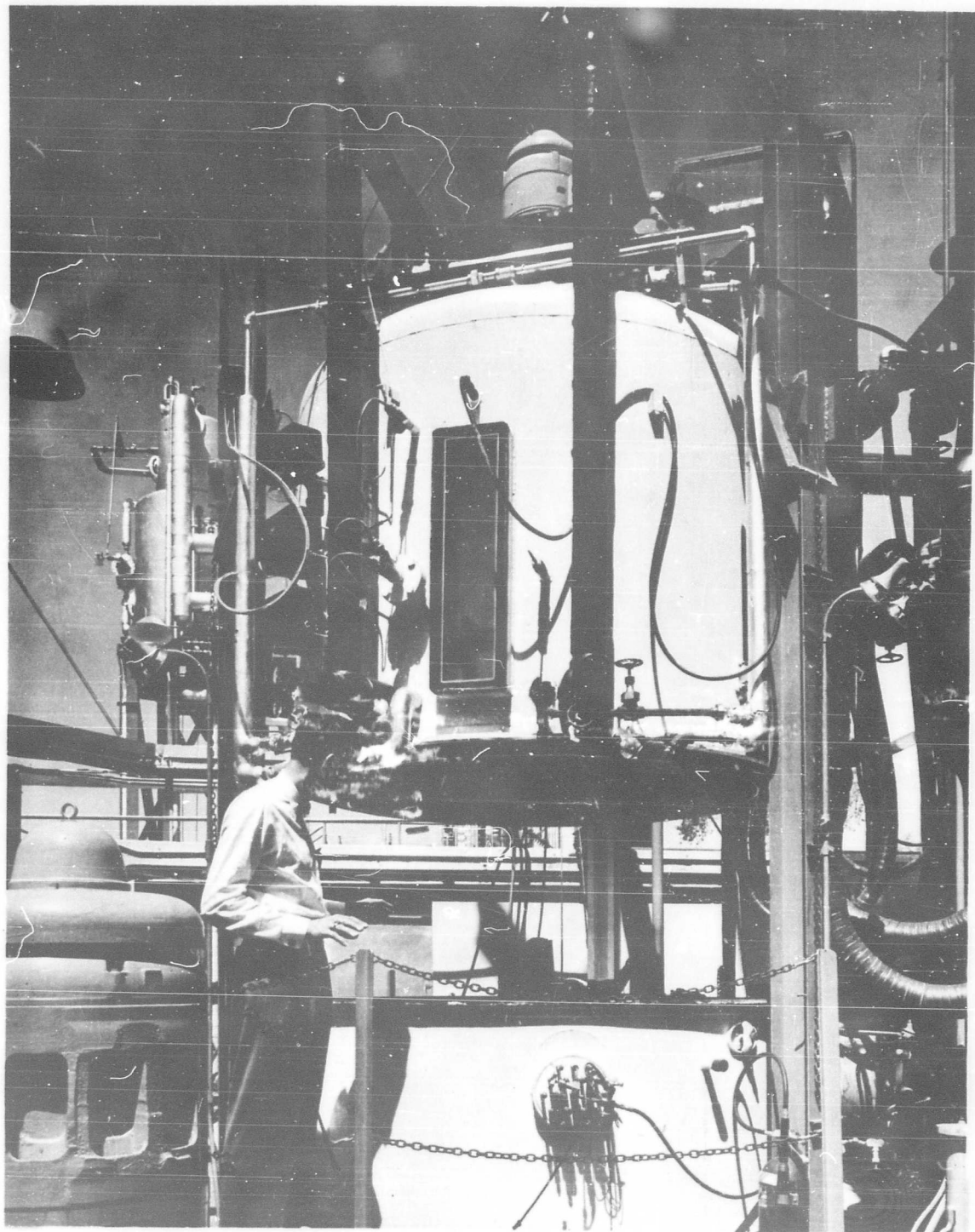


Figure 11. Test Chamber at the High Altitude Facility

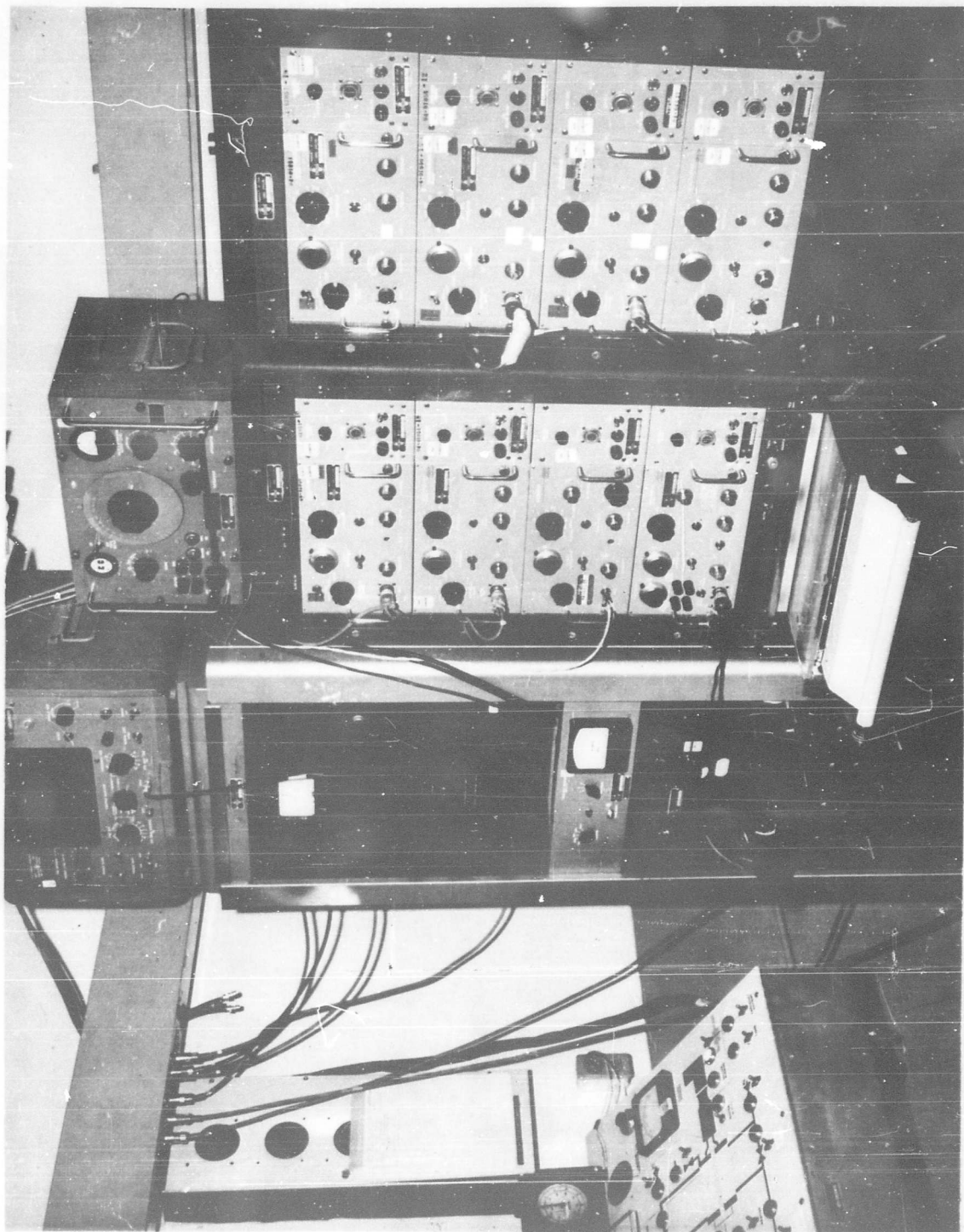


Figure 12. Recording Instruments of High Altitude Facility

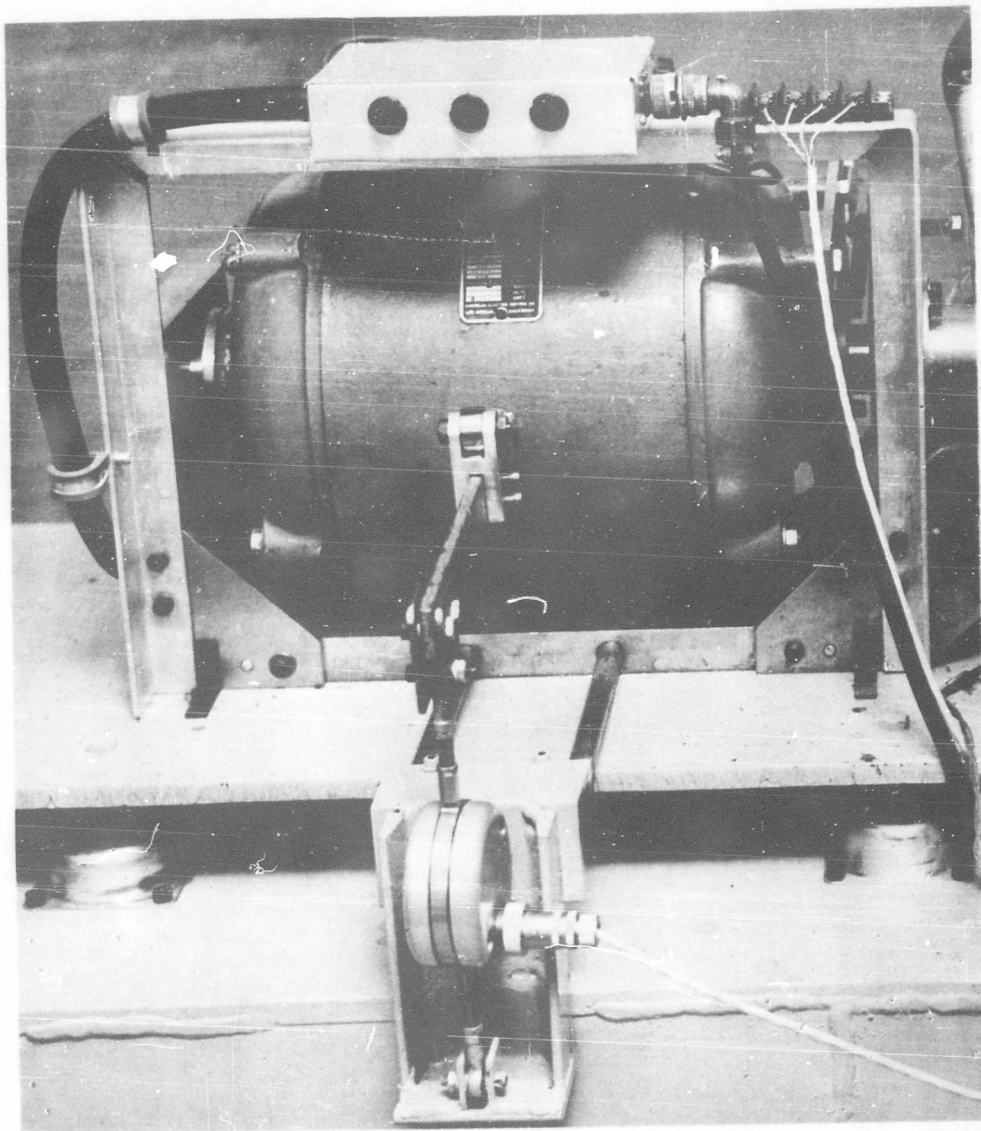
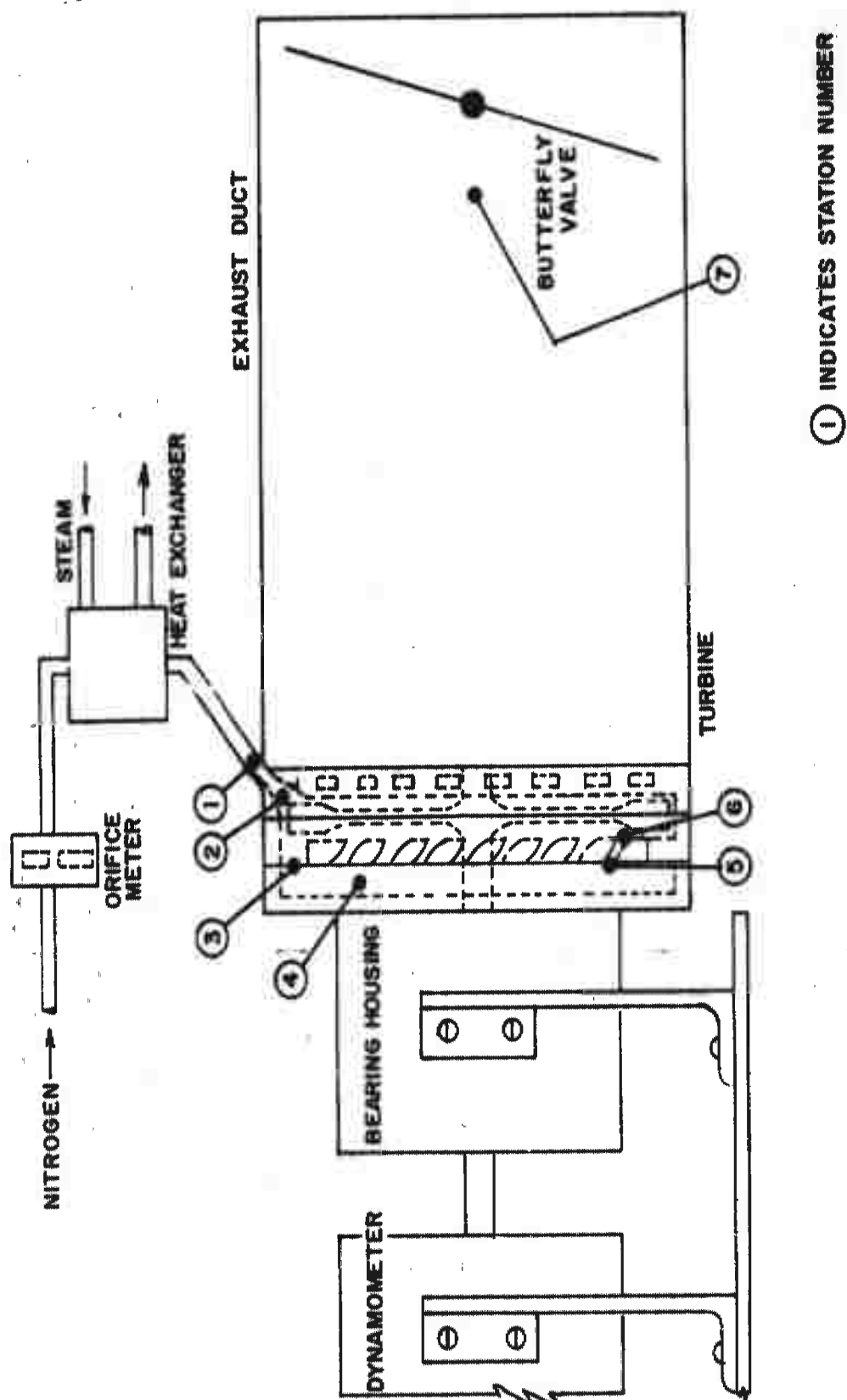


FIGURE 13. DYNAMOMETER WITH TORQUE RING

SUNDSTRAND TURBO
DIVISION OF SUNDSTRAND CORPORATION



SUNDSTRAND TURBO
DIVISION OF SUNDSTRAND CORPORATION

FIGURE 14.
SCHEMATIC—INSTRUMENTATION STATIONS

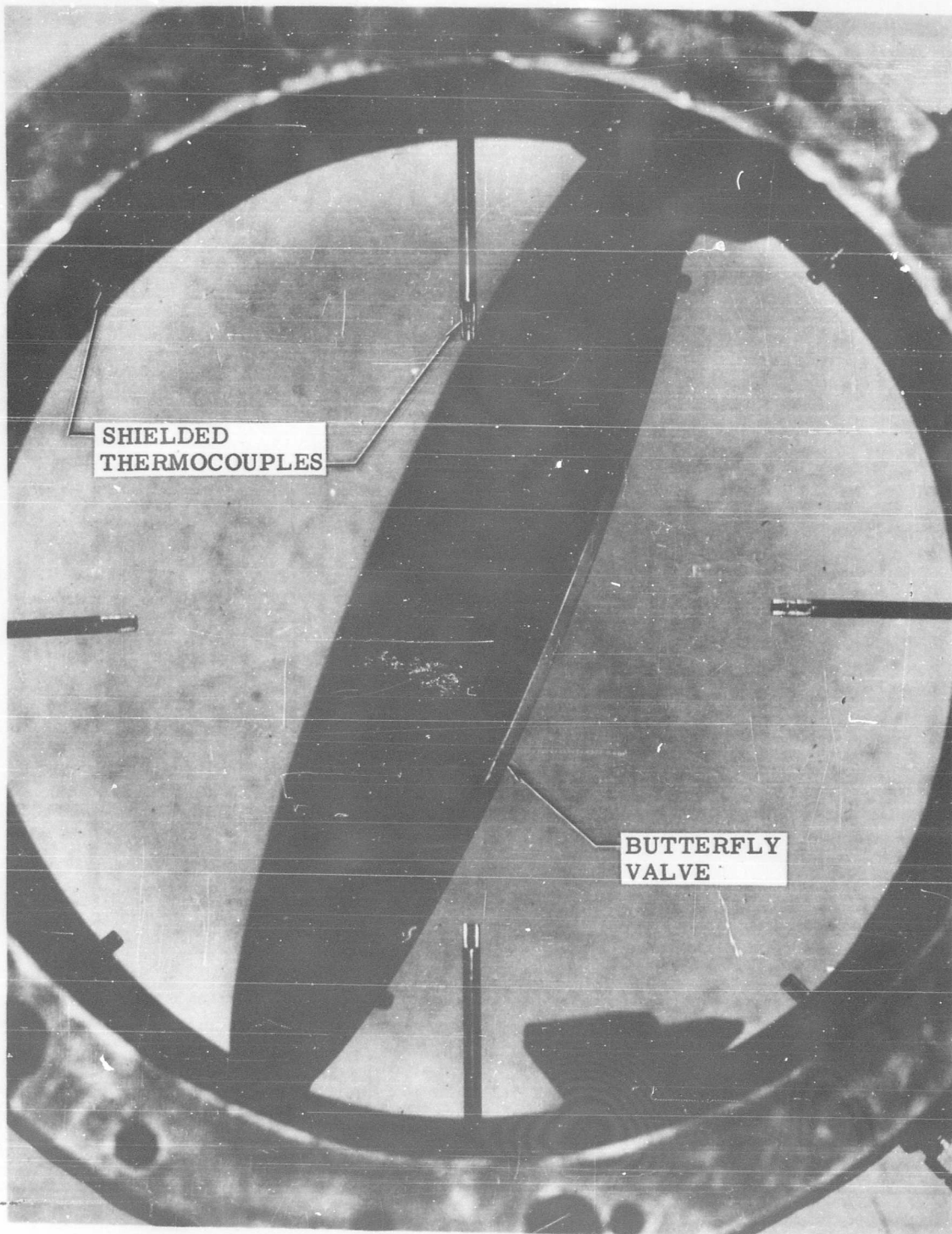


Figure 15. Downstream Measuring Station

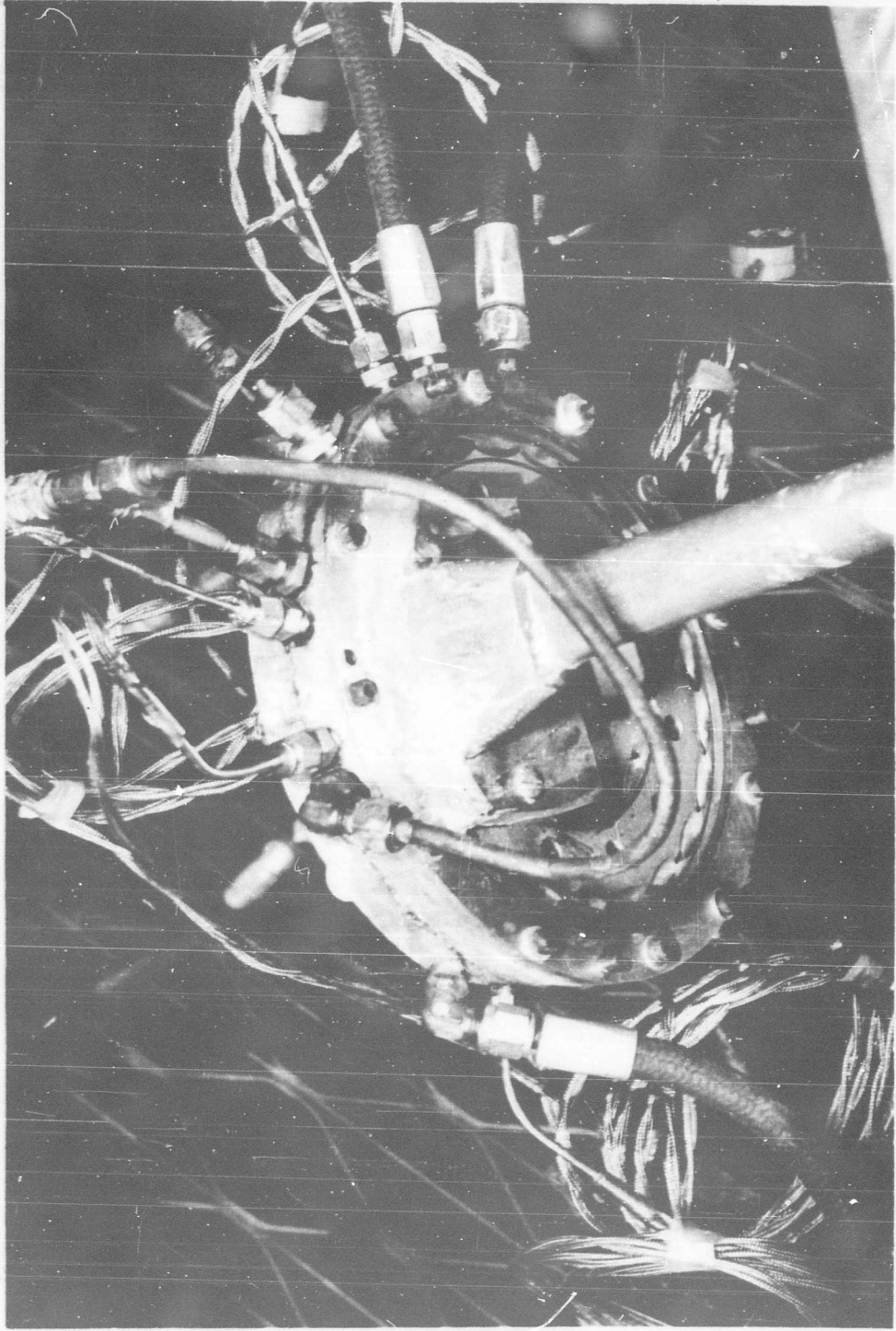


Figure 16. Calibration of Reentry Duct in High Altitude Chamber

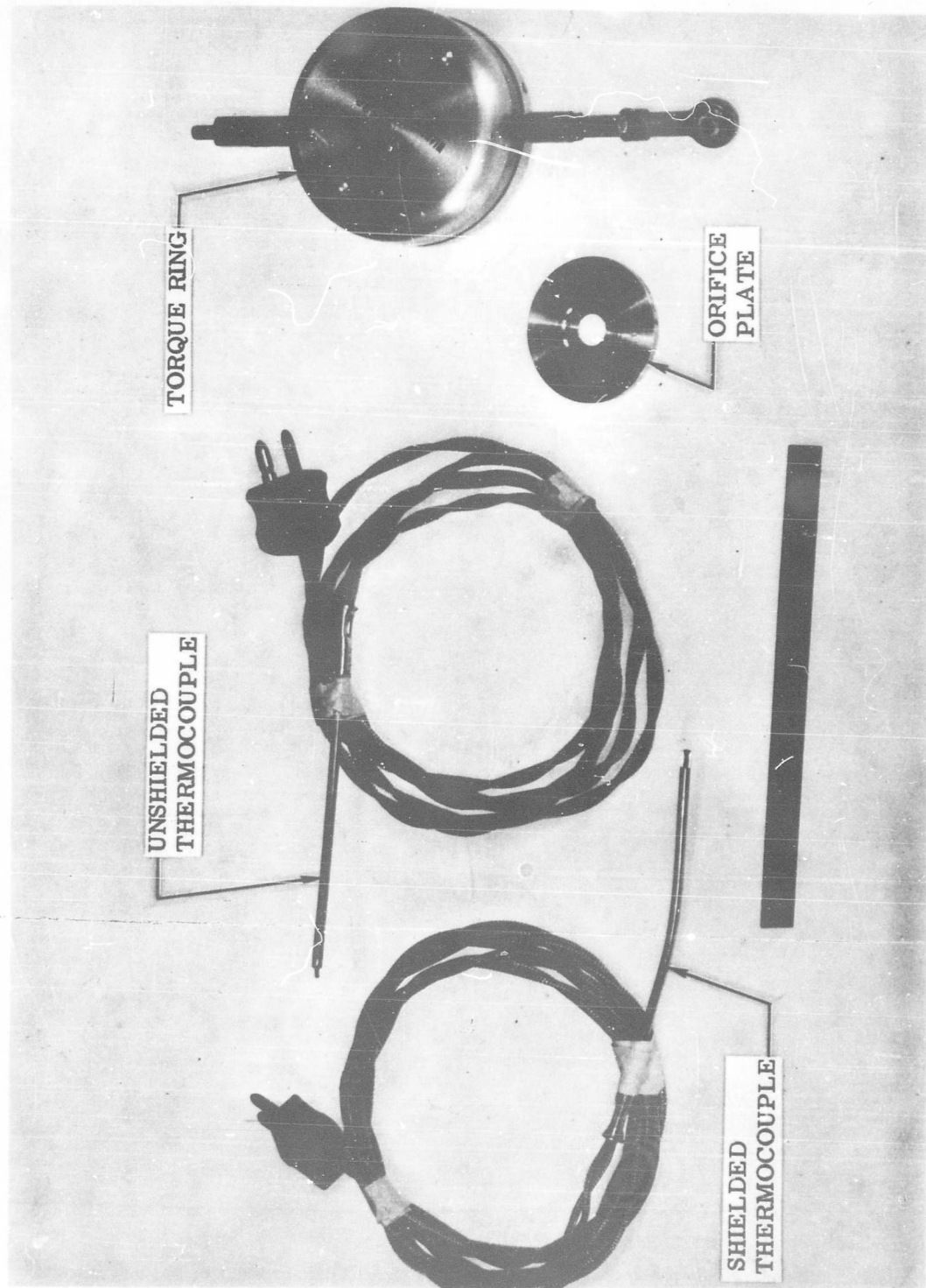


Figure 17. Instrumentation

FIGURE 18

DESCRIPTION OF INSTRUMENTATION

Instrument	Station	Manufacturer		Range	Accuracy % Full Range ASME Power Test Code
Inlet Orifice	0	Barton Instrument Corp.			
		<u>Gage</u>	<u>Transducer</u>		
P ₁	1	Acragage	Wiancko Engr. Co.	0-200 psi	1/2%
P ₂	2	"	"	0-30 psi	"
P ₃	3	"	"	0-30 psi	"
P ₄	3	"	"	0-30 psi	"
P ₅	4	"	"	0-30 psi	"
P ₆	4	"	"	0-30 psi	"
P ₇	4	"	"	0-30 psi	"
P ₈	4	"	"	0-30 psi	"
P ₉	7	"	"	0-5 psi	"
P ₁₀	7	"	"	0-5 psi	"
P ₁₁	7	"	"	0-5 psi	"
P ₁₂	7	"	"	0-5 psi	"
P ₁₃	6	"	"	0-5 psi	"
P ₁₄	7	"	"	0-5 psi	"
T ₀	0			-100 to + 500° F	0.5%
T ₁	1			"	"
T ₃	3	Copper Constantan Unshielded Type Total Tempera- ture measuring		"	"

S/TD No. 1735

30 January 1960
Page 118a

Instrument	Station	Manufacturer		Range	Accuracy % Full Range ASME Power Test Code
Inlet Orifice	0	Barton Instrument Corp.			
		<u>Gage</u>	<u>Transducer</u>		
T ₄	3	"	"	"	"
T ₅	4	"	"	"	"
T ₆	4	"	"	"	"
T ₇	4	"	"	"	"
T ₈	4	"	"	"	"
T ₉	7	"	"	"	"
T ₁₀	7	"	"	"	"
T ₁₁	7	"	"	"	"
T ₁₂	7	"	"	"	"
T ₁₃	Ambient	"	"	"	"
T ₁₄	Ambient	"	"	"	"
Read out		Brown Potentiometer		-200 to + 200°F	0.5%

SUNDSTRAND TURBO
DIVISION OF SUNDSTRAND CORPORATION

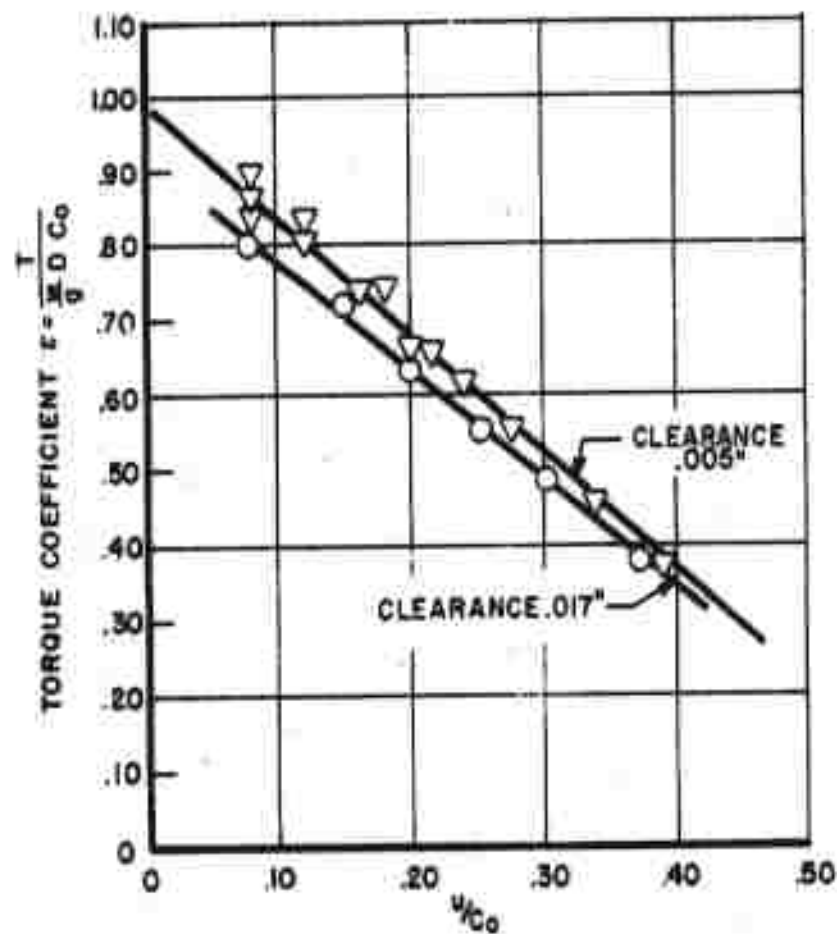


FIGURE 19.
PERFORMANCE OF TWO-STAGE RE-ENTRY TURBINE
FOR PRESSURE RATIO 300:1

SUNDSTRAND TURBO
DIVISION OF SUNDSTRAND CORPORATION

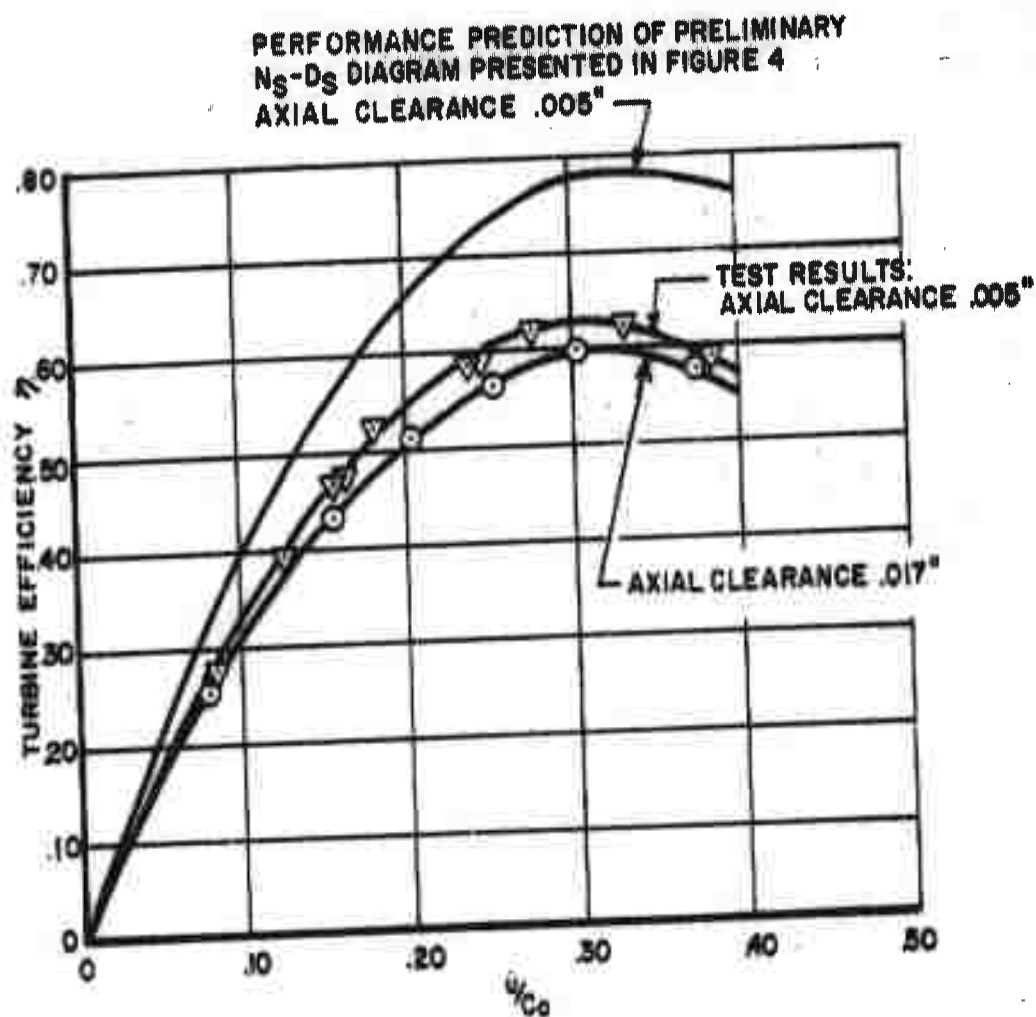


FIGURE 20.
 PERFORMANCE OF TWO-STAGE RE-ENTRY TURBINE
 FOR PRESSURE RATIO $P_r = 300:1$

SUNDSTRAND TURBO
 DIVISION OF SUNDSTRAND CORPORATION

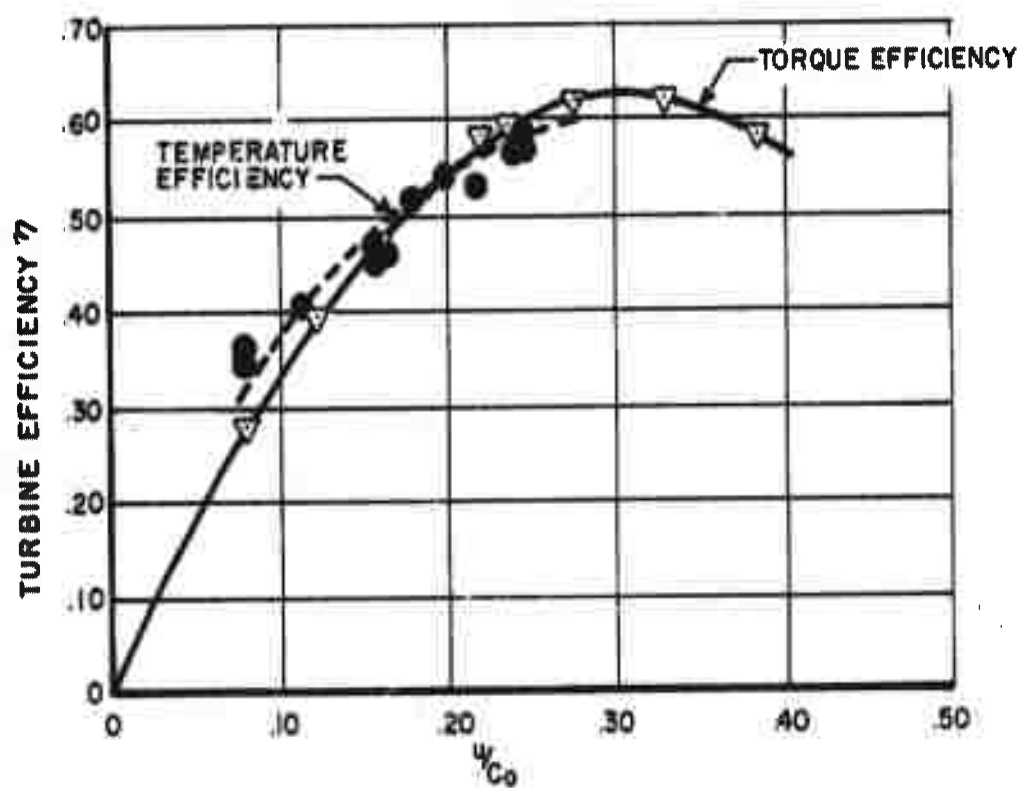


FIGURE 21.
COMPARISON OF TORQUE AND TEMPERATURE EFFICIENCY FOR CLEARANCE
 $C^* = .005''$

SUNDSTRAND TURBO
DIVISION OF SUNDSTRAND CORPORATION

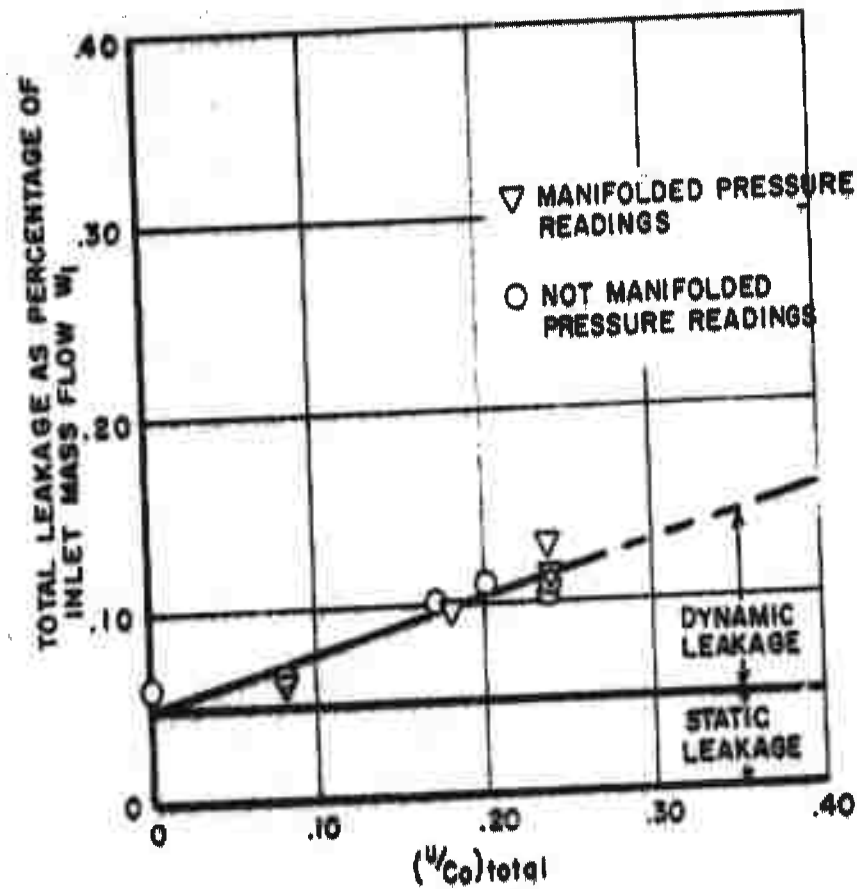


FIGURE 22.
MEASURED LEAKAGE OF TWO-STAGE SINGLE DISK TURBINE
PR: 300:1 CLEARANCE: .005"

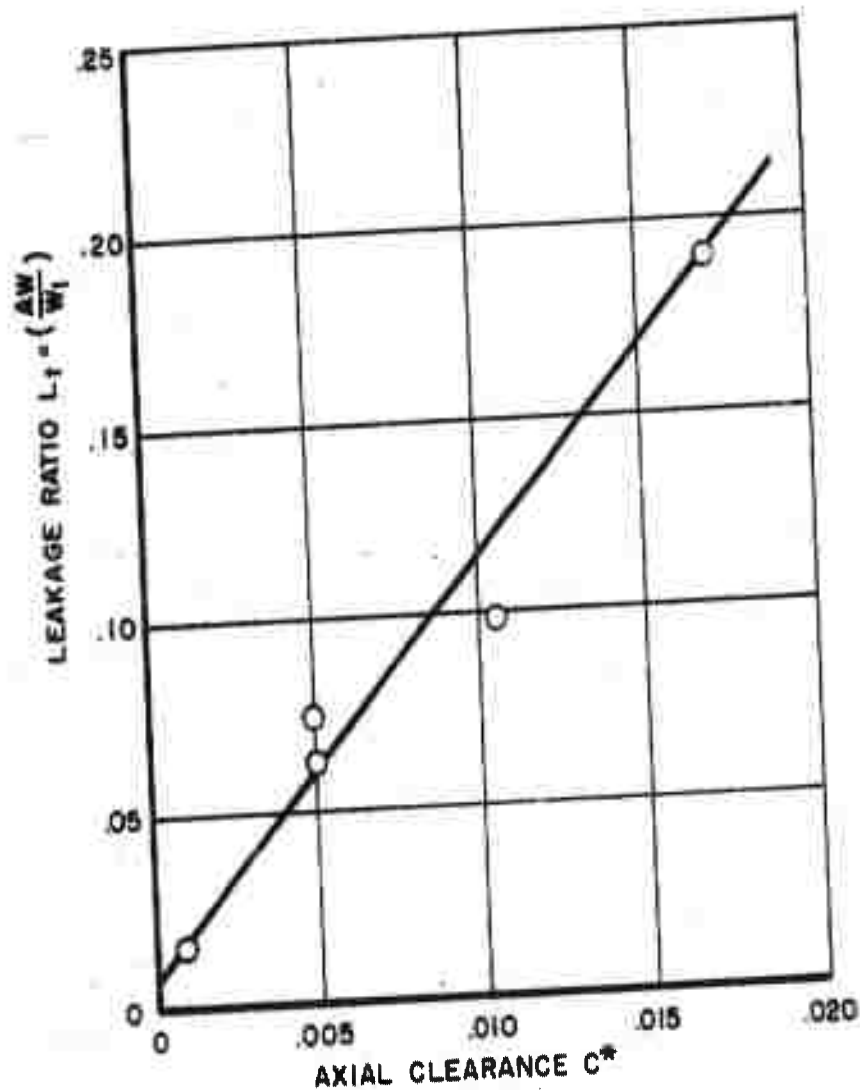


FIGURE 23.
STATIC LEAKAGE OF TWO-STAGE SINGLE DISK TURBINE PR: 300:1

SUNDSTRAND TURBO
DIVISION OF SUNDSTRAND CORPORATION

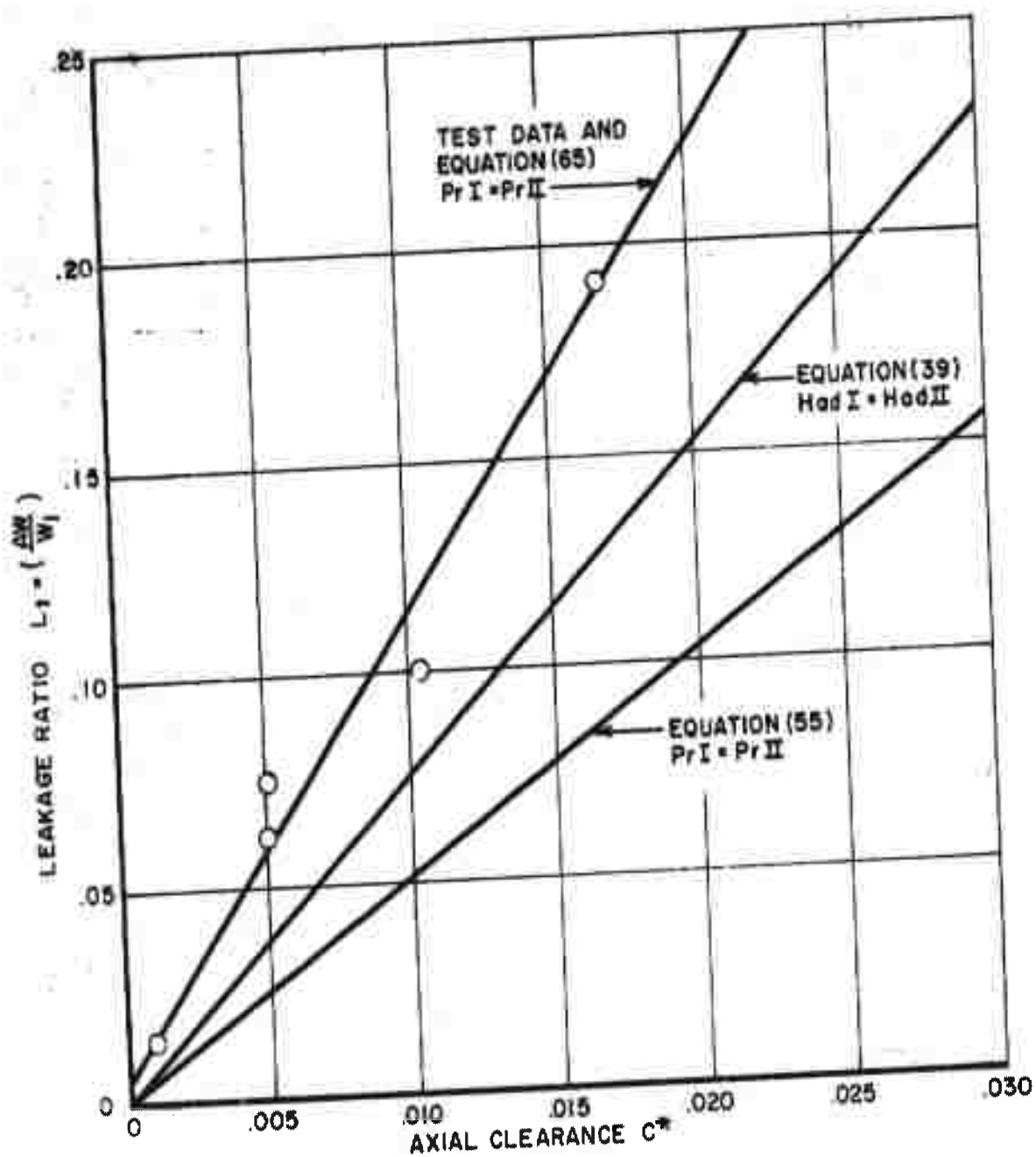


FIGURE 24.
COMPARISON OF MEASURED AND PREDICTED STATIC LEAKAGE

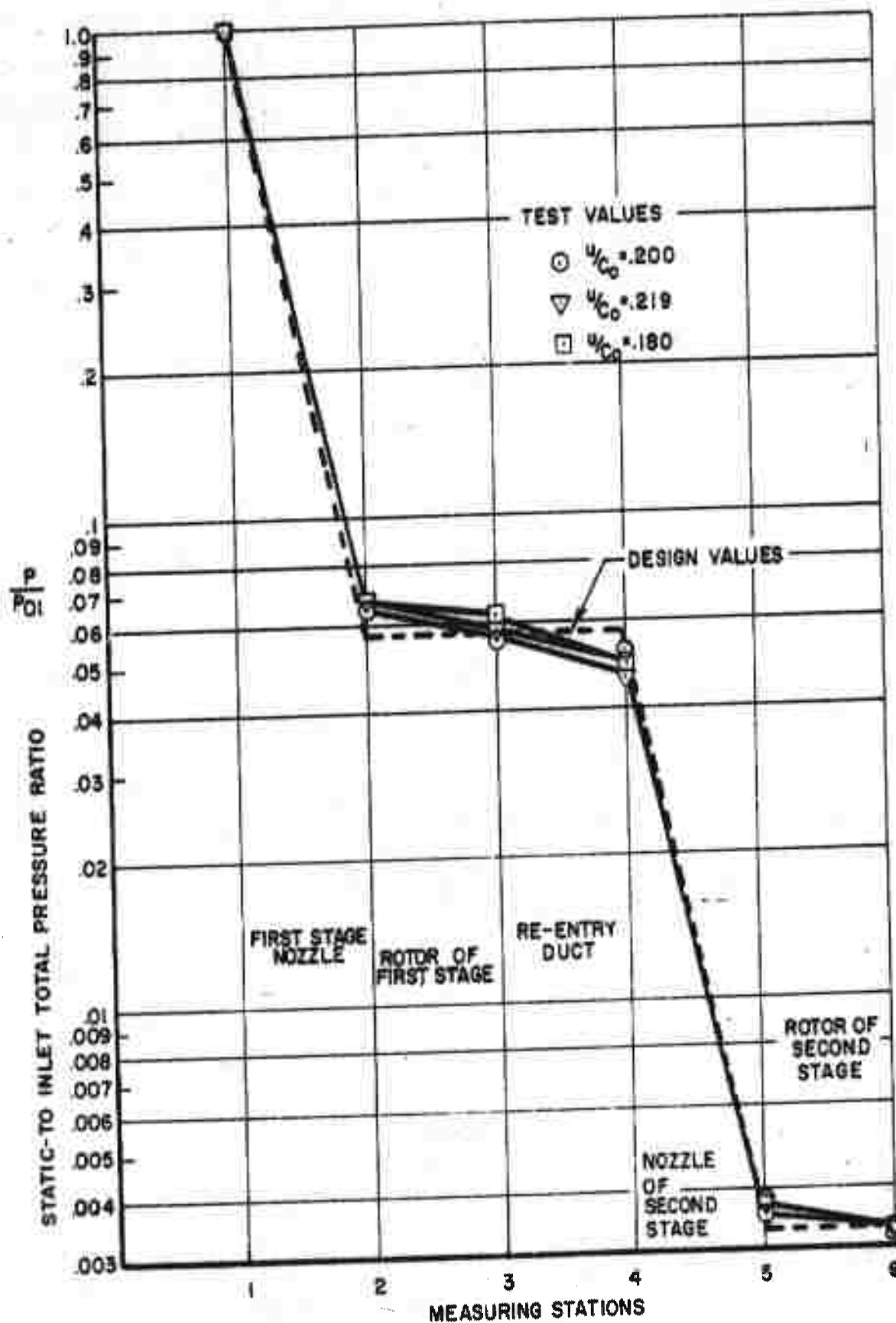


FIGURE 25.
 STATIC PRESSURE VARIATION INSIDE TURBINE NEAR DESIGN POINT
 $u/c_0 = .20$ AT DESIGN PRESSURE RATIO $P_r = 300:1$

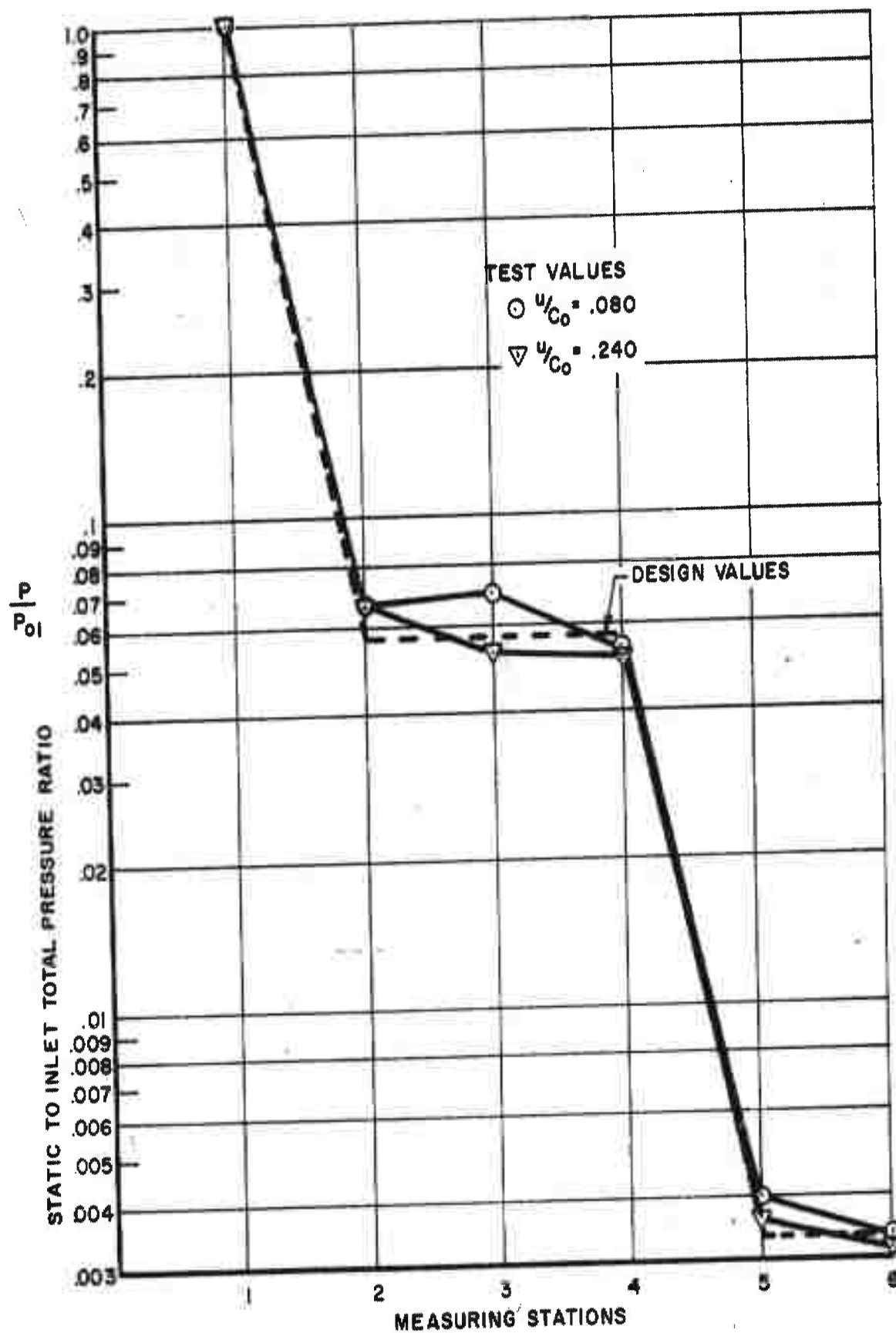


FIGURE 26.
 STATIC PRESSURE VARIATION INSIDE TURBINE FOR OFF-DESIGN
 CONDITIONS $u/c_0 = .080$ & $u/c_0 = .240$ AT PRESS. RATIO 300:1

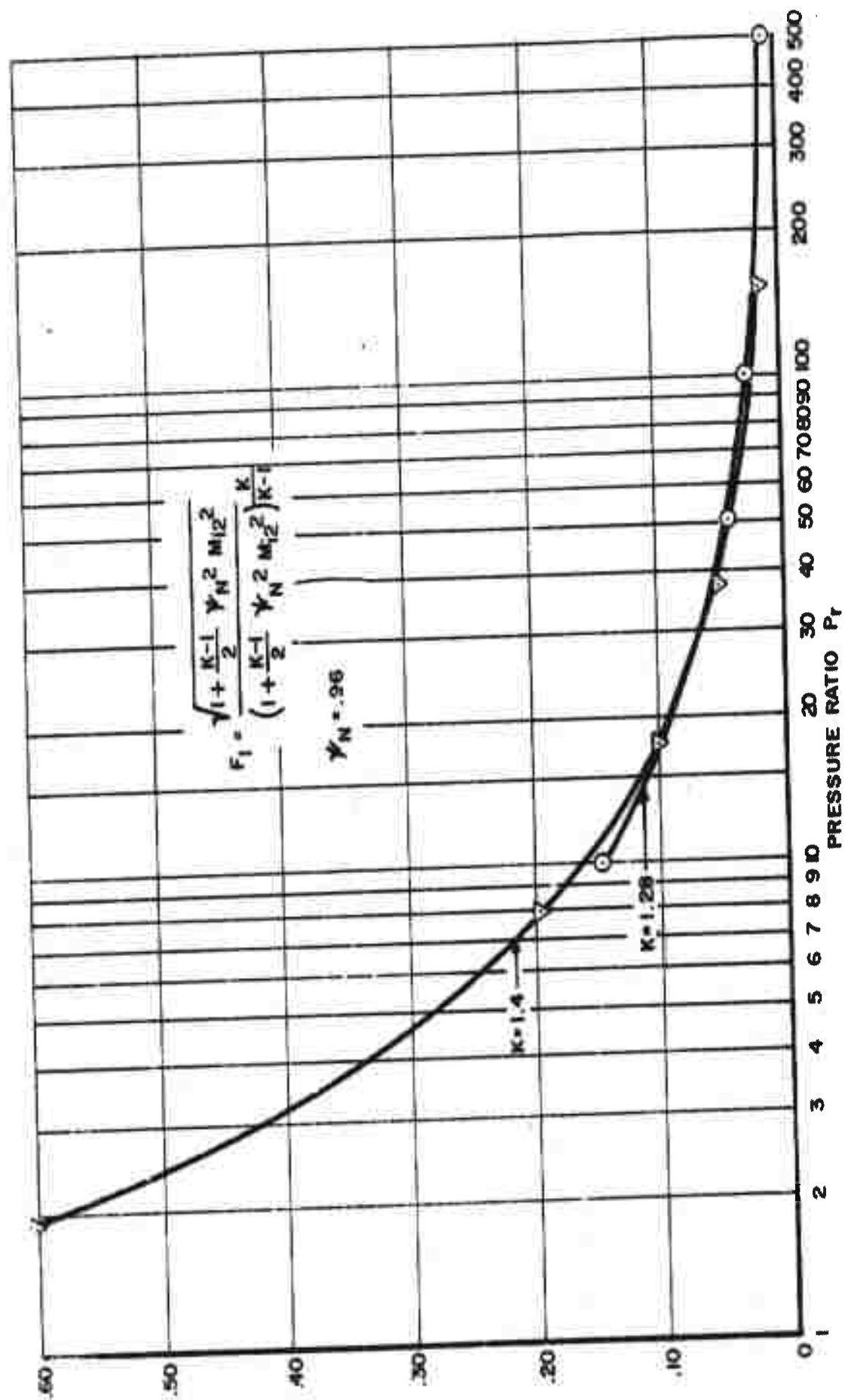


FIGURE 27.
STATIC LEAKAGE FUNCTION F_1

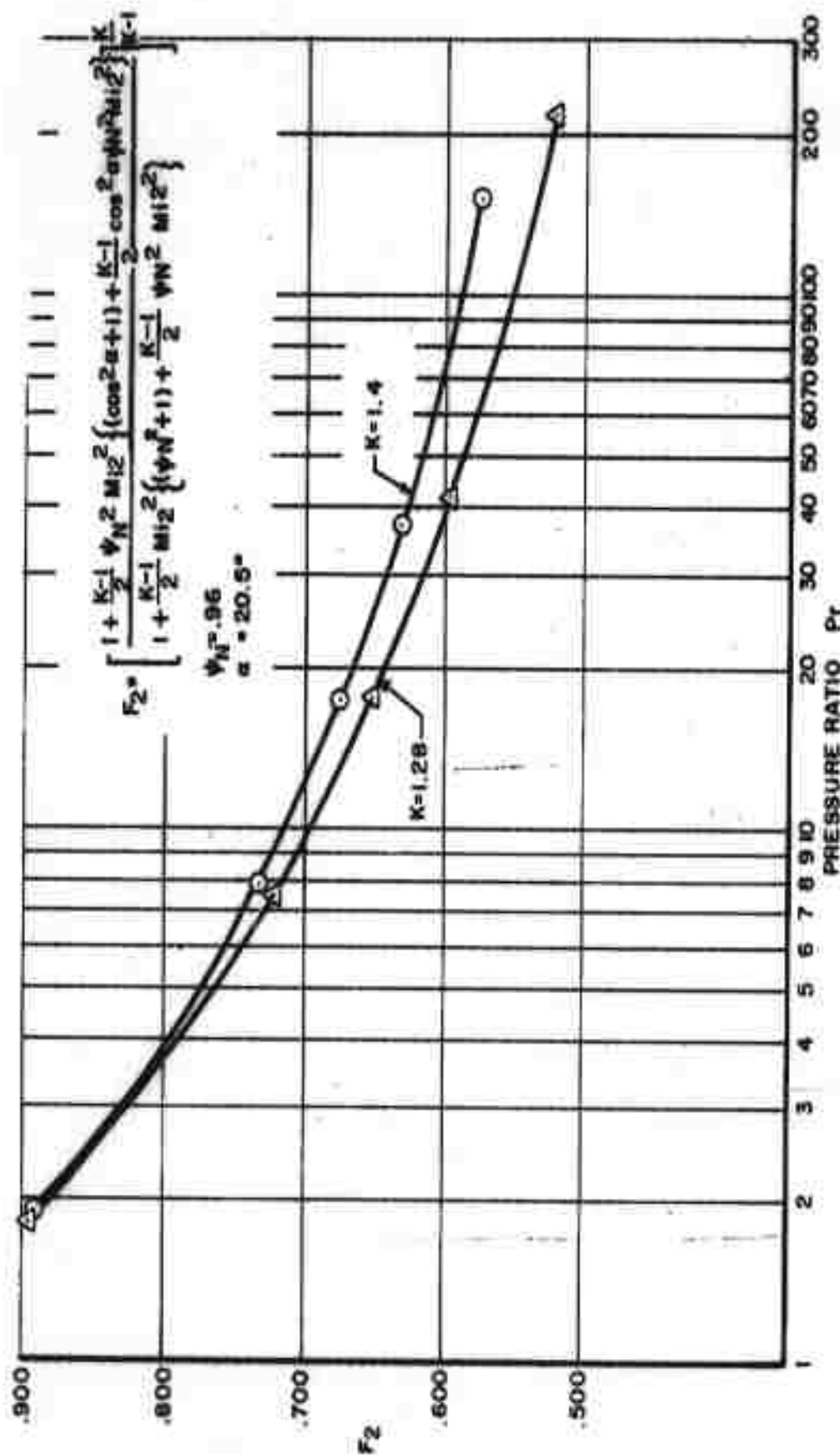


FIGURE 28.
TOTAL LEAKAGE FUNCTION F_2

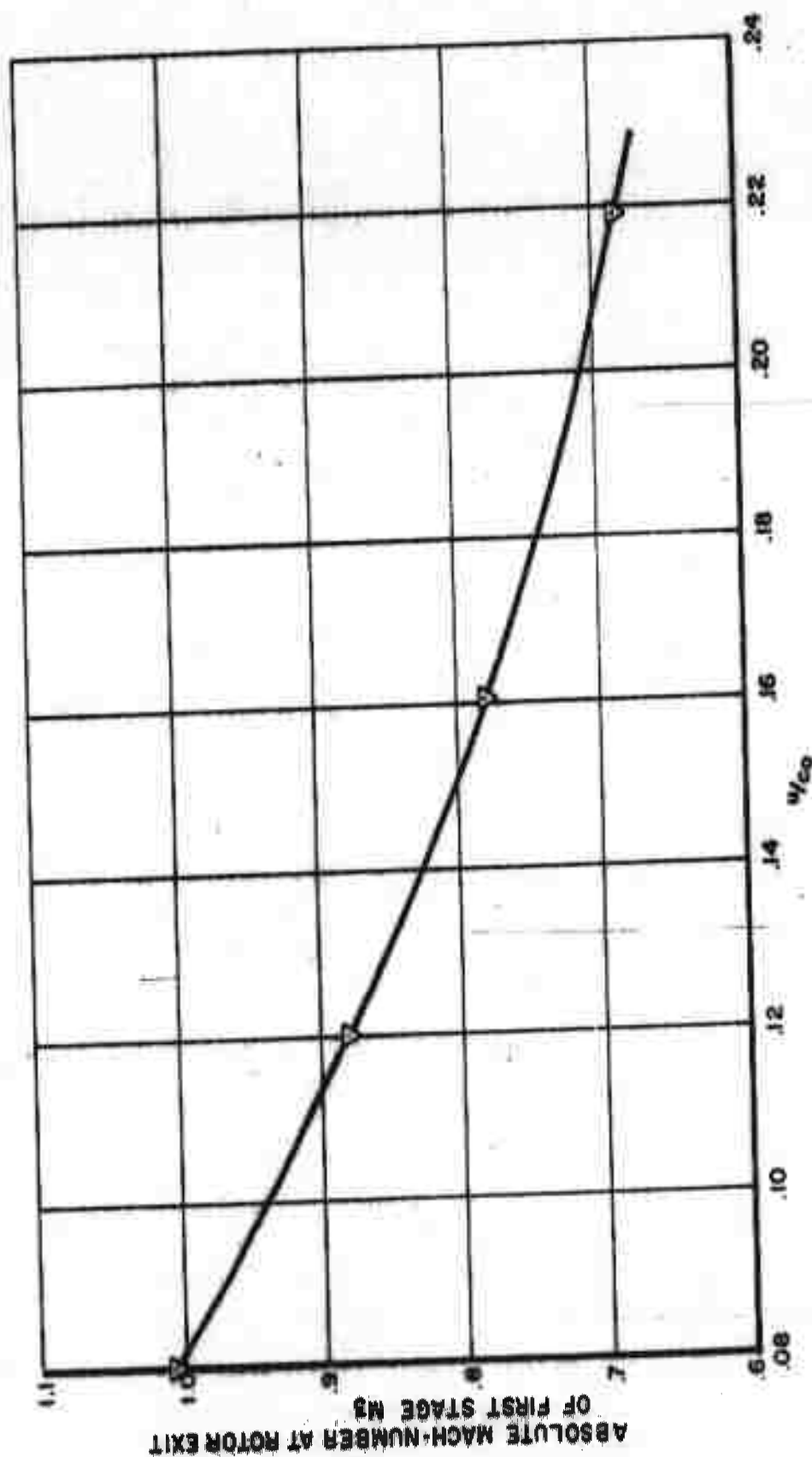


FIGURE 29.
ABSOLUTE MACH-NUMBER AT ROTOR EXIT OF FIRST STAGE M_3 vs. u/c_o

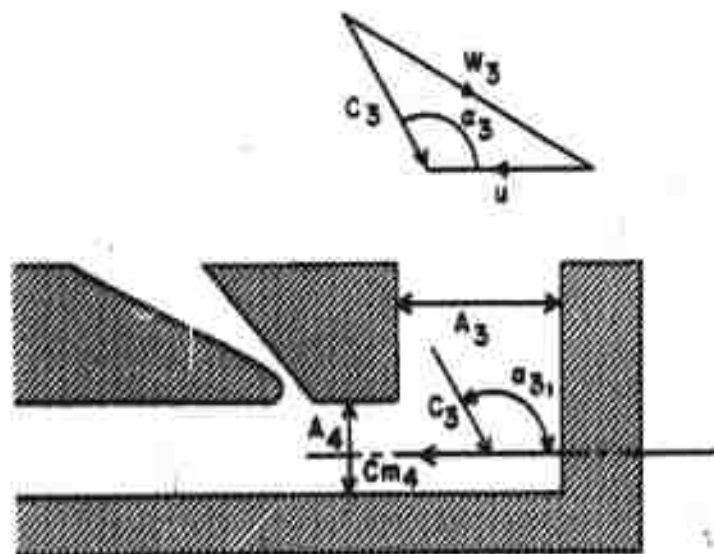


FIGURE 30.
ILLUSTRATION OF TURNING LOSS
AT INLET TO RE-ENTRY DUCT

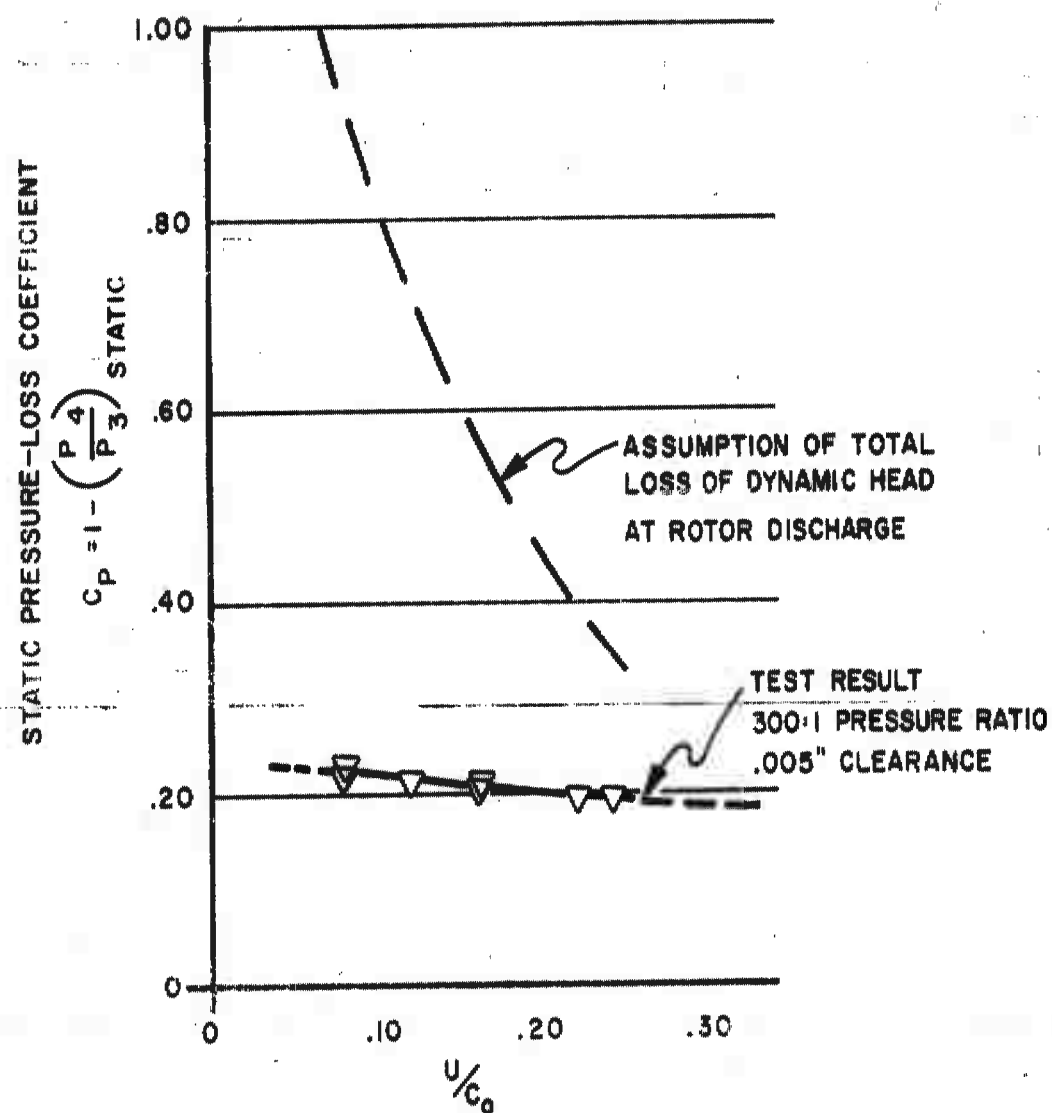


FIGURE 31.
DUCT LOSS OF RE-ENTRY STAGE

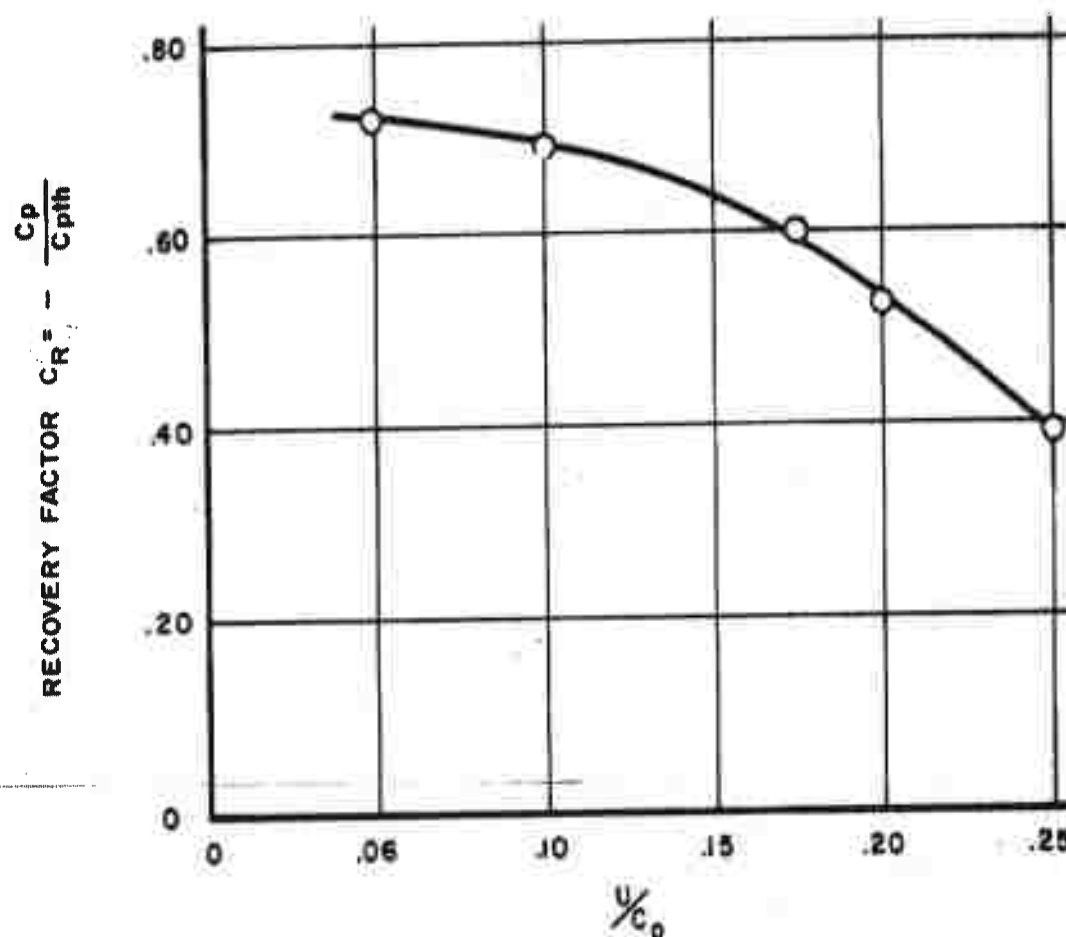


FIGURE 32
RECOVERY OF ROTOR DISCHARGE
TOTAL PRESSURE IN RE-ENTRY DUCT
PR = 300:1 $C^* = .005''$

SUNDSTRAND TURBO
DIVISION OF SUNDSTRAND CORPORATION

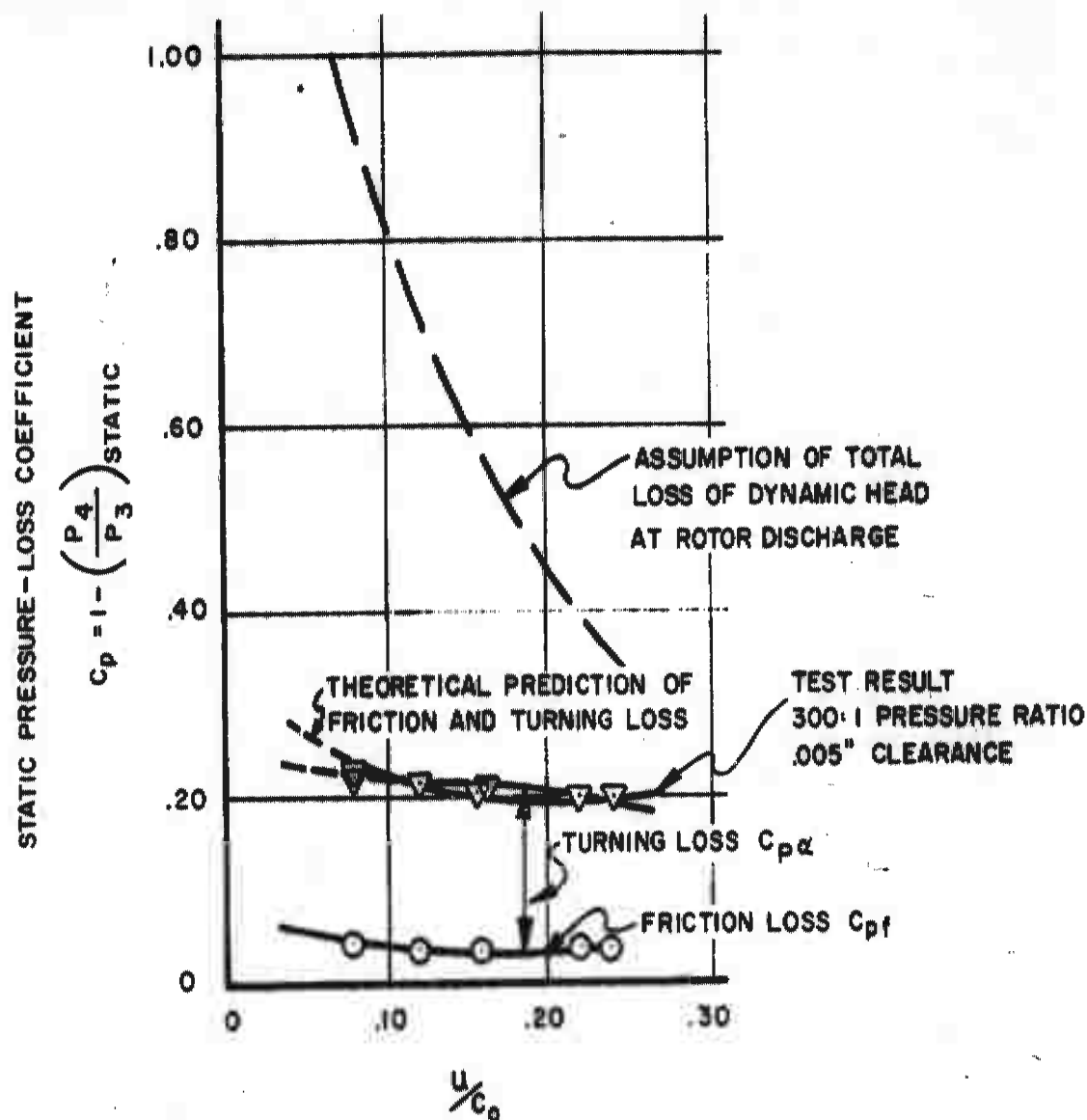


FIGURE 33
DUCT-LOSS OF RE-ENTRY STAGE

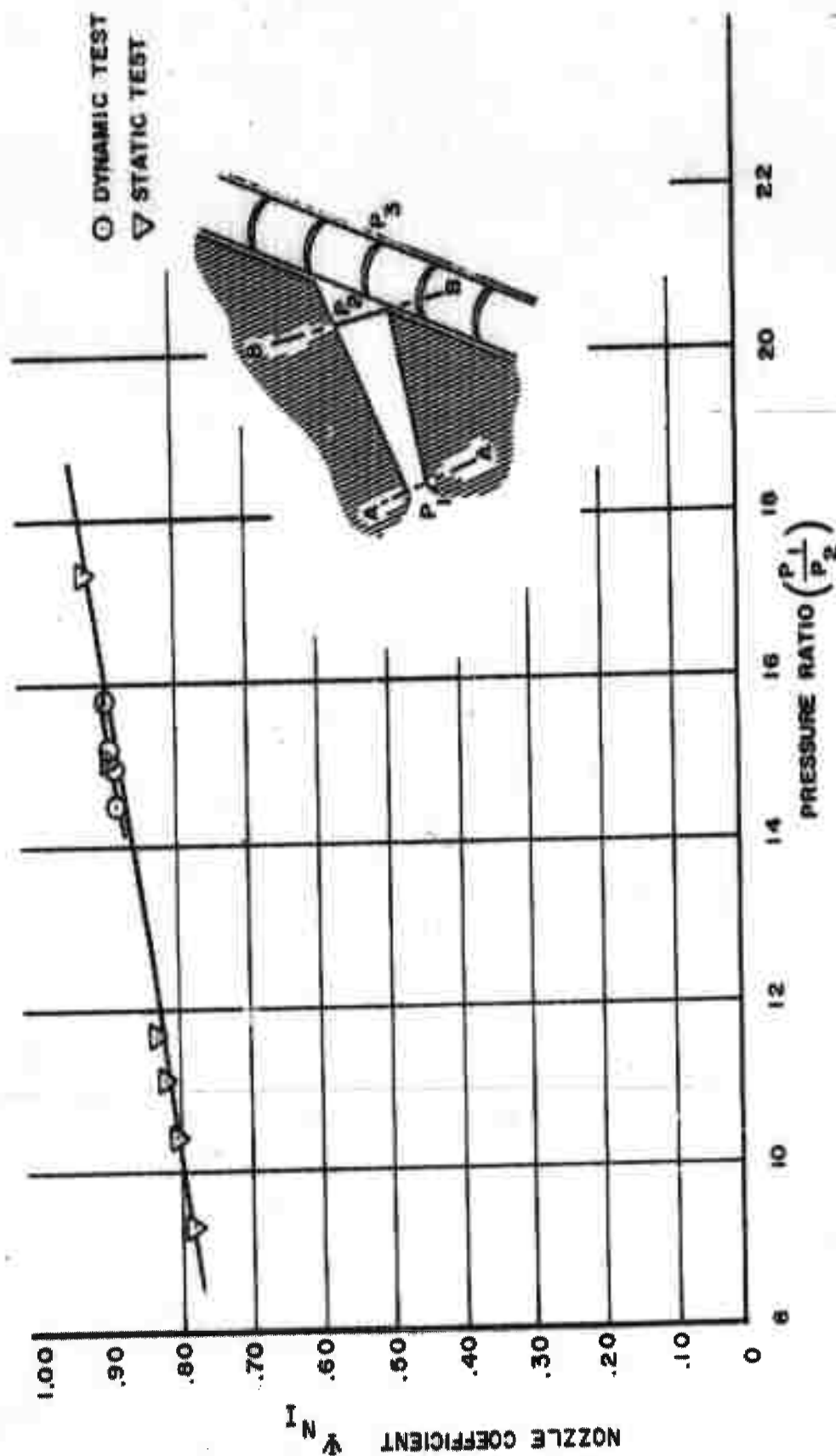


FIGURE 34.
 NOZZLE COEFFICIENT OF FIRST STAGE
 $R_0 = 1 \times 10^5 - 5 \times 10^5$

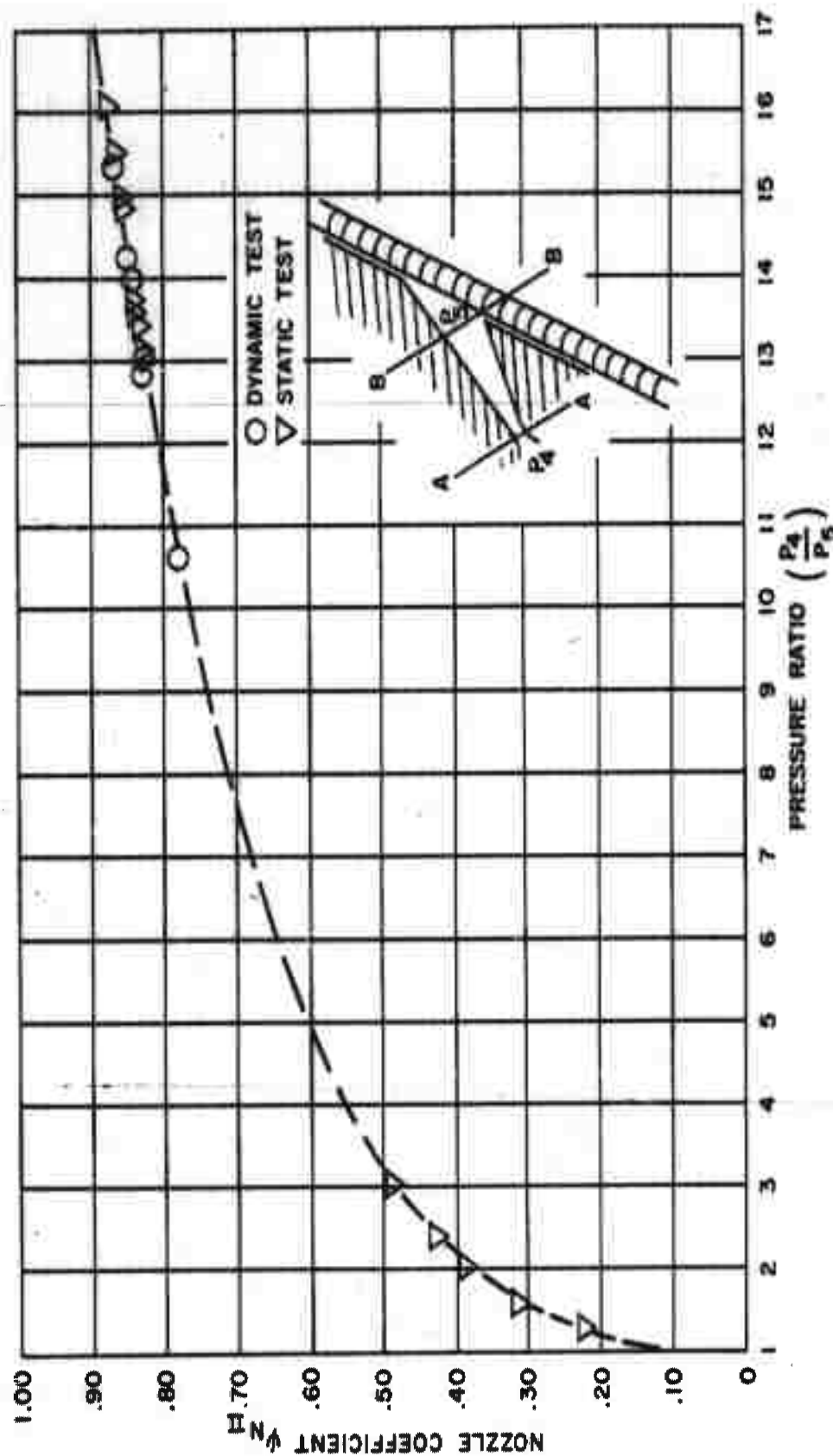


FIGURE 35
NOZZLE COEFFICIENT OF SECOND STAGE
 $Re = 3 \times 10^4 \rightarrow 1.2 \times 10^5$

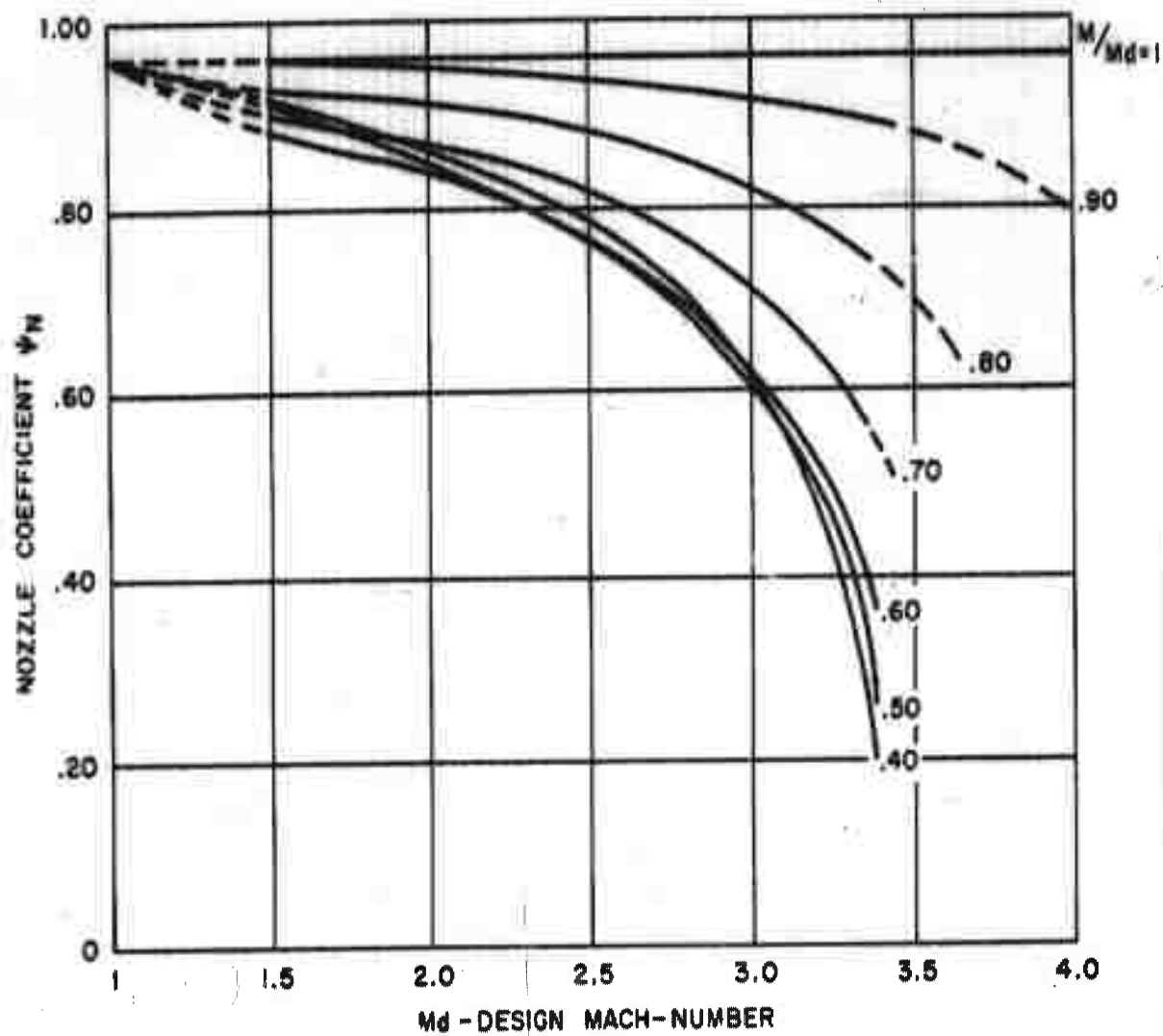


FIGURE 36
PREDICTED NOZZLE COEFFICIENTS
OF REFERENCE (5)

—— DESIGN VELOCITY TRIANGLE
 ---- OFF-DESIGN VELOCITY TRIANGLE

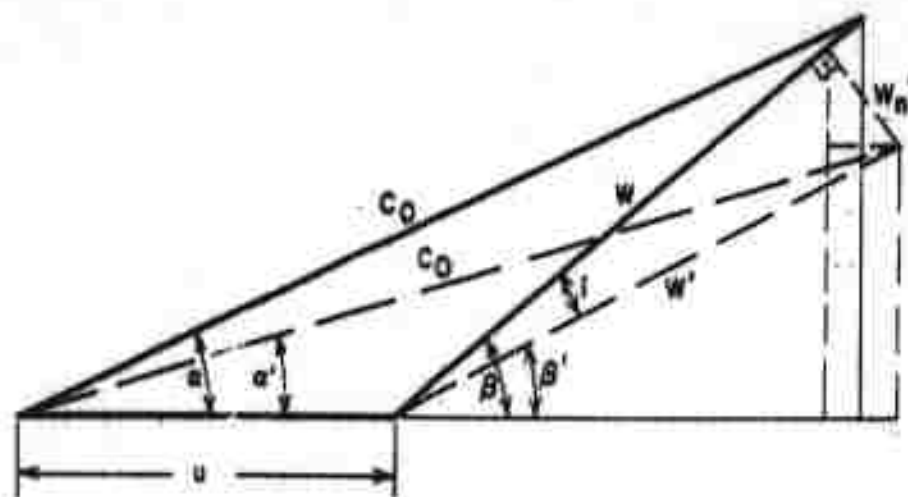


FIGURE 37
 ILLUSTRATION OF INCIDENCE
 LOSS FOR ψ_{c_0} CONSTANT

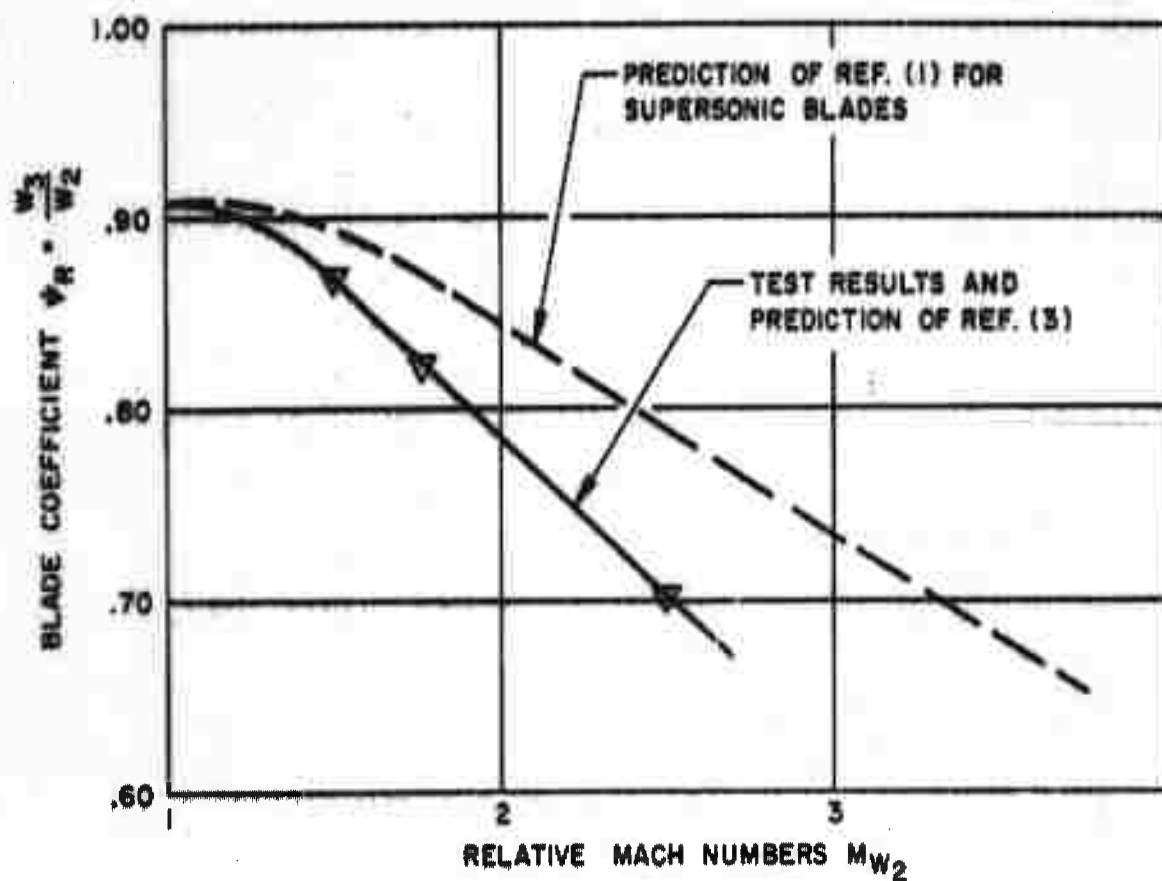


FIGURE 38
MACH NUMBER RELATION FOR
 $\beta = 30^\circ$ SUBSONIC BLADES

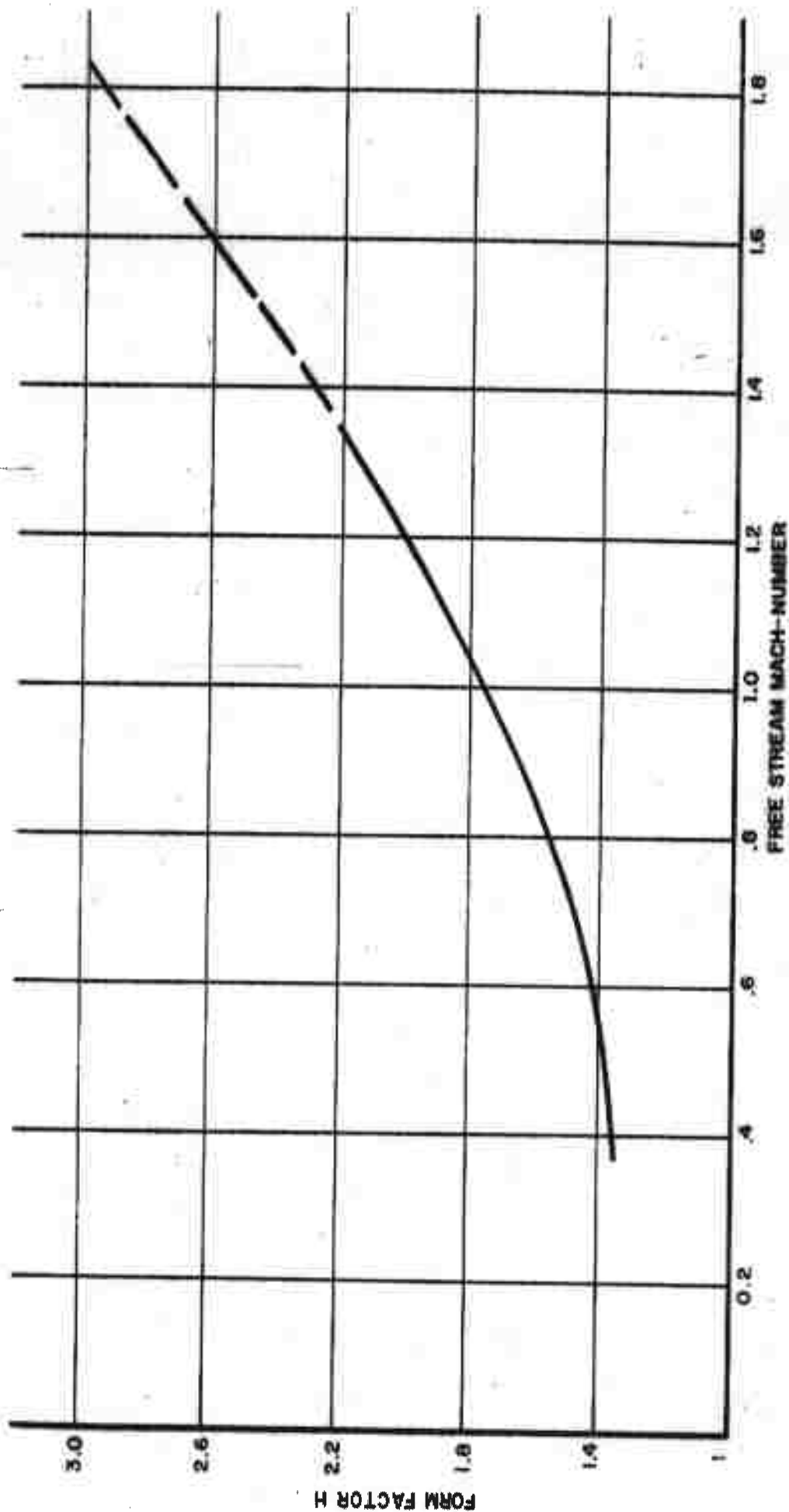


FIGURE 39
FORM FACTOR VERSUS FREE-STREAM MACH NUMBER

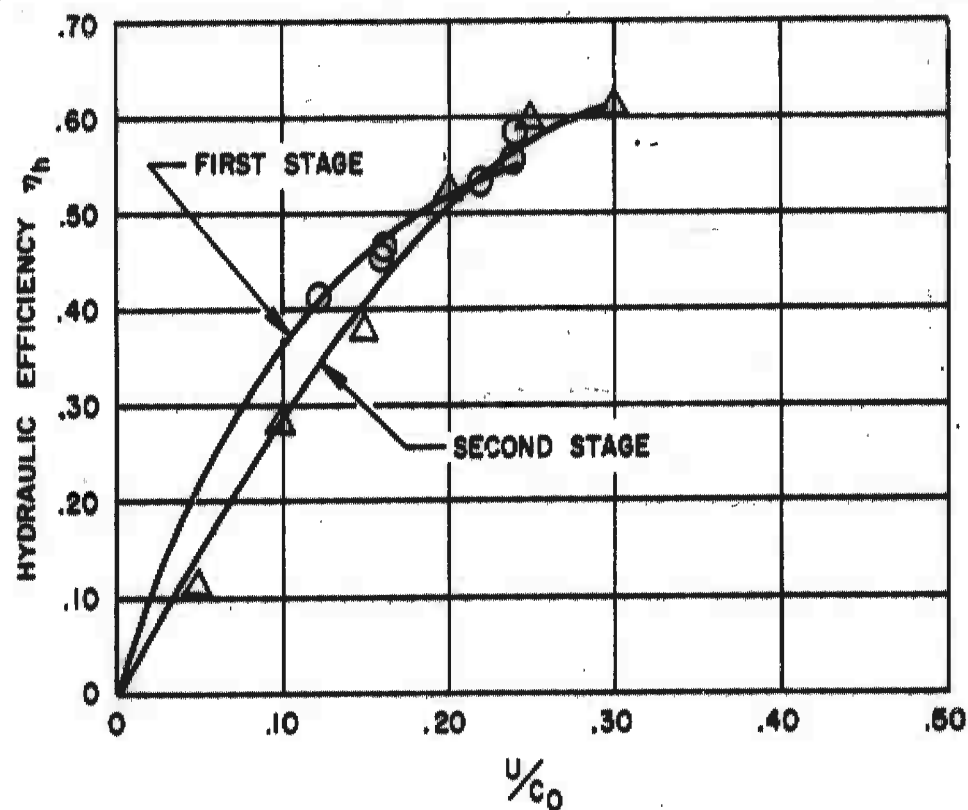


FIGURE 40
STAGE PERFORMANCE OF TWO-STAGE
RE-ENTRY TURBINE FOR PRESSURE
RATIO 300:1 AND AXIAL CLEARANCE $C^* = .005''$

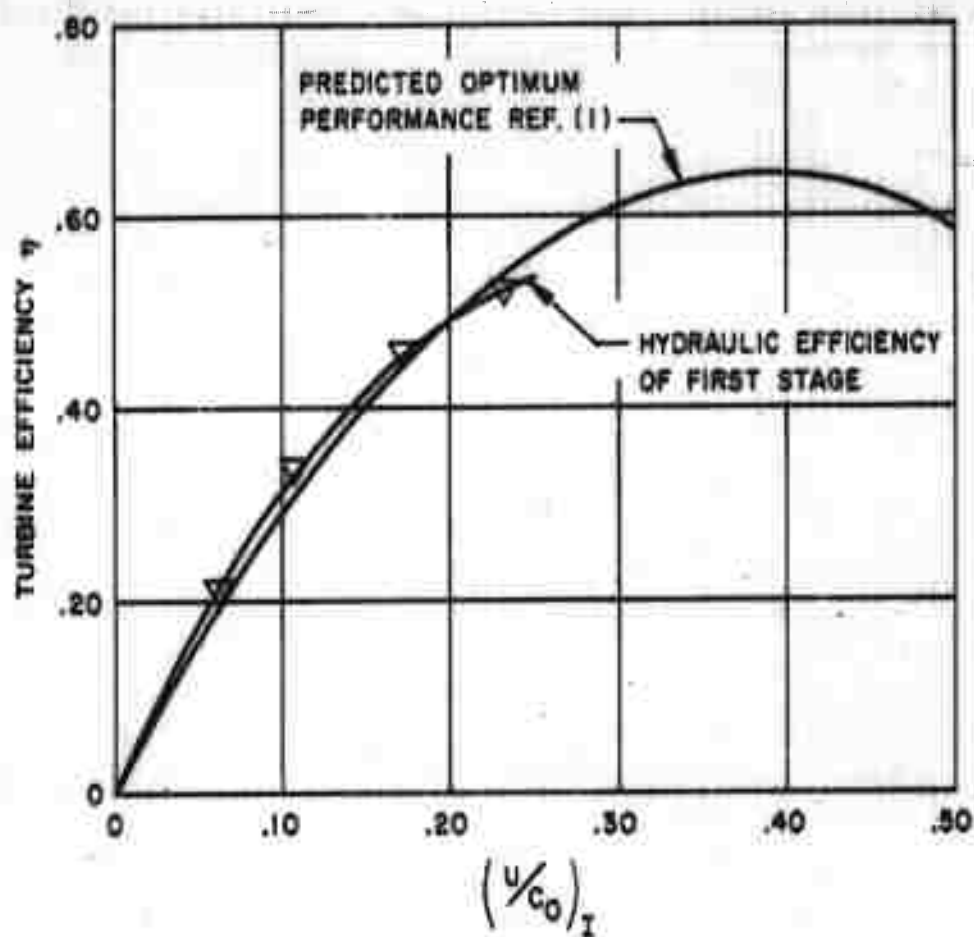


FIGURE 41
PERFORMANCE OF FIRST STAGE

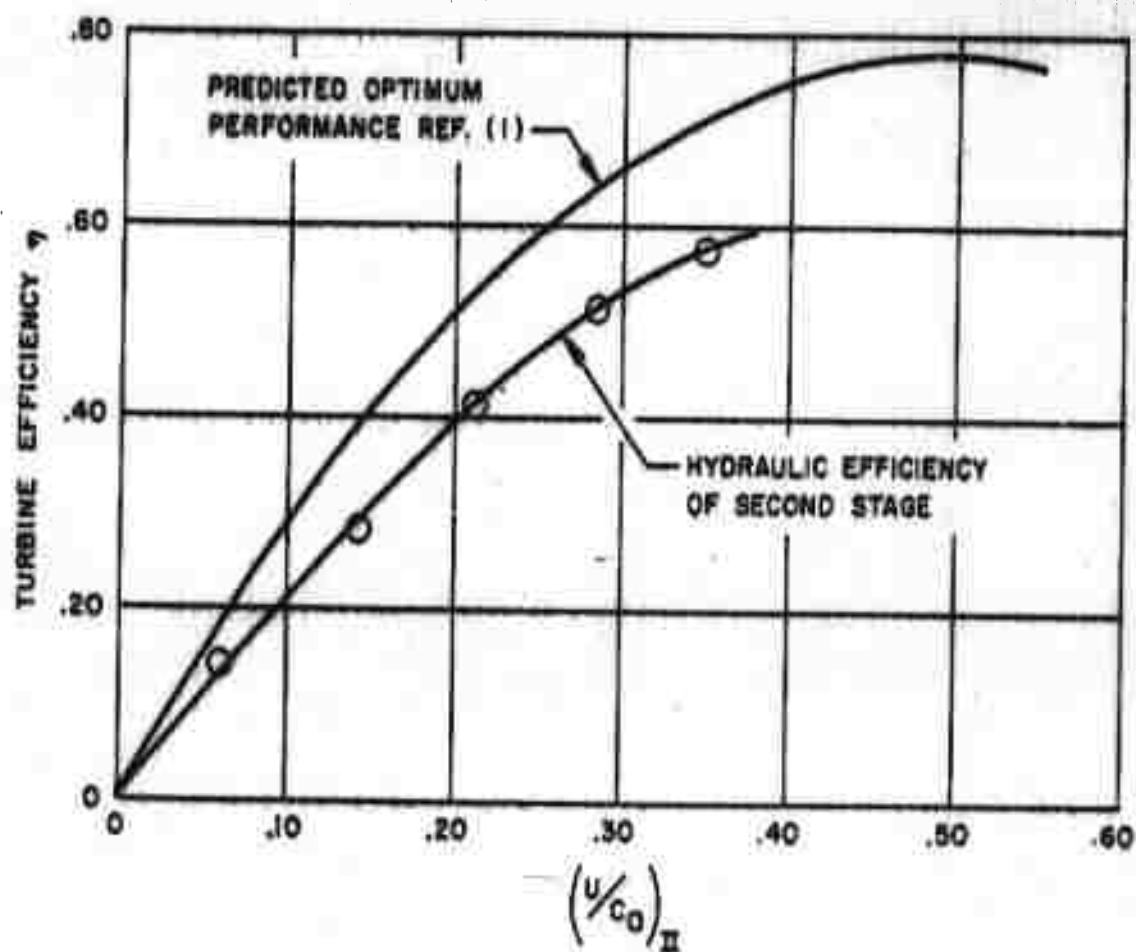


FIGURE 42
PERFORMANCE OF SECOND STAGE
 $P_r = 300 : 1$ $C^* = .005''$

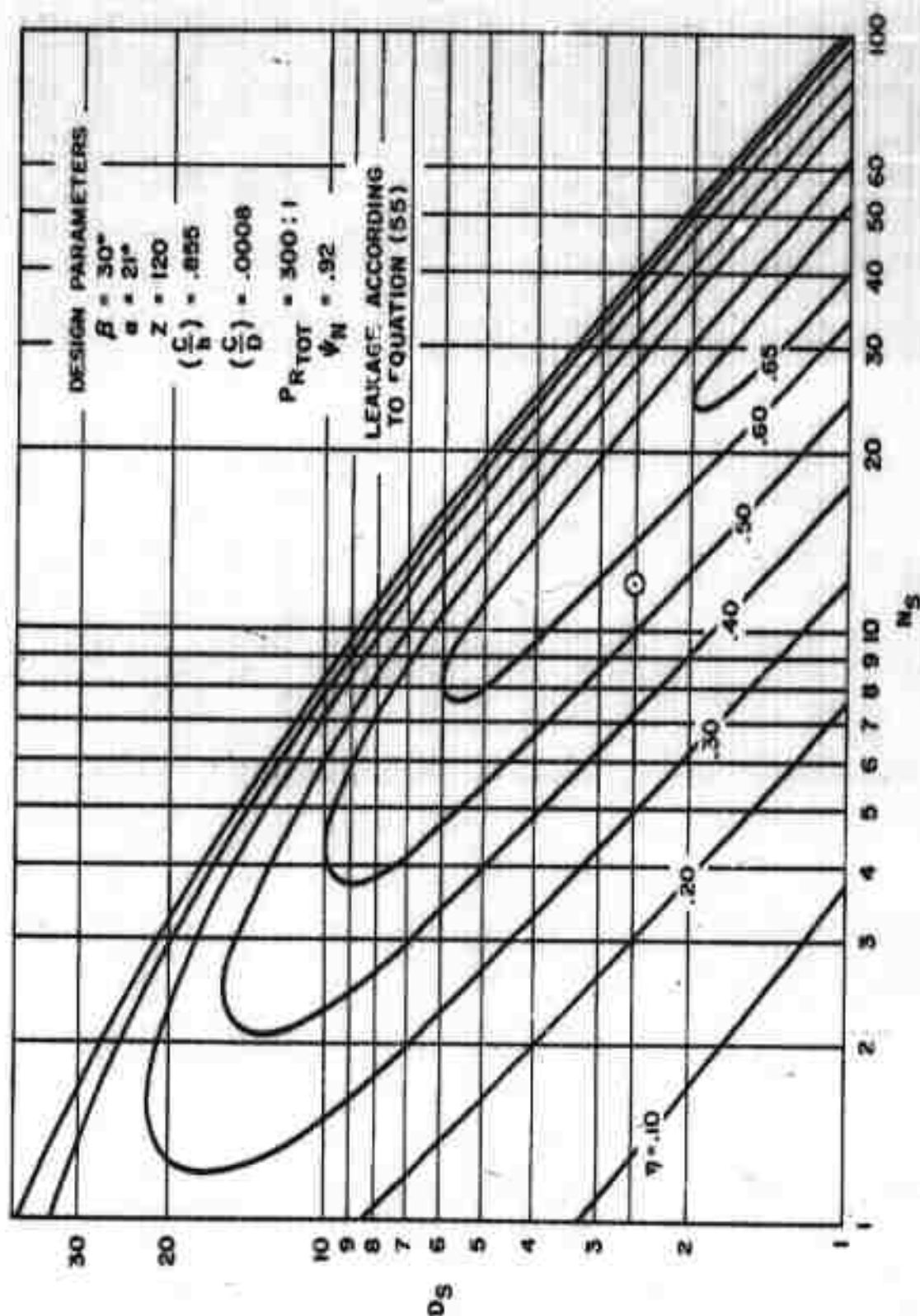


FIGURE 43
FINAL N_s - D_s DIAGRAM FOR TWO-STAGE RE-ENTRY TURBINES WITH EQUAL PRESSURE RATIO IN BOTH STAGES AND 300:1 OVER-ALL PRESSURE RATIO

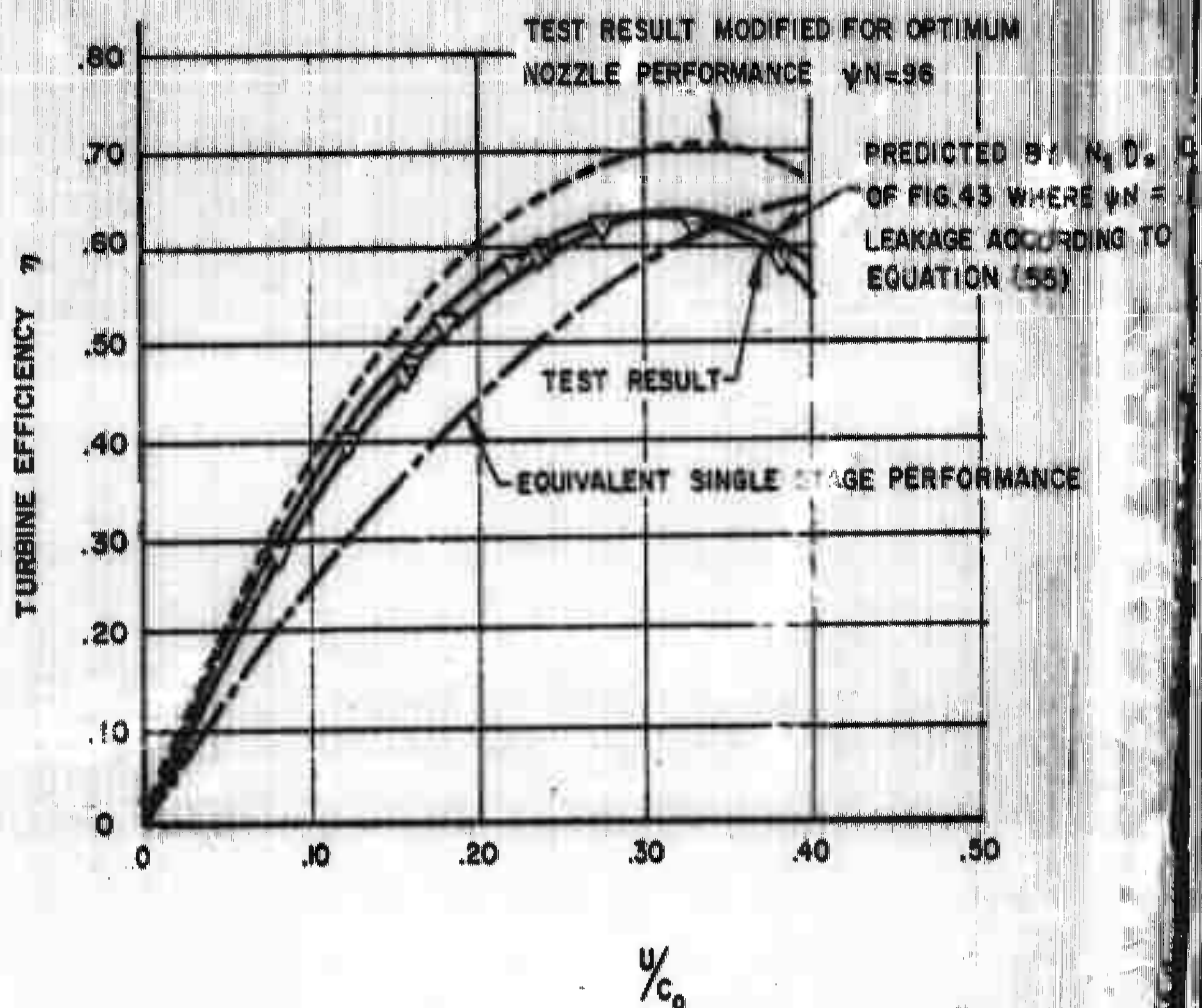


FIGURE 44
COMPARISON OF PERFORMANCE OF TWO STAGE RE-ENTRY TURBINE WITH THEORETICAL PERFORMANCE PREDICTED BY REFINED ANALYSIS AND PERFORMANCE OF EQUIVALENT SINGLE STAGE TURBINE ($C^* = .005$)

UNCLASSIFIED

UNCLASSIFIED